J. A. van Loenhout

Electrochemical reduction of CO_2 to CO on a S-doped flat Ag surface

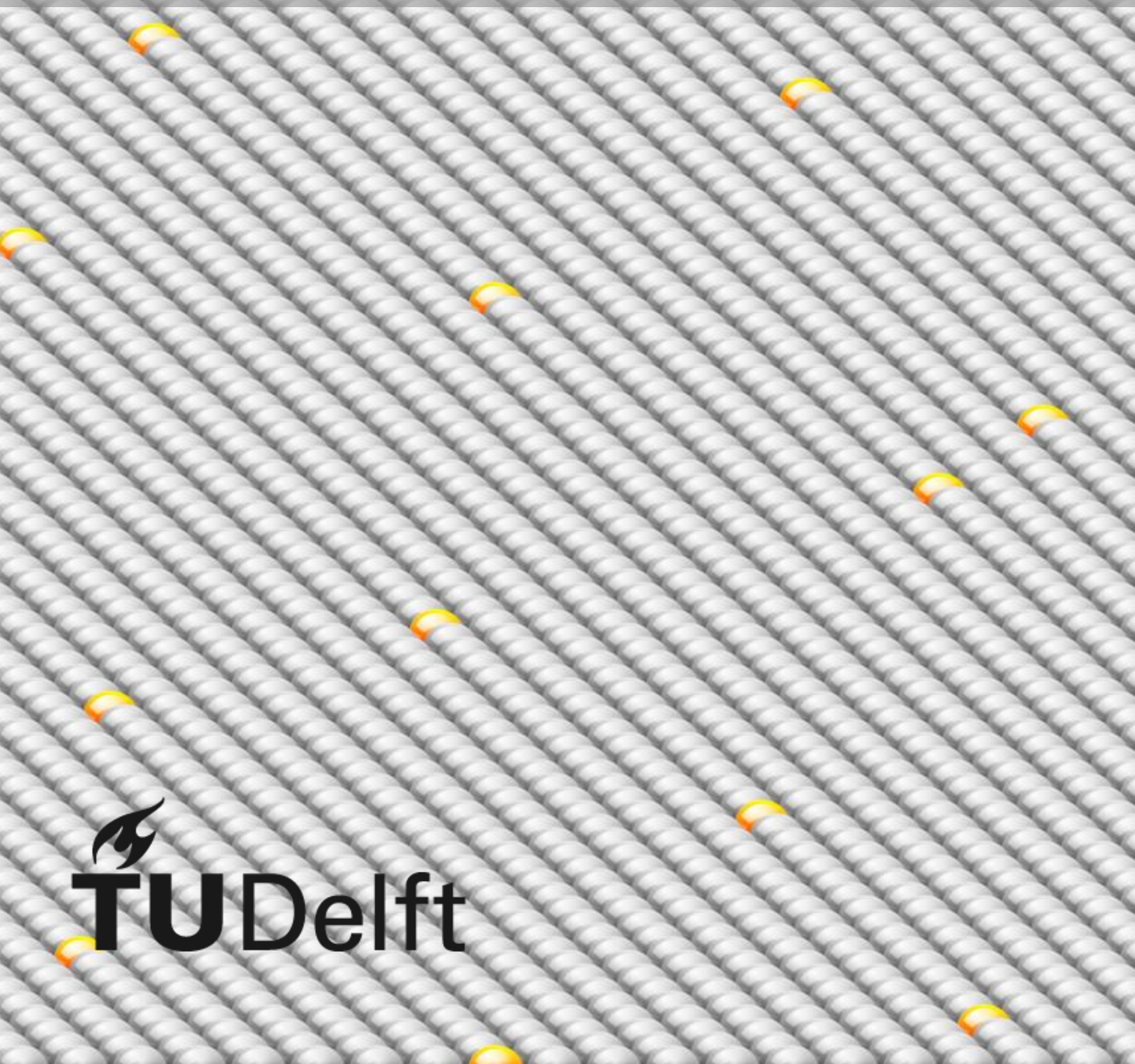

TU Delft

Electrochemical reduction of CO_2 to CO on a S-doped flat Ag surface

By

J.A. van Loenhout

in partial fulfilment of the requirements for the degree of

Master of Science

Sustainable Energy Technology

at the Delft University of Technology,

to be defended publicly on Wednesday July 25, 2018 at 10:30 AM.

Supervisors:	Dr. W.A. Smith	
	N.J. Firet	
Thesis committee:	Prof. Dr. B. Dam	TU Delft
	Dr. R. Eelkema	TU Delft

TU Delft

Preface

First of all I want to thank Nienke for all her help with the experiments, theory, discussions on the subject and focusing more on the positive outcome of the experiments. I also want to thank Wilson for making this thesis possible, the discussions and being thoughtful when I needed some extra time. Next I want to thank Professor Bernard Dam and Dr. Rienk Eelkema for accepting to be a member of my thesis committee. Herman and Joost thank you for helping me with the experiments. I also want to thank Kai for helping me with the NMR measurements. I am also grateful to Marijn who helped me out in the lab and other problems. Furthermore I want to thank all the people of the MECS group for their discussion and interesting group talks.
Next I want to thank my parents for making it possible doing this research while living in Amsterdam and still supporting me after all these years. Special thanks to my girlfriend Milou who cheered me up after a frustrating lab day and tolerated all my many stressful episodes. And last but not least I want to thank my sister Ceciel very much for all the help, support and cheerful times the last 5 years.

Abstract

Since the industrial revolution the use of fossil fuels has increased exponentially, this increase caused a higher concentration of carbon dioxide in the atmosphere, which is responsible for climate change. To prevent a large-scale change of the earth's climate humanity needs to switch to renewable energy sources. A large drawback of current renewable energy sources is that they almost all exclusively produce electricity which is hard to store for long periods of time. A possible solution to this energy storage issue is the electrochemical reduction of CO_2 with electricity from renewable sources. Catalysts used for this process are transition metals but there are several problems that prevent large-scale implementation. Two fundamental problems with these catalysts are: Low activity causing low reaction rates, and low selectivity causing the formation of undesired products. A possible solution was proposed by Lim *et al.* (2014)[1] where they suggested doping a silver electrode with sulphur to enhance the selectivity and activity for carbon monoxide production. This proposal was put the test in this thesis where silver was doped with sulphur by two different methods and were characterized by different techniques and tested at four different potentials. The method where a sample was immersed in a sulphur containing solution and subsequently annealed proofed to be the most effective way to dope a silver electrode. With the help of gas chromatography it was found out that at lower overpotentials the addition of sulphur is beneficial to its performance to produce CO but at higher potentials this advantage is lost. However if the results of this thesis are compared to literature it is clear that doping with sulphur is not effective. Furthermore it was seen that the sulphur doped Ag electrodes were not very stable and therefore not suited for large-scale implementation.

Table of contents

List of figures

1 Introduction

1.1 Introduction to the subject

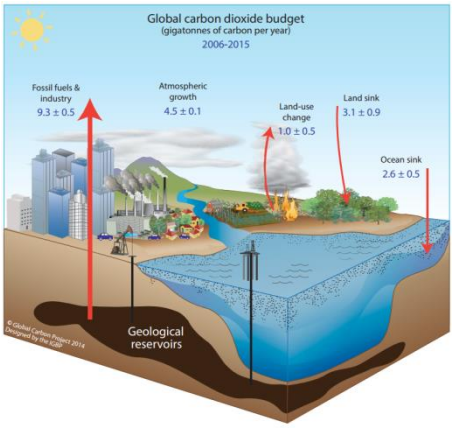

Figure 1: Global carbon dioxide budget.[2]

Since the industrialization started approximately in the middle of the 18th century the demand for energy has increased.[3] This increased demand for energy and the difference in land use e.g. deforestation, large scale agriculture caused an increase in the amount of CO_2 and greenhouse gases (GHG) in the atmosphere.[2,4] this extra CO_2 that was added to the atmosphere disturbed the natural carbon cycle, which is shown in Figure 1. In this natural carbon cycle the amount of CO_2 that was added to the atmosphere, by for example organic decay, was in balance with the amount of carbon that was taken up by the land sink and the ocean sink.[2]

From the 1920s the use of fossil fuels became the largest source of the increasing CO_2 concentration in the atmosphere.[2] But from the 1950s the amount of CO_2 in the atmosphere spiralled out of control because of the growth of the human population, increasing welfare of the entire planet, new technologies and the large scale exploitation of earth's resources.[5] The change of the amount of CO_2 in the atmosphere can be seen in Figure 2.

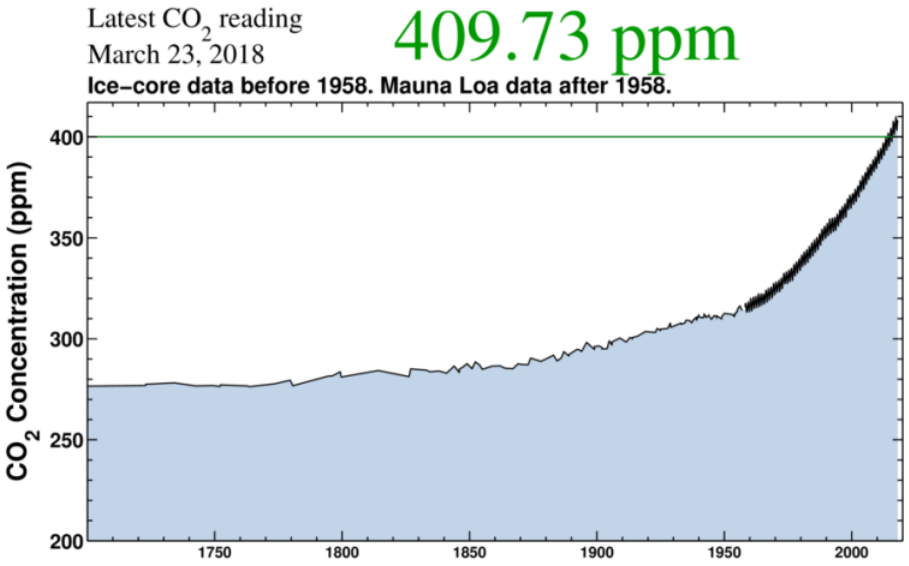

Figure 2: CO_2 concentration in the atmosphere over time. [6]

The amount of GHG in the atmosphere is directly linked to the climate change on earth that is currently taking place.[7-8] To put a hold to climate change the international treaty United Nations Framework Convention on Climate Change (UNFCCC) was created in 1992 to structure this change.[9] Since this treaty multiple conferences have been held with the latest being the Paris Agreement of 2015. At this conference it was decided that the global average temperature should not increase to 1.5 ˚C above the pre-industrial level.[10] To achieve this goal the amount of fossil fuels that are currently being used should decrease and eventually drop to zero. Instead of using fossil fuels as our main source of energy, renewable energy sources should be the main and only source of energy. However the use of renewables has some large drawbacks; first of all most renewable energy sources exclusively produce electricity as their output. This is a problem since our world is fully designed for the use of liquid and gaseous fossil fuels: our power plants, transportation, heating and product manufacturing. The distribution of the world final energy use by fuel is shown in Figure 3.[11]

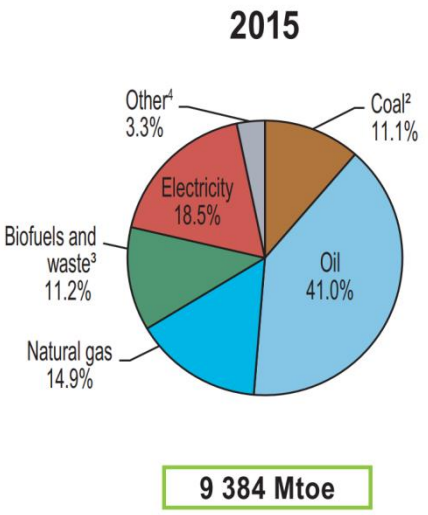

Figure 3: World total final energy consumption of 2015 by fuel

Secondly the amount of energy that is produced fluctuates throughout the day and even throughout the year, besides is the supply of energy from these sources not synchronous with the demand.[12-13] The solution for both these problems are in the way electricity is stored that is produced by renewable energy sources.

Batteries could offer a solution for short time storage of electricity but for long time storage at seasonal scale the use of batteries are not suitable because of scalability and cost problems.[14] Another solution could be the use of hydrogen as an energy carrier but there are again problems with storage, especially the low volumetric energy density. Another drawback is that hydrogen is an energy carrier so it needs to be produced, which lowers the overall efficiency of the use of hydrogen. Finally large initial costs are required because the most efficient way to make use of hydrogen are fuel cells, which are currently not widely available.[13]

A possible solution that both tackle the problem of storage and implementation is the direct conversion of CO_2 to useable products. The source of the CO_2 can be for example the flue gas of coal fired electricity plants, steel factories or the petrochemical industry. And with the help of CCS techniques high purity CO_2 can be obtained from this flue gas.[15] The obtained CO_2 can then be converted to intermediates or end products that can be used as feedstock for the petro-chemical industry or directly as fuels. A possible method of converting CO_2 to useful chemicals or fuels is the electrochemical reduction of CO_2. In this process we assume sustainable produced electrical energy is converted into chemical energy by converting CO_2 with an applied potential into other chemical products.

1.2 Problem definition

The electrochemical reduction of CO_2 has gained a lot more attention over the last years.[16] The main problem in the electrochemical reduction of CO_2 is the high overpotentials that are needed to convert CO_2 and the low selectivity of end products that are formed. The inert nature of the CO_2 molecule makes it difficult to alter the molecule and in this case reduce the molecule. A reduction reaction involves the transfer of electrons towards the molecule that is reduced. In the most simple case where there are only two electrons transferred towards the CO_2 molecule CO is formed, a more complex example is the transfer of eight electrons towards the CO_2 molecule to form CH_4.[17] A lot of intermediate steps are needed to form these products, this means that at all of these intermediate steps undesired steps can occur which ends up in the formation of an undesired product. To reduce the chance of failure the choice to produce CO, with a minimum of two electrons that have to be exchanged, is a reasonable choice. CO together with H_2 is the feedstock of the Fischer-Tropsch process which can produce a wide set of hydrocarbons.

But there are still problems with the CO_2 reduction reaction (CO_2RR) on metallic surfaces. First of all there is competition with the hydrogen evolution reaction (HER), which causes a low selectivity for CO. Secondly there is the high overpotential needed to uptake the CO_2 molecule on the surface of the metal.

Hatsukade *et al.*[18] investigated the electrochemical reduction of CO_2 to CO on a flat Ag surface but still encountered the problems described above. To overcome these problems Lim *et al.*[1] showed by Density Functional Theory (DFT) calculations that by embedding covalency into a metal catalyst the overpotential needed to drive the CO_2RR is reduced. It was suggested that by embedding S into an Ag catalyst the overpotential needed for CO_2RR could be decreased by 0.4-0.5 V.

1.3 Research objective & questions

To combine these two articles of Hatsukade *et al.*[18] and Lim *et al.*[1] the case of a S-doped Ag catalyst will be compared to an Ag foil catalyst in an experimental setting.

The main research question is:

> *Does a S-doped Ag electrode perform better than an all Ag electrode in the electrochemical reduction of CO_2 towards CO?*

To help answer the main research question and give structure to this research the following sub-questions will be answered:

- *What is a suitable method to produce S-doped Ag electrodes?*
- *Does a S-doped electrode convert CO_2 more efficiently to CO than an all Ag electrode?*
- *Is the produced S-doped Ag electrode stable when it is used to reduce CO_2?*

.

1.4 Research design

To see if the addition of S to an Ag film increases the activity for the electrode to reduce CO_2 to CO first a theoretical investigation was done on the different aspects of the subject. From this theoretical study different methods were tried to dope Ag with S. To characterize the electrodes the following techniques were used; Scanning Electron Microscopy (SEM); X-Ray Diffraction (XRD); Grazing Incidence X-ray Diffraction (GIXD); Energy-dispersive X-ray spectroscopy (EDX); Cyclic-Voltammetry (CV); Electrochemical Surface Area (ECSA) measurements; The produced electrodes where tested in a electrochemical cell using a potentiostat to deliver the needed potential and a Gas Chromatograph (GC) to analyse the produced products.

1.5 Report overview

First the theoretical background of CO_2RR and especially on Ag surfaces and the influence of S will be discussed. Furthermore in this chapter the current state of research in the field will be treated. In chapter three the various characterization methods will be shortly explained as well as the step-by-step producing of the S-doped Ag electrodes by the methods used and the experiments that have been conducted to test the electrodes in operation are explained. Chapter four will contain the results of the experiments. In chapter five the outcome of the theoretical background and the experiments will be discussed. In chapter six a conclusion will be drawn based upon the work performed in this thesis. Finally in chapter seven a future outlook will be given on the field of this thesis and subject.

2 Theory

In this chapter the theory behind the reduction of CO_2 will be treated. First a general overview of CO_2 reduction on metal surfaces will be given. Next the particulate case of CO_2 reduction on an Ag surface towards CO is discussed, where the problems and different reaction steps will be shown. In this part also the effect of incorporation of an S molecule in an Ag electrode is explained. Finally the structural and physical properties of the new-formed S-doped Ag electrode are examined.

2.1 CO2 reduction on metal surfaces

Electrochemical reduction of CO_2 or the CO_2 reduction reaction (CO_2RR) is a redox reaction, a reaction that involves the exchange of electrons between the reductant and the oxidator.

The reduction of CO_2 towards other products has been researched since the 1980's and the research in the last few years has been growing a lot.[16]

It is possible to convert CO_2 to a lot of different products; the main thing that changes is the amount of electrons that are exchanged between the electrode surface and the CO_2 molecule. One of the simplest conversions is the addition of two electrons to form CO as shown in Equation 1. But the addition of electrons can go up to twelve electrons forming more complex molecules.[16,19]

$$CO_2(g) + 2H^+ + 2e^- \rightarrow CO(g) + H_2O\ (l) \qquad \textbf{Equation 1}$$

The products that are mostly produced of CO_2 are CO, $HCOO^-$/HCOOH, CH_4, CH_3OH, C_2H_4 and CH_3CH_2OH.[18,20–27] The three major classes of CO_2 reduction catalysts are the following:[28] Non-metallic catalysts e.g. 3-D graphene foam incorporated with nitrogen defects;[29] molecular catalysts e.g. transition-metal-centred molecules;[30] and finally there are metallic catalysts which form the largest group. The metallic catalysts can be subdivided into:[28,31] Ion-modified metallic e.g. Ag-O; Bimetallic alloys e.g. AuCu and the monometallic subgroup e.g. Ag, Cu; Nano-structured subgroup e.g. nanoparticles, Nano foam, Nano corals.

In this study only heterogeneous catalysts are discussed because these are believed to have most potential for large-scale implementation because of their recyclability and lower cost. The heterogeneous catalysts that are used in CO_2 reduction can roughly be grouped in four classes. First there is the class that produces CO (Ag, Au, and Zn). Secondly there is the class that produces formate and/or formic acid (Pb, Pd, Hg, In, Sn, Cd, Tl, Bi) and thirdly the subclass that produces hydrogen (Pt, Fe, Ni, Ti, Ga, Co).[28,32] The fourth class consists of only the element Cu. Cu is somewhat different because it is the only transition metal that can produce higher C products like methane but also alcohols like methanol.[33]

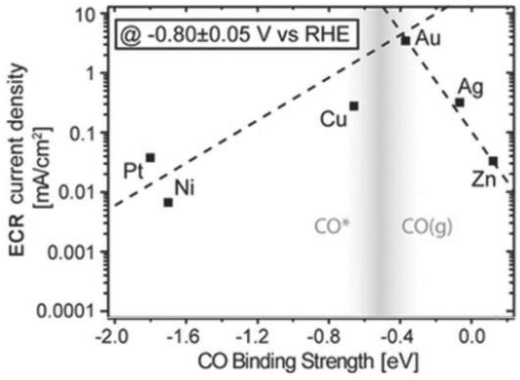

Figure 4: Volcano plot of current density vs binding strength of CO. (figure from Zhu *et al.*[17], 2016; slightly adjusted)

Why a certain catalyst produces either CO, Formate/formic acid, H_2 or higher C products is because of the binding strength of the intermediates in CO_2RR to the catalyst' surface. Especially the binding of the *CO intermediate on the surface of the catalyst determines what end products are formed. Catalysts that produce H_2 (e.g. Pt, Fe, Ni, etc.) bind the *CO intermediate very strongly this means that the catalyst surface becomes poisoned with CO and therefore only produces H_2. When the *CO intermediate binds at an intermediate strength higher hydrocarbons will be formed. At low *CO intermediate binding strength CO will be the end product, because it is energetically more favourable for CO to leave the surface of the catalyst.[33] So there is an optimal binding strength for molecules adsorbed on the surface of a catalyst this is called the Sabatier principle and this can be visualised in a volcano plot.[33] An example of such a volcano plot is shown in

Figure 4[17] where the electrochemical CO_2 reduction (ECR) current density (i.e. activity) is plotted against the binding strength of various metals.

The most suitable catalyst for CO_2 reduction towards CO are Zn, Ag and Au because of their low binding energy ($\Delta G_{B,CO}$) of CO. So because of the binding energy of CO on the surfaces of Au, Ag and Zn the favourable end product is CO. But between these catalysts there is a difference in the performance of CO_2RR towards CO. This is because of the binding energy of the COOH intermediate that is formed on the surface of the catalyst. It turns out that a good binding with the COOH molecule is the key to effective CO_2RR towards CO this will be explained in more detail in the next paragraph.

Au is the best candidate for the CO_2RR towards CO because of the best binding energy with COOH. Ag and Zn have lower binding energies with COOH where the latter one has the lowest binding energy and is therefore the least active in CO_2RR. Combining the cost of the catalyst and activity Ag is the best candidate for CO_2 reduction towards CO.[34]

There are some important definitions that are crucial to understand the electro catalytic conversion of CO_2 towards other products. Since different products can be formed in the CO_2RR the selectivity of a catalyst to produce a particular products is important. A measurement for the selectivity towards a certain product is the Faradaic efficiency.

The Faradaic efficiency (FE) is defined as the ratio between the electrons used to form a certain product and the total electrons that are used in an experiment.[35] As shown in Equation 2.

$$Faradaic\ efficiency = \frac{number\ of\ electrons\ used\ for\ product}{total\ electrons\ used} \qquad \textbf{Equation 2}$$

With the help of the FE it is possible to tell something about where the electrons end up and thus say something about the selectivity of catalyst for certain products.

The current density (Equation 3) is a measurement for the activity of a catalyst with the unit mA/cm^2 by dividing the current by the surface area of the catalyst it is possible to compare different catalyst (i.e. different sizes).

$$J = \frac{1000 \cdot ppm \cdot Q \cdot n \cdot F \cdot p_0}{R \cdot T \cdot A} \qquad \textbf{Equation 3}$$

$J = Partial\ current\ density\ \left(\frac{mA}{cm^2}\right)$
$ppm = Amount\ of\ product\ interested\ in\ (ppm)$
$Q = Flow\left(\frac{m^3}{s}\right)$
$n = Number\ of\ electrons\ per\ product\ (-)$
$F = Faraday\ constant\left(\frac{A \cdot s}{mole}\right)$
$p_0 = Pressure\ (Pa)$
$R = Gas\ constant\ \left(\frac{m^3 \cdot Pa}{K \cdot mole}\right)$
$T = Temperature(K)$
$A = Surface\ area\ (cm^2)$

This is called the geometric current density this is an effective physical quantity to compare flat surfaces but electrocatalysts usually do not have perfectly flat surfaces. So to incorporate the nano-structured or not flat surfaces the electrochemical surface area current density can be used. In this current density the influence of the three dimensional area is eliminated by dividing the current through the area of the electrode that is used during electrochemical experiments.[35]

2.2 CO2 reduction towards CO on an Ag surface

In this research the electrochemical reduction of CO_2 towards CO is investigated, to put this research in contrast with results already reported in literature other research performed in the field will be discussed. Three articles are treated were different varieties of an Ag catalyst are investigated. All of the articles use 0.1 M CO_2 saturated $KHCO_3$ as electrolyte solution. Figure 5 and Figure 6 show the results of experiments conducted by Hatsukade *et al.*[18] In the figures the relation between the applied overpotential and the corresponding FE for each product and the relation between overpotential and current density is shown.[18] The catalyst used in these figures is a polished Ag foil with a thickness of 0.1 mm. From Figure 5 it can be seen that at overpotentials lower than -0.8 V vs RHE the formation of H_2 is dominant over CO production. At intermediate overpotentials the formation of CO is favoured over H_2 and the highest FE is seen at -1.1 V vs RHE. At the highest overpotentials higher than -1.2 V vs RHE CO selectivity decreases and H_2 is favoured, also in very small amounts higher hydrocarbons are formed. $HCOO^-$, as a two-electron product, also formed at all potentials but only in very small amount reaching only an average faradaic efficiency of 5%. The current densities that were monitored by Hatsukade *et al.*[18] are shown in Figure 6. The partial current density for CO range from -0.007 mA/cm^2 at -0.6 V vs RHE and reaches the highest current density of -5 mA/cm^2 at -1.1 V vs RHE. When the partial current density and CO FE reached its peak at -1.1 V vs RHE the FE and current densities of the other products start to increase indicating that CO is further reduced, the Hydrogen Evolution Reaction (HER) is more prominent and more $HCOO^-$ is produced. The total current density reaches from -0.25 mA/cm^2 at -0.6 V vs RHE to -10 mA/cm^2 at -1.4 V vs RHE.

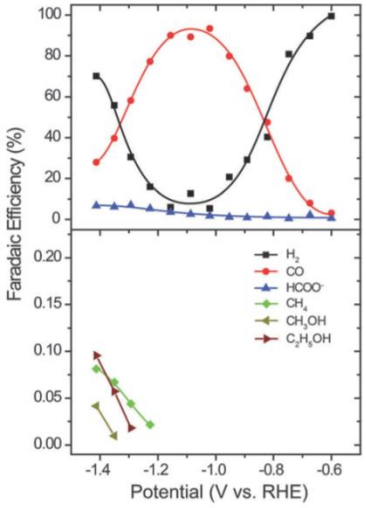

Figure 5: Faradaic efficiency as a function of overpotential.

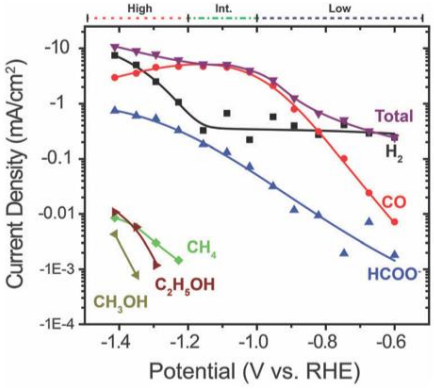

Figure 6: Current density as a function of overpotential.

Figure 7 show the result of Ma *et al.*[36] in this work polycrystalline Ag and oxide-derived nanostructured Ag were tested at different potentials for the production of CO. By nano-structuring the surface of Ag the FE increases substantially at lower overpotentials reaching already an FE of 10% at -0.4 V vs RHE and reaching 90% at -0.8 V vs RHE. Besides the high CO FE the HER is successfully suppressed at higher overpotentials. Also the current density is increased at lower overpotentials reaching a peak at -1.0 V vs RHE of 2.8 mA/cm^2. Probably because of mass transport limitations the peak is reached at -1.0 V vs RHE and is not further increased.

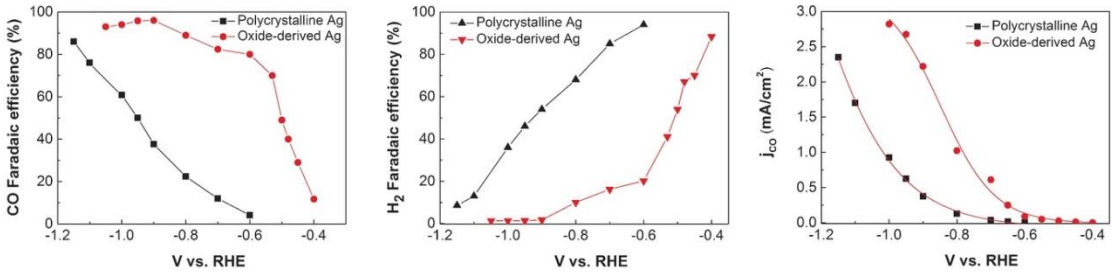

Figure 7: Faradaic efficiency and current density for CO on polycrystalline Ag and oxide-derived Ag

In Figure 8 the results of research performed by Hsieh et al.[37] the CO_2RR to CO was tested at Ag foil, Ag Nanoparticles (NPs) and AgCl-derived nano-corals. The Ag nano-coral performs the best on CO FE reaching a FE of 95% at -0.5 V vs RHE and a minor FE for H_2 at all potentials. The Ag NP's perform less than the nano-corals on CO FE but better than Ag foil. Ag foil performs similar as in the article of Ma *et al.*[36] but less than Hatsukade *et al.*[18] The partial CO current density at a potential of -0.6 V vs RHE is for the nano-coral, Ag NP's and Ag foil: 6.62, 0.4 and 0.01 mA/cm^2 respectively. The total current density is for the Ag nano-corals high in comparison with Ma *et al.*[36] and Hatsukade *et al.*[18] with ~10 mA/cm^2 at -0.7 V vs RHE.

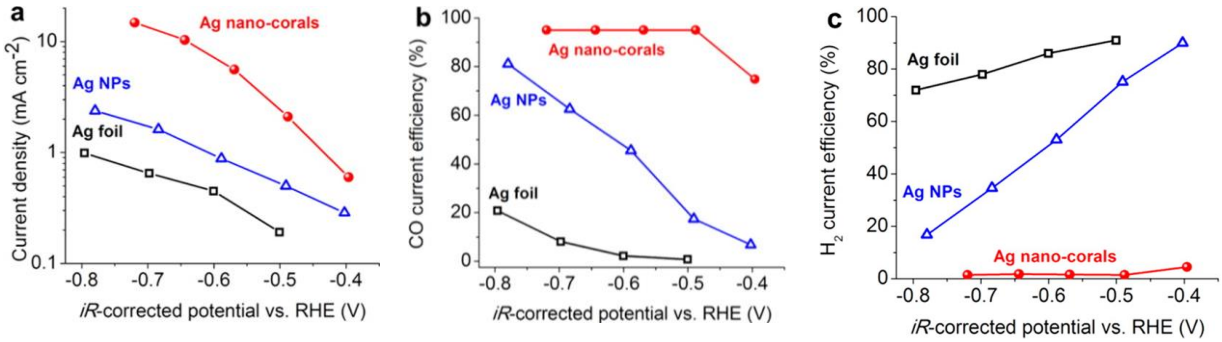

Figure 8: Faradaic efficiency and total current density for Ag foil, Ag NPs and Ag nano-corals

The oxide-derived nanostructured of Ma *et al.*[36] and the Ag nano-corals and Ag NPs significantly outperform the ordinary Ag foil. Ma *et al.*[36] name the more favourable sites for the intermediate of COOH* to bind to, next to these sites also a high pH near the surface is mentioned. This is mainly because of the increased active surface area of these electrodes and the more favourable facets needed for CO_2 reduction. Hsieh *et al.*[37] name besides the nanostructured morphology also the adsorbed chloride anions as a reason for the increased activity and a HER suppressant.

Now the general picture of CO_2RR is given we go in more depth on the CO_2RR towards CO on the surface of an Ag surface. Above already some solutions are mentioned for the CO_2RR on an Ag surface. In the next part the fundamentals of these problems will be discussed. Firstly there is the competition with the Hydrogen Evolution Reaction (HER) that is shown in Equation 4.

$$2H^+ + 2e^- \rightarrow H_2(g) \qquad \textbf{Equation 4}$$

The HER is mainly active in the low overpotential region, the equilibrium potential is 0 V vs RHE.[23] This causes a low selectivity towards other products than H_2.

Secondly there are problems of low activity i.e. current density.

Thirdly there are problems with high overpotentials that are needed for CO_2RR to CO. To give more insight in this problem the reactions that are taking place on the surface of the Ag electrode will first be discussed. There are two theories on what intermediates form on the surface of the Ag electrode in the CO_2RR the first theory is shown in Figure 9.

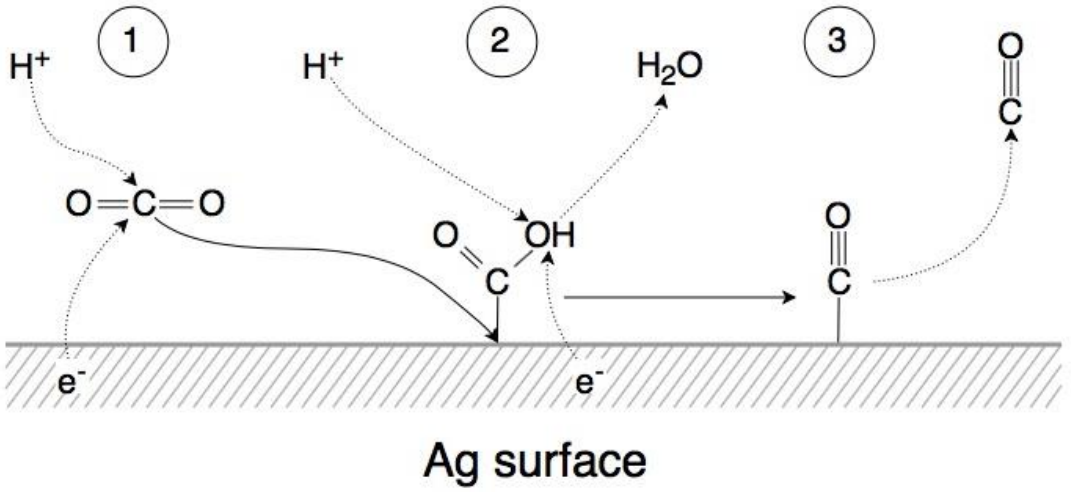

Figure 9: Two possible intermediates in CO_2RR

The two theories on the reaction mechanism differ in the way the CO_2 molecule is bound to the surface of Ag. The first theory is shown in Equation 5; here it is assumed that there is a Proton Coupled Electron Transfer (PCET). So the transfer of a proton from the electrolyte towards the CO_2 molecule occurs together with the electron transfer from the Ag electrode towards the CO_2 molecule. This step is also pointed out by Hatsukade *et al.*[18] and Lim *et al.*[1] In Equation 5 the * is the symbol for a bound molecule or a surface active site at the catalyst as in Equation 9.

$$CO_2(g) + * + H^+ + e^- \rightarrow COOH* \qquad \textbf{Equation 5}$$

The other theory the decoupled proton and electron transfer (Figure 10) presumes a decoupled proton and electron transfer in other words the binding of the CO_2 molecule and the formation of the COOH* on the surface of Ag is not a one-step mechanism but a two-step mechanism. This sequential electron proton transfer has been reported by Koper[38], the decoupled transfer has influence on the reaction because in this case there will a pH dependence on the overall reaction rate and therefore also an optimal pH for the reaction to occur. Firet & Smith[39] have shown with ATR-FTIR measurements that on an Ag surface in a KCl electrolyte the PCET in a potential window of -1.4 V and -1.55 V vs Ag/AgCl was dominant and at a potential of -1.6 V vs Ag/AgCl the decoupled mechanism was dominant.

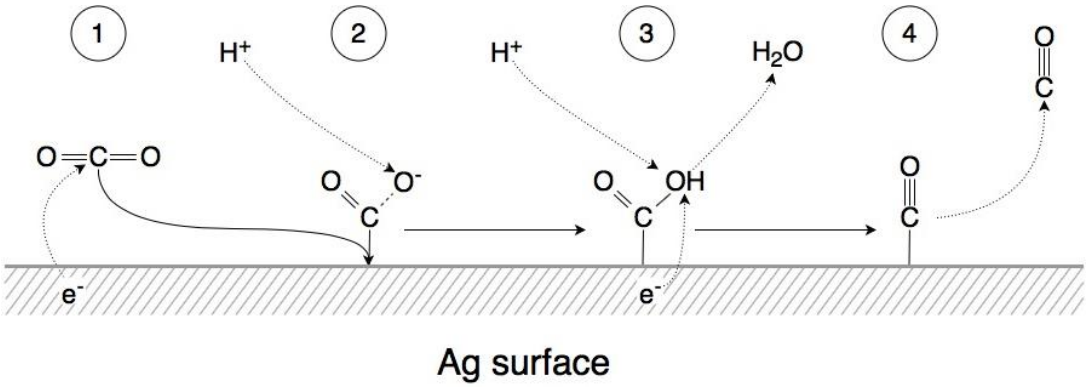

Figure 10: Decoupled proton electron transfer in CO_2RR

In Equation 6 the first step of the decoupled proton electron transfer is the adsorption of CO_2 and the simultaneous electron transfer.

$$CO_2(g) + * + e^- \rightarrow COO^- * \qquad \textbf{Equation 6}$$

Subsequently there is a proton transfer from the electrolyte towards the COO^-* radical as shown in Equation 7.

$$COO^- * + H^+ \rightarrow COOH * \qquad \textbf{Equation 7}$$

The next step is the same for both mechanisms, there is a simultaneous proton and electron transfer towards the COOH* intermediate in which it forms a CO molecules bound to the surface. (Equation 8)

$$COOH * + H^+ + e^- \rightarrow CO * + H_2O(l) \qquad \textbf{Equation 8}$$

Finally the CO is desorbed into the electrolyte in the gas phase as shown in Equation 9.

$$CO * \rightarrow CO(g) + * \qquad \textbf{Equation 9}$$

Since the CO_2RR includes multiple intermediates there is a rate-determining step (RDS). The bending of the linear CO_2 molecule, the sp-hybridization, which is needed to adsorb the molecule on the surface of the catalyst is the RDS.[1] This RDS has a reduction potential of E°= −2.02 V vs SHE without a catalyst present. By using Ag as a catalyst this overpotential is lowered to E°= −0.91 V vs SHE.[1]

To overcome the problems of a high overpotential at an Ag surface, the reaction must be further catalysed. Since the reaction of CO_2 to CO requires multiple intermediates and therefore different reaction steps it is important that the right reaction steps are catalysed. It has been shown that the first reaction step, the bending and adsorbing of the CO_2 molecule on the surface of Ag, is the RDS. So to lower the overall potential needed, this reaction has to be catalysed, without altering the binding strength of CO maintaining the energetically

favourable desorption of CO. Because when the energy that is necessary for the first step is less than the second step this will be the RDS of the overall reaction. In the article by Lim *et al.*[1] the thermodynamic energy change for the three intermediate steps is as following, where the first step is the same as Equation 5, the second step is Equation 8 and the third and final step is the same as Equation 9.

Step 1 $$\Gamma_1 \rightarrow \Delta G_1 + \Delta G_{B,COOH}$$ **Equation 10**

Step 2 $$\Gamma_2 \rightarrow \Delta G_2 + \Delta G_{B,CO} - \Delta G_{B,COOH}$$ **Equation 11**

Step 3 $$\Gamma_3 \rightarrow \Delta G_3 + \Delta G_{B,CO}$$ **Equation 12**

Γ represents in these formulas the thermodynamic energy change. ΔG is the free reaction energy needed for every reaction (without a catalyst) and ΔG_B is the binding free energy. With the help of DFT calculations the thermodynamically required energy needed for each step has been calculated at a certain current density. In summary the $\Delta G_{B,COOH}$ should decrease thereby increasing the stabilization of the COOH* on the surface of Ag, maintaining or increasing $\Delta G_{B,CO}$ so desorption is favoured over another reduction step.

Doping is a method to alter the binding conditions of the surface of a catalyst. Lim *et al.*[1] used DFT calculations to determine a suitable dopant. They looked into *d*-block and *p*-block dopants, by replacing one surface Ag atom in an Ag FCC (111) structure of three atomic layers of 48 atoms. The following explanation is based upon the work of Lim *et al.*[1]

Because of scaling relations, the decrease in $\Delta G_{B,COOH}$ when *d*-block dopants were introduced ended up in a linear decrease of $\Delta G_{B,CO}$ causing a limit to which the binding energy needed could be lowered (i.e. otherwise the CO desorption step would get unfavourable). This is due to the fact that *d*-block dopants in Ag, a *d*-block element, alter the *d*-band, which binds to the CO and COOH in the same way thus the binding energies of these intermediates are correlated. By introducing a *p*-block element, there is a singly occupied p_z orbital available that is highly hybridized with the *d*-band of the Ag atoms. This singly occupied p_z can stabilize the radical electron present in COOH of the $2p_z$ orbital C atom. The binding of the COOH radical on the surface of the *p*-block doped Ag catalyst can be separated in two steps. The first step is the energy preparation cost (E_{rp}) of the radical; because the *p*-orbitals are highly hybridized with the *d*-band of Ag an energy input is necessary to spatially localize the singly occupied p_z orbital of the dopant atom to prepare $(p_z)^1$. The second step is the covalent bond stabilization energy step ($E_{\sigma\text{-bond}}$) which originates from the energy that is needed to form the σ-bond of the $(p_z)^1$ orbital of the new dopant atom and the $(2p_z)^1$ orbital of the COOH-intermediate molecule. These two steps are shown in Figure 11.

The binding of CO, which has a couple of non-binding electrons, needs a $(p_z)^0$ orbital. In order to reach this state all electrons from the p_z orbital should be removed which is energy intensive. Therefore the binding energy of CO on the doped Ag catalyst is not favourable thus leading to desorption. In this way the scaling relation between $\Delta G_{B,COOH}$ and $\Delta G_{B,CO}$ is

successfully circumvented and it is possible to further decrease the overpotential that is needed. This doping is called covalency-aided electrochemical reaction (CAER).[1]

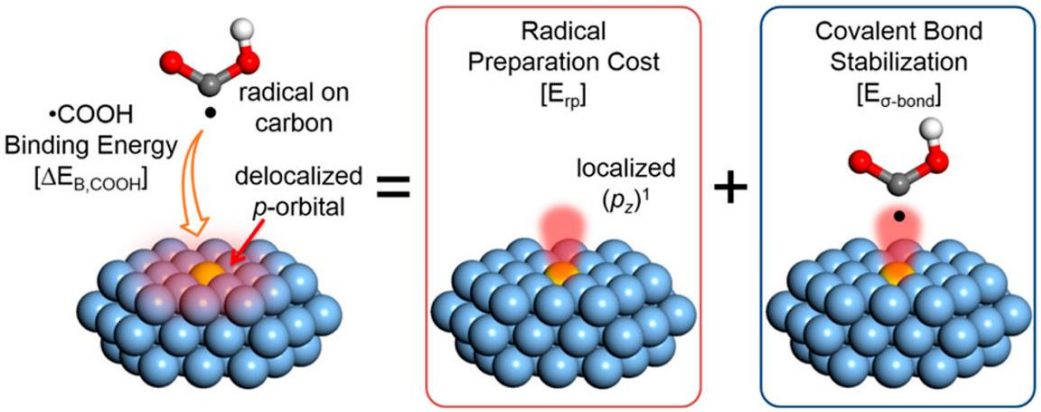

Figure 11: Covalency-aided electrochemical reaction[1]

These DFT calculations that are described above were performed for *d*-block and *p*-block dopants that are shown in Figure 12.

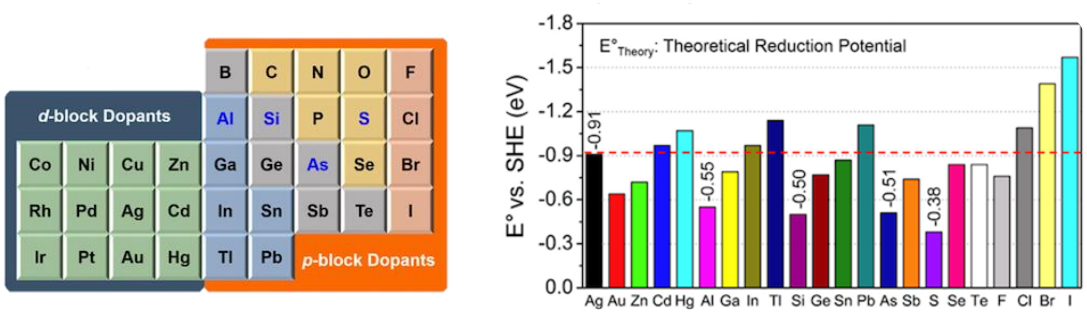

Figure 12: List of *d*-block and *p*-block dopants (left) and the theoretical reduction potential (right) when incorporated in Ag[1]

The use of S in Ag gave the best result lowering the theoretical reduction potential to -0.38 V vs SHE. Other dopants that decreased the theoretical potential significantly are Si, Al and As.

To examine the stability of the dopant element in the Ag slab, electrochemical hydrogenation reaction simulations were performed. This gave a leaching potential of -0.58 V vs SHE and was therefore stable during CO_2 reduction.

2.3 Ag_2S

The addition of S ions to the structure of polycrystalline Ag will have consequences. In this thesis the amounts of S that are incorporated in the polycrystalline Ag will be relatively small, so there will be a mixture of metallic Ag and Ag_2S.[40] The aim is, taken from the research of Lim *et al.*[1], an atomic ratio of 1:48 ≈ 2.1 at% S. the structure of the Ag_2S and Ag will be discussed here.

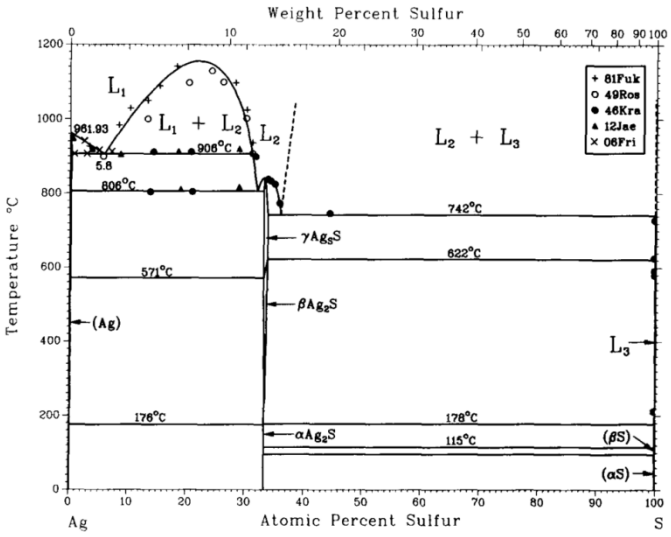

Figure 13: Phase diagram Ag + S[40]

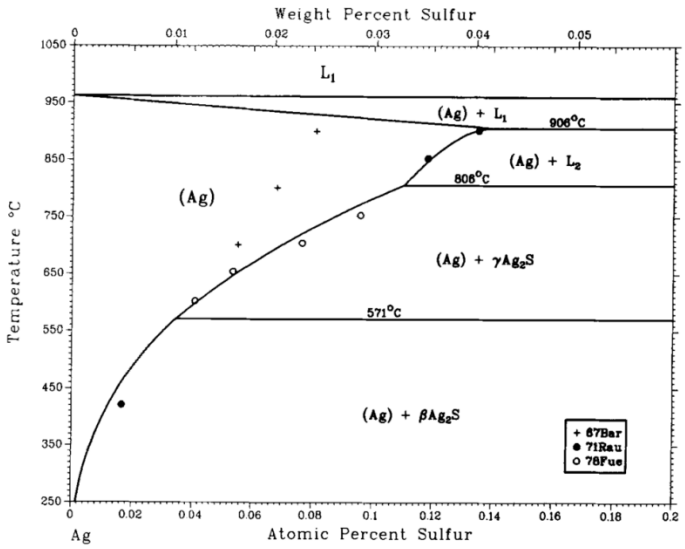

Figure 14: Phase diagram low S content[40]

There are two methods tried to produce S-doped Ag electrodes which will be discussed in the experimental section. In one of these methods the electrode is annealed at 523 K (250 °C). In the other method, the electrode is not annealed and the temperature of the electrode is not raised above 333 K (60 °C). This temperature difference in both production methods is of importance because that would mean there are different phases present in the different materials. In the phase diagrams of Figure 13 and Figure 14 it can be seen that there are two phases present in each material. At temperatures up to 451 K (178 °C), the α-Ag_2S phase, also known as the acanthite phase, is present in the material.[40,41] The α-phase is transformed to the ß-phase, or argentite, at a temperature of 451 K (178 °C) and is stable up to 844 K (571 °C).[40,41] Above 844 K (K (571 °C) there is also a third phase the γ-Ag_2S phase.[40]

The α-Ag_2S phase has a total conductivity that is comparable to the behaviour of a semiconductor (i.e. the conductivity increases with increasing temperature). The structure consists of a S monoclinic lattice (vectors have differing lengths), the Ag atoms are in close proximity to the tetra- and octahedral positions and equally spread.[41] Figure 15 shows the monoclinic structure of α-$Ag_{2+\delta}S$ where the Ag atoms numbered 1 are closest to the octahedral sites and Ag atoms numbered 2 are closest to tetrahedral sites.

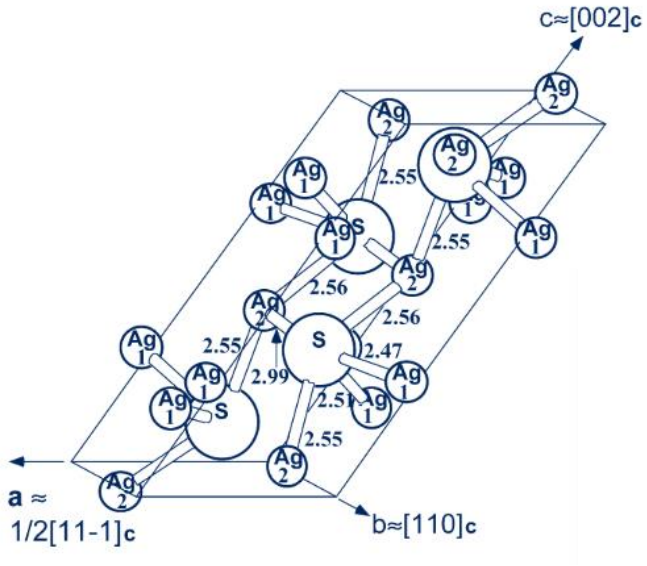

Figure 15: Monoclinic structure of acanthite α-$Ag_{2+\delta}S$, Ag(1) closest to octahedral sites and Ag(2) closest to tetrahedral sites.[41]

ß-Ag_2S consists of a S BCC lattice, but the Ag atoms are more located at the tetrahedral sites than the octahedral sites. The total conductivity of the ß-phase is in the order of 2-3 magnitudes larger than in the α-phase, it is also more or less independent of the temperature and therefore shows more metallic behaviour.[41]

The produced electrode in this thesis will thus exist for the largest part exist of a large Ag-phase with either small amounts of α-Ag_2S or ß-Ag_2S phases incorporated in the polycrystalline structure of the Ag phase.

2.4 Doping of Ag

The doping of Ag to enhance the electro catalytic properties of Ag is a much-researched topic in the field of CO_2RR. Besides Lim *et al.*[1] also Liu *et al.*[42] looked into doping Ag with S[42], they formed Ag_2S nanowires, that were then used for the CO_2 reduction towards CO. Increased partial current densities for CO and improvement in the CO FE were observed. Also the onset potential for the formation of CO was lowered successfully to a potential of -0.164 V. They performed their experiments with Ag_2S nanowires in 0.1 M $KHCO_3$ and ionic liquid and, the use of an ionic liquid as a electrolyte increased the partial current density to 12.37 mA/cm^2, almost 14 times higher than the same experiment performed in $KHCO_3$ and 17.5 times higher than Ag in $KHCO_3$.

Another research were doping of Ag nanoparticles with S stood central was performed by Kim *et al.*[43] were they doped Ag nanoparticles with cysteamine on a carbon support. By using cysteamine and a nanoparticle size of 5nm the overpotential was effectively lowered and at -0.75 V vs RHE the FE was four times higher than at Ag foil. Next to the lowered overpotential and increased FE also the durability was strongly improved. Finally DFT calculations showed that the improved performance was due to the Ag-S bond that favoured the COOH intermediate over CO.

Park *et al.*[44] reported on the electro deposition of Ag catalysts in the presence of different additives. By using different additives the morphology, crystal structure and electrochemical properties of the catalyst were altered. So by choosing the right additive an Ag catalyst with the right Ag(220)/Ag(111) ratio could be produced. Because of the relation between the ratio of the crystalline structures and the ratio of the produced CO and H_2, with the help of additives syngas with the right CO/H_2 ratio can be produced which can be immediately used in for example in Fischer-Tropsch.

Choi *et al.*[45] used electrodeposition to produce dendritic Ag-Cu catalysts. The dendritic pure Ag catalyst had the highest FE; the activity was higher for a mix of Ag-Cu in a dendritic catalyst. By tuning the ratio between Ag and Cu the ratio between the produced products CO and H_2 could be controlled.

Doping however is not always helpful for a catalyst, Sun *et al.*[46] showed that by doping an Ag with Ni they deteriorated the active efficiency for CO of Ag. By adding Ni the amount of unoccupied density of states of d-character was reduced which had a negative effect on the overall catalytic performance of Ag.

3 Experimental methods

In this chapter the two techniques of producing S-doped Ag electrodes are being discussed step-by-step. Furthermore the used equipment, characterization methods and operation conditions are briefly explained.

3.1 Production of Electrodes

3.1.1 Ag preparation

Polycrystalline Ag with a thickness of 0.125 mm (Mateck, 99.9% purity) was cut into samples of 2x2 cm. These samples were then thoroughly cleaned with soap and rinsed with Milli-Q water. Next the samples were rinsed and sonicated for 10 minutes at 40 °C in an ultrasonic cleaner (Emmi Emag 30-HC) subsequently with acetone, ethanol and Milli-Q water. Afterwards the clean samples were blown dry with N_2.

3.1.2 Chemical Bath Deposition

A solution of 100 mL of 1 mM S_8 (99.998% trace metal basis, Sigma-Aldrich) in acetonitrile solution was prepared after Liu *et al.*[47] where it was used to produce Ag_2S nanoparticles. 25.652 mg of S_8 was added to a volumetric flask thoroughly cleaned with ethanol and acetone and blown dry with N_2. Next, 100 mL acetonitrile (anhydrous 99.8%, Sigma-Aldrich) was added to the volumetric flask. A stirring flea was added to the volumetric flask. The mixture was heated to 60 °C to dissolve the S_8 in the acetonitrile and stirred simultaneously using a magnetic stirrer with a heating element (RSM-05-H, Phoenix Instrument). When the S was dissolved 50 mL of the solution was poured into a beaker glass. The temperature of the solution in the beaker was raised again to 60 °C. When the temperature was stable at 60 °C the cleaned Ag sample was lowered into the solution with help of a titanium tool. The sample was immersed for 1 minute while closely monitoring the temperature of the solution. When the temperature plummeted the beaker was covered with a lid or when the temperature raised the sash of the fume hood was closed. After 1 minute the sample was taken out of the solution and was immersed into a beaker filled with pure acetonitrile. Subsequently the sample was rinsed with ethanol and Milli-Q water and finally was blown dry with N_2. This method is called the Chemical Bath Deposition (CBD).

After the samples were doped with S the samples were annealed in a tube furnace oven (3210, ATS) at a temperature of 523 K (250 °C) for 3 hours with a ramp of 5 °C/s in a stream of Ar. This annealing step was needed to distribute the S over the Ag sample. After this anneal step the samples were ready for testing.

In Figure 16 samples before the anneal step can be seen and in Figure 17 afterwards, this were test samples to see what conditions (i.e. concentration solution, immersion time) are best to fulfil the requirement of ~2 at% S. There is a correlation between the colour change and the amount of S in an Ag sample. When the Ag sample was exposed for a longer

amount of time or a higher concentration of S_8 the colour of the Ag sample changed from metallic silver through yellow, violet, blue to finally dark grey.[48]

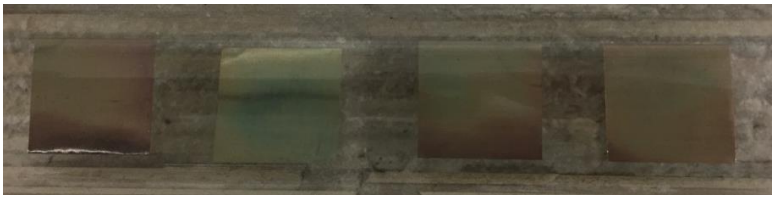

Figure 16: 0.125 mm Ag samples before annealing

Figure 17: 0.125 mm Ag sample after annealing

3.1.3 Pre-reduction

A slightly different method to produce the S-doped Ag samples was shown by Huang *et al.*[21] First a prepared Cu_2O disk was doped with S by immersing it in an ammonium polysulfide solution of concentration varying from 1 to 5000 µM for 5 minutes. The prepared samples were rinsed with large quantities of water before drying overnight in an oven at 50 °C. Next the samples were pre-reduced at -0.8 V vs RHE for 5 min. in 0.1 M $KHCO_3$ to remove excess S and obtain a sample with ~2.7 at% S.

In this thesis Ag is used instead of Cu, so to dope the Ag samples the CBD method was used as described on the previous page with one adjustment: the samples were doped for 2, 2.5 or 3 min. instead of 1 min. The samples were immersed longer to increase the S content of the samples. It was found out that the best reduction potential was -1.0 V vs RHE, the amount of time the sample was electrochemically reduced varied for the different samples. Because the samples were immersed for different amounts of time and the temperature of the acetonitrile + S_8 solutions also varied different over time for each sample therefore the S content also fluctuated. With EDX the initial S content of one sample was determined the sample was then reduced at -1.0 V vs RHE, the reduction was stopped when the linear voltammogram stabilized and thus all the S in the sample was reduced (i.e. leached out of the Ag). The loss of all the S was confirmed by EDX and by analysing the linear voltammograms and the speed of loss of S during reduction at -1.0 V vs RHE was roughly determined. So for every different sample first the initial S content was measured, with EDX, and then the amount of that was needed to reduce the S content to ~2 at% was estimated. After pre-reduction the samples were rinsed wit Milli-Q water and blown dry with N_2. The pre-reduction experiments were conducted in a fume hood, because when the high S content samples were pre-reduced H_2S was being formed. Examples of a pre-reduced sample and the intermediate steps are shown in Figure 18.

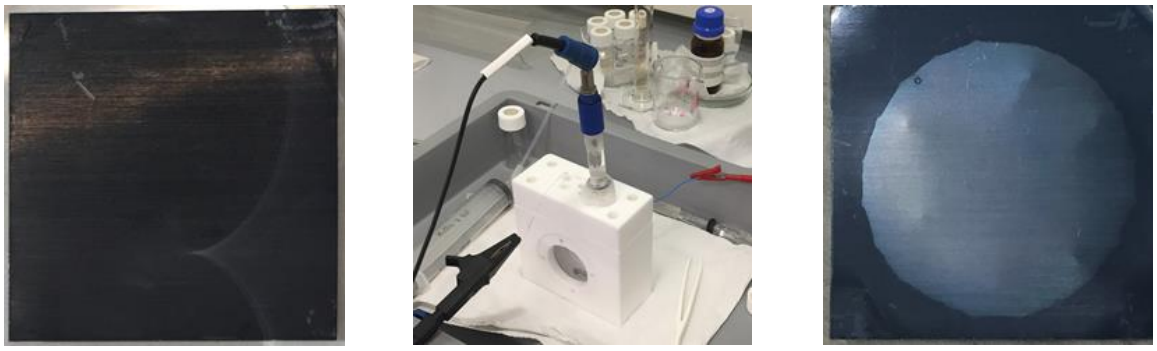

Figure 18: Steps of producing S-doped samples via pre-reducing. A) Example of a sample after CBD for 2-3 minutes. B) Pre-reducing at -1.0 V vs RHE. C) Example of sample produced by pre-reducing.

3.2 Electrochemical Cells

3.2.1 Poly (methyl methacrylate) (PMMA) cell

All the cyclic voltammetry (CV) and gas chromatography (GC) experiments were conducted in a two compartment three electrode setup where the two compartments were separated by a Nafion^{TM} (ION Power) proton exchange membrane. The cell was made from poly (methyl methacrylate) (PMMA) and can be seen in Figure 19. In the cathodic compartment of the cell the following elements were present: First the working electrode, the catalyst for CO_2RR, in this case Ag or S-doped Ag, with a diameter of 1.6 cm and a surface area of 2.0114 cm^2. Second the reference electrode which was an Ag/AgCl reference system (Radiometer Analytical XR300 filled with sat. AgCl). Third, a Teflon coated stirring flea was added which was stirred at a rate of 1000 rpm. There was one gas stream going into the cathodic compartment, that could be used to purge CO_2 and another gas stream exited the compartment at the top towards the GC. Furthermore the compartment was completely sealed off from the air so only products formed on the surface of the electrode or that were added were measured in the GC. During measurement both compartments were purged with CO_2 (The Linde Group) at a rate of 15 mL/min. The pressure and temperature were at ambient conditions. The anodic compartment of the cell consisted of a Pt electrode with a larger surface area than the working electrode so the flow of current was not restricted. And again there was an inlet for a gas stream and an outlet for a gas stream towards the atmosphere.

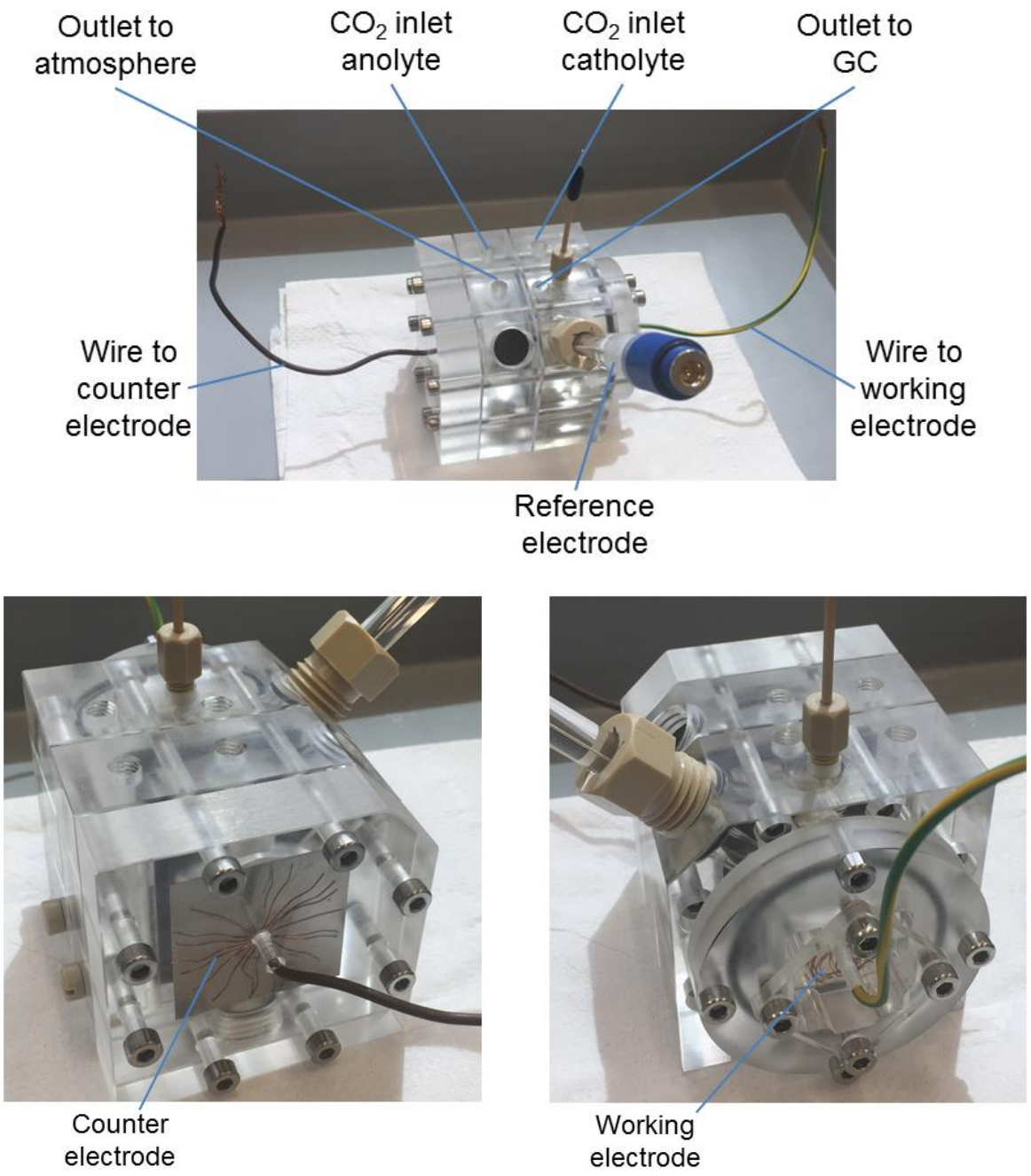

Figure 19: Pictures with descriptions from the PMMA cell.

3.2.2 Teflon cell

Electrochemical Surface Area (ECSA) measurements and the pre-reduction were conducted in a Teflon cell that has a setup of a three electrode beaker type cell i.e. all of the electrodes are in the same space. The working electrode was the sample that had to be pre-reduced or an ECSA was conducted. The reference electrode was an Ag/AgCl reference system (Radiometer Analytical XR300 filled with sat. AgCl) and the counter electrode was a coiled Pt wire. The resistance of the electrolyte between the reference electrode and the working electrode was determined with electrochemical impedance spectroscopy. An image of the Teflon cell can be seen in Figure 20.

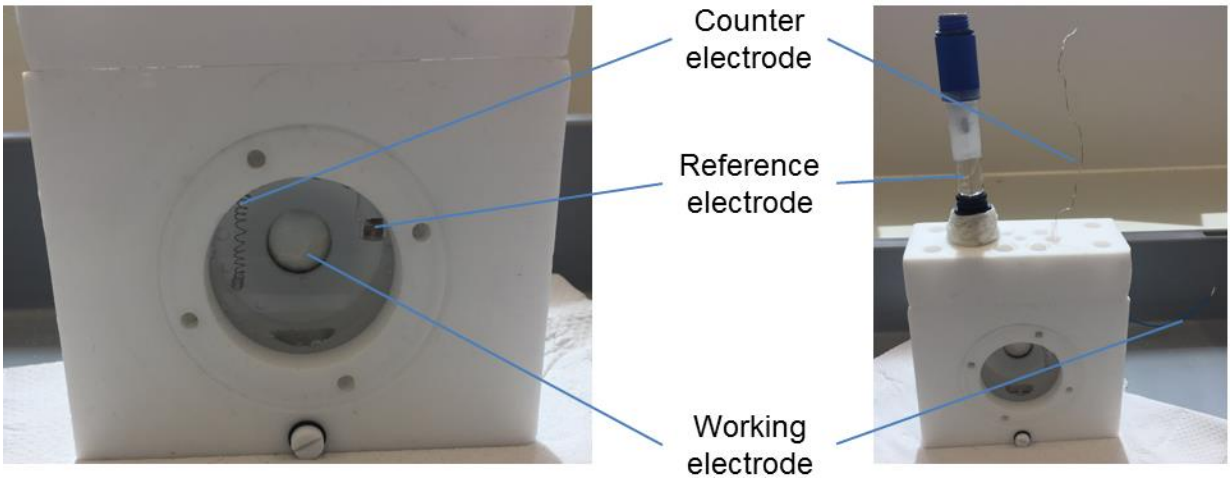

Figure 20: Teflon cell with all it components

3.3 Operation and Characterization

3.3.1 Scanning Electron Microscopy (SEM) and Energy-dispersive X-ray spectroscopy (EDX)

Scanning Electron Microscopy (SEM) is used to give a 'visual' representation of the sample that is observed and Energy-dispersive X-ray spectroscopy (EDX) to give a chemical overview of the elements that are present in the sample. An electron gun with a W filament creates an electron bundle, this bundle is then accelerated by a ring anode towards the sample. A series of magnetic lenses, called condenser lenses, focus this electron bundle onto the sample. When the high-energy electrons come into contact with the surface of the sample secondary electrons are released from the sample. The electron bundle is scanned over the sample and for every point of the sample the secondary electrons are detected and are magnified giving an image of the sample, this is called Second Electron Imaging (SEI).

Besides the secondary electrons also backscatter electrons are generated, these are the electrons that are reflected from the surface and also from deeper parts of the sample.[49] This characterization method is based upon the detection of electrons that are either reflected or released by the surface of the sample. X-rays that are released by interaction between high-energy electrons and the atoms of the sample can also be detected, this is called Energy-dispersive X-ray spectroscopy (EDX). If an electron from an inner shell of a sample atom is removed from its place by an electron of the electron bundle an outer shell electron will move to this place to restore the energy balance. This atom is now however in an ionized state, to return to the ground state a characteristic X-ray is released. These characteristic X-rays are detected and in this way the chemical composition of the sample can be determined.[49]

In this thesis a JEOL-6010LA is used: SEI will be used to give high-resolution images of the surface of the sample and in what way the surface is changed by doping or after operation. EDX will be used to determine the S content in the samples before and after use.

3.3.2 X-ray Diffraction (XRD)

X-ray Diffraction (XRD) is the based upon on the phenomenon that crystalline materials will deflect X-rays in a consistent manner. An X-ray source causes an incident beam of X-rays this incident beam is reflected by the sample onto a detector, the so-called diffractive X-rays. This is done while continuously changing the angle between the incoming X-rays and the sample but by keeping the angle of the incident X-rays, Θ, and the angle of the diffractive X-rays 2Θ. The diffraction of X-rays is a form of elastic scattering so the wavelength stays the same. X-rays will deflect by the atoms that are present and the lattice spacing between the different planes in the crystal structure. Because of destructive and constructive interference a diffraction pattern is formed. From this diffraction pattern a graph is made that shows the intensity distribution of reflectance for every 2Θ angle. This distribution can then be used to qualitatively characterize the structure of the sample.[50] In this thesis a Bruker D8 Advance is used with a Co X-ray source, it will be used to determine the phases and the difference between the different samples and also the effect of doping and use in the cell. The settings

that were used are: divergent slit 0.3; scan speed 0.2 s/step; increment 0.02; start 25˚; end 100˚. For the identification of the peaks the JCPDS No. 14-0072 file was used.

3.3.3 Grazing incidence X-ray Diffraction

Grazing incidence X-ray Diffraction is just as XRD a technique that uses X-rays to characterize materials. The difference between XRD and GIXD is the geometry of the X-ray tube and the detector. In XRD the X-ray tube and detector move simultaneously in such a way that the angle between the incident X-rays and the angle of the diffractive X-rays is always 2Θ. With GIXD the angle of incidence is fixed and small $\alpha < 5°$ and the detector moves around the sample. The advantages of this technique are that with GIXD because the angle of incidence is fixed and the detector moves also facets with a different orientation can be measured. The second advantage is that because of the low angle of incidence the penetration depth is limited and only the top of the sample is examined.[51] In this thesis a Bruker Discover is used with a Cu X-ray source. It is used because it focuses more on the top of the sample instead of the bulk and it thereby takes also facets with different orientations in regard. The settings that were used are: Incidence angle, α, 3˚; divergent slit 0.6; scan speed 0.4 s/step; increment 0.02; start 20˚; end 116.5˚. For the identification of the peaks the PDF 65-2871 file was used.

3.3.4 Cyclic Voltammetry (CV)

Cyclic Voltammetry (CV) is an electrochemical method to determine electrochemical properties of an electrode. In CV the potential is first ramped down to a certain potential when this potential is reached the potential is ramped up again to the initial value where the cycle began. The output is a current which resembles the activity that takes place at the surface of the electrode. The ramping up and down of the potential shows the reductive and oxidative reactions on the electrode. These cycles can be repeated multiple times to get understanding of the stability of the electrode.[52] CV in this thesis is used to determine at which potential the working electrode is most active and it also gives insight in the stability of the electrode. A PARSTAT 4000A Potentiostat Galvanostat and a PARSTAT MC Multichannel potentiostat both from Princeton Applied Research where used for these experiments. The settings that were used are: Initial potential 0.0 V vs RHE; Vertex potential -1.4 V vs RHE; Final potential 0.0 V vs RHE; Scan rate 0.02 V/s.

3.3.5 Gas Chromatography (GC)

Gas Chromatography (GC) is a qualitative and quantitative method to determine what products are being formed and in what quantities under operation of the cell. Every three minutes a gaseous sample is taken from the overhead compartment of the cathodic part of the cell. This sample is lead through a column, a carrier gas (the mobile phase) is added to transfer the gas through the column and towards the detector. The carrier gas usually consists of H_2 and/or He. The column of the GC consists of the mobile phase and the stationary phase, the mobile phase flows through the column and the stationary phase is situated on the wall of the column. When a sample consisting of multiple gases flows through the column, the separate molecules will interact differently with the stationary phase and the

mobile phase. So the different components of the sample will stay for different amounts of time in the column until they reach the detector, this is called the retention time and this is the value upon which the distinction of the different components is made.[53] The output of the GC is a chromatogram in which the different peaks represent the different components of the analysed gaseous sample, by integrating the area beneath the peaks the amount of a certain component can be calculated. In this thesis the GC is used to specify what gases are formed in operation of the cell and at what amounts these components are formed, a CompactGC$^{4.0}$ from Global Analysis Solutions was used.

The electrolyte used was 0.05 M K_2CO_3 (Sigma-Aldrich) this was purged overnight with CO_2, at a rate of 12.4 SCCM, by doing this the 0.05 M K_2CO_3 was converted to 0.1 M $KHCO_3$ with a pH of 6.8. This electrolyte was used for GC measurements, pre-reduction and CV measurements.

Before the cell was loaded with a new sample the compartments were thoroughly rinsed three times with Milli-Q water and when the new sample was loaded it was rinsed once more to remove any pollution that could be on the surface of the electrode. When loaded with the electrode and rinsed with Milli-Q water both compartments were filled with 14 mL of electrolyte and placed upon a magnetic stirrer (RSM-10-B, Phoenix Instrument). The cell was connected to a stream of CO_2 (The Linde Group) through a mass flow controller (EL-FLOW, Bronkhorst) this mass flow controller was not very accurate therefore it was verified with a flowmeter (ProFLOW 6000, Restek) and adjusted with the mass flow controller until a flow of 15 mL/min was reached. To enable that the overhead compartment in the both the cathodic and anodic part of the cell was saturated with CO_2 the flow of CO_2 through the cell was started at least 10 minutes before performing the GC measurements. Every 3 min. the GC was injected with a sample from the cathodic side of the cell for a total operation time of 60 min.

A potentiostat (PARSTAT 4000A, Princeton Applied Research) supplied the working electrode with the needed overpotential. Before an overpotential was applied the iR compensation between the reference electrode and the working electrode was determined. The samples were tested at the following overpotentials: -0.4, -0.55, -0.7 and -0.8 V vs RHE.

The current density is calculated with the help Equation 13 and the FE with Equation 14 where J_i and FE_i are the respectively current density and faradaic efficiency of a certain product. J_{real} is the real current measured divided by the area of the sample. The parameters used in these formulas are as following. Flow of CO_2, Q, was 15 mL/min which equals $2.5 \cdot 10^{-7}$ m^3/s. The amount of electrons transferred, n, is 2 for CO. Faraday constant, F, is 96485 A·s/mole. Gas constant, R, is 8.314 $m^3 \cdot Pa/K \cdot mole$. Pressure, p, was 101000 Pa. Temperature, T, 298 K. The surface area of the sample with a diameter of 1.6 cm was 2.0114 cm^2.

$$J_i = \frac{1000 \cdot ppm \cdot Q \cdot n \cdot F \cdot p_0}{R \cdot T \cdot A}$$ **Equation 13**

$$FE_i = \frac{J_i}{J_{real}}$$ **Equation 14**

3.3.6 Electrochemical Surface Area measurement (ECSA)

Electrochemical Surface Area Measurement (ECSA) is performed to get insight in the active surface area of the working electrode. Since the surface of the Ag and S-doped Ag electrodes is not perfectly flat and is different for every sample and production method a characterization technique is needed to determine the active surface area. This is done through ECSA, the sample that is used for GC measurements is loaded in a Teflon beaker type three-electrode cell, with an Ag/AgCl reference electrode and a Pt wire counter electrode. First the sample is reduced at -0.4 V vs RHE for 10 minutes in 30 mL 0.1 M KOH (Sigma-Aldrich) electrolyte, which was purged with N_2 until saturated with a pH of 12.6. Next the electrodes were oxidized at 1.15 V vs RHE (without changing the electrolyte), which formed a monolayer of oxide on the surface either Ag_2O or AgOH that corresponds to a charge of about 400 $\mu C\ cm^{-2}$. The amount of electrons that are passed through during the oxidation process are a measure of the surface area. By comparing this amount for every sample a relative surface area can be determined.[54–56]

4 Results

In this chapter the results of the experimental part of this thesis are discussed. First the motivation for choosing the doping methods is treated. Secondly the SEM images and EDX measurements are discussed. Subsequently the XRD and Cyclic voltammetry part is explained. Finally the gas chromatography measurement and electrochemical surface area measurements are presented.

4.1 Doping methods

Two methods were used to dope the Blanco Ag samples with S. Both of the methods start with by immersing a cleaned Blanco Ag sample in a solution of acetonitrile and S_8 as described in the experimental section. This method was described by Liu *et al.*[47] in this article TiO_2 nanotube arrays sensitized with Ag_2S were used for photocatalytic H_2 generation. This method was used because of its simplicity, the absence of dangerous components and its scalability. For the next phase of doping two different methods were tried, the anneal treatment and pre-reduction. Anneal treatment was used to spread the S atoms more evenly over the Ag sample and reduce the internal stresses of the crystal lattice.

The other treatment after the CBD, pre-reduction, was described by Huang *et al.*[21] In this research Cu_2O-derived Cu catalyst doped with S by immersing Cu in to an ammonium polysulfide solution. The S-doped Cu showed a very high selectivity towards formate where a S content of 2.7 at% showed the highest current density for formate. Although Cu was used instead of Ag, the prior immersion technique used and the final S content in the Cu gave reason to try this with Ag.

4.2 SEM and EDX

To observe the surface of the samples and to see if there is a morphological change occurring because of the doping with S SEM is used. Next to SEM also EDX is performed to quantify the S content of the annealed samples before operation in GC and afterwards to check the stability of the sample. First a Blanco Ag sample will be examined followed by an annealed sample and finally a pre-reduced sample is investigated. All measurements were conducted with a JEOL-6010LA.

4.2.1 Blanco Ag

In Figure 21 the SEM images of a Blanco Ag sample are shown. The Blanco Ag samples were not polished to smoothen the surface or grinded to increase the roughness. The surface of the Blanco Ag is ridged, this due to the production method of the Ag foil.

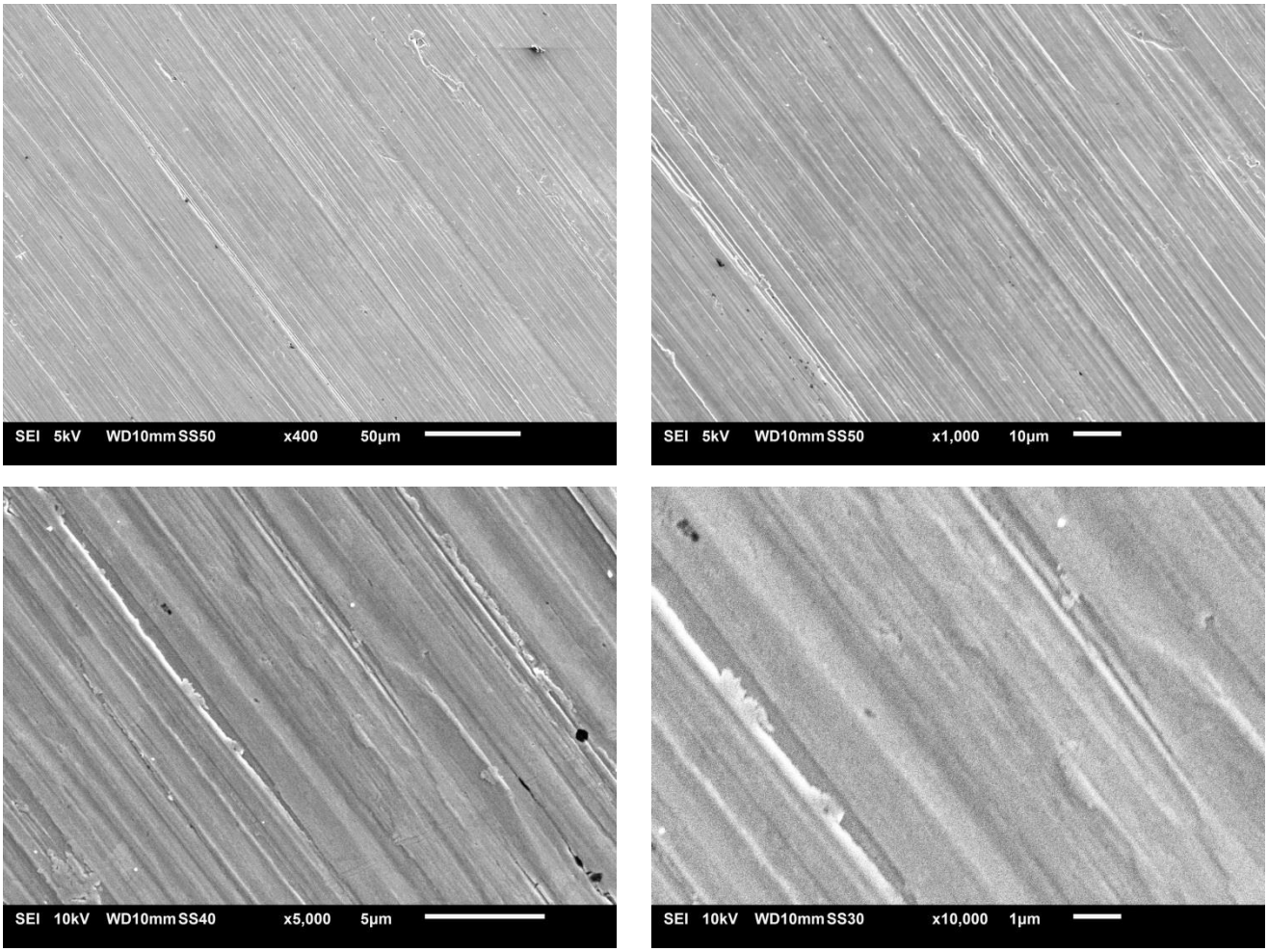

Figure 21: SEM images of a Blanco Ag sample. Magnification starting upper left clockwise: 400x, 1000x, 5000x and 10000x

4.2.2 Annealed samples

In Figure 22 SEM images of an annealed sample before testing it in an electrochemical cell is shown. The doping step and annealing step change the surface morphology. There are now cavities present and also is the surface more battered than in the Blanco Ag sample. The S content of this sample is 5.41 at% and was determined by EDX. In Table 4 in the Appendices there is an overview with all samples used in this thesis with the S, Ag and C content for three points of the sample and the average amount.

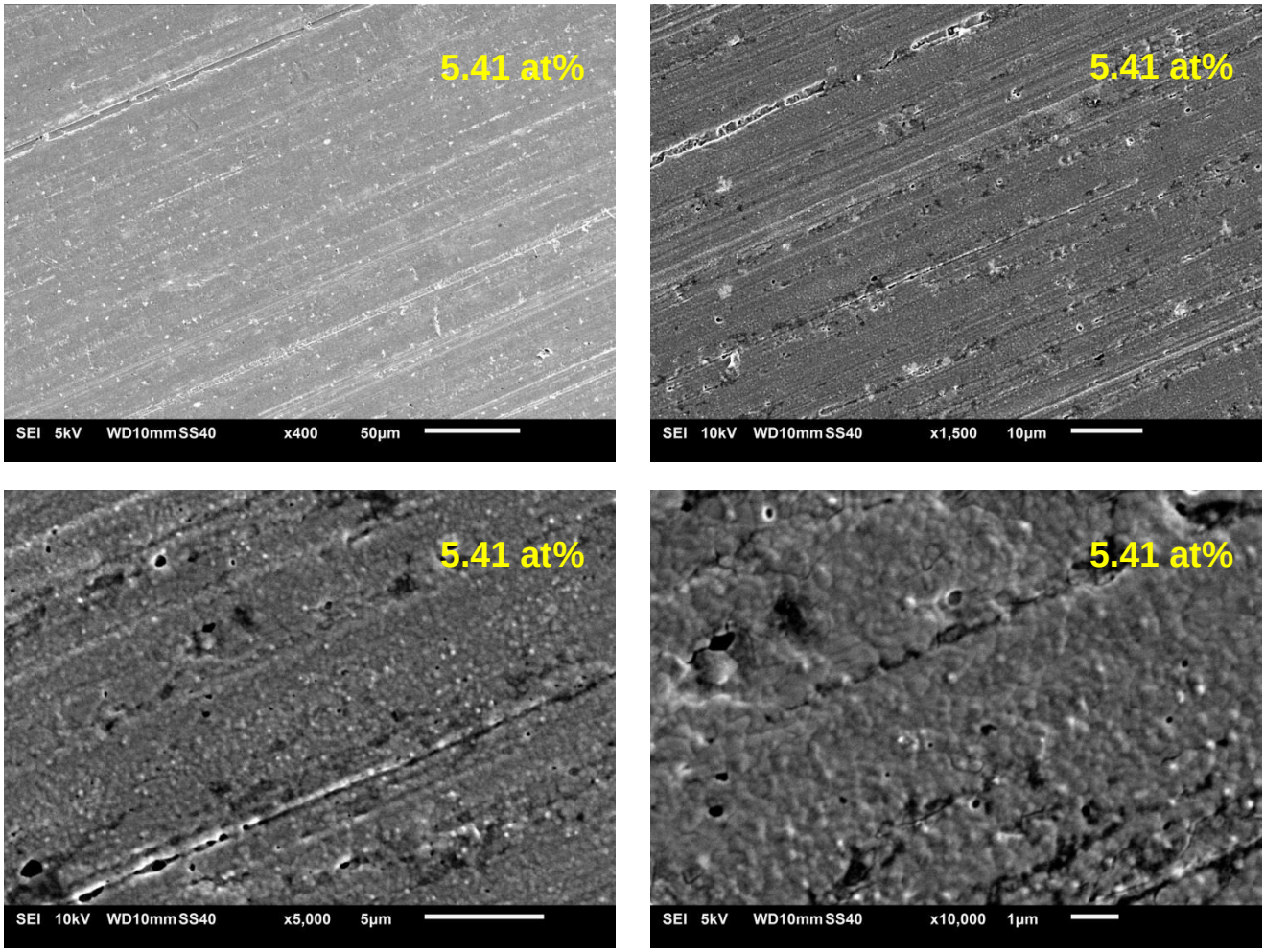

Figure 22: SEM images of annealed sample with a S content of 5.41 at%. Magnification starting upper left clockwise: 400x, 1500x, 5000x and 10000x. The yellow percentage in the picture represents the atomic S content.

The amount of S at the top layer of the sample is probably higher than that measured with EDX. Since the S diffused from the acetonitrile + S_8 solution through the surface that was in contact with this solution towards the centre of the sample. Therefore the amount of S in the top layer is probably higher than in the centre of the sample. During the anneal treatment the S was more evenly spread over the sample but it is plausible that the content of S near the surface of the sample was still higher. Due to the material and measuring parameters the penetration depth of the electrons used in EDX is roughly 1.2 µm, this is explained in more detail in Figure 52 in the Appendices.

So when the amount of S is determined this is done for a large amount of the sample instead of just the top layer that is active in CO_2RR, and thus is the amount of S on the top probably higher.

Figure 23 shows the same sample as in Figure 22 only now after testing in an electrochemical cell at -0.7 V vs RHE. The surface looks more irregular almost as if the surface has been etched. To learn more about the stability of the sample after use in an electrochemical cell EDX was performed. The EDX results revealed that all of the S was lost during testing in an electrochemical cell.

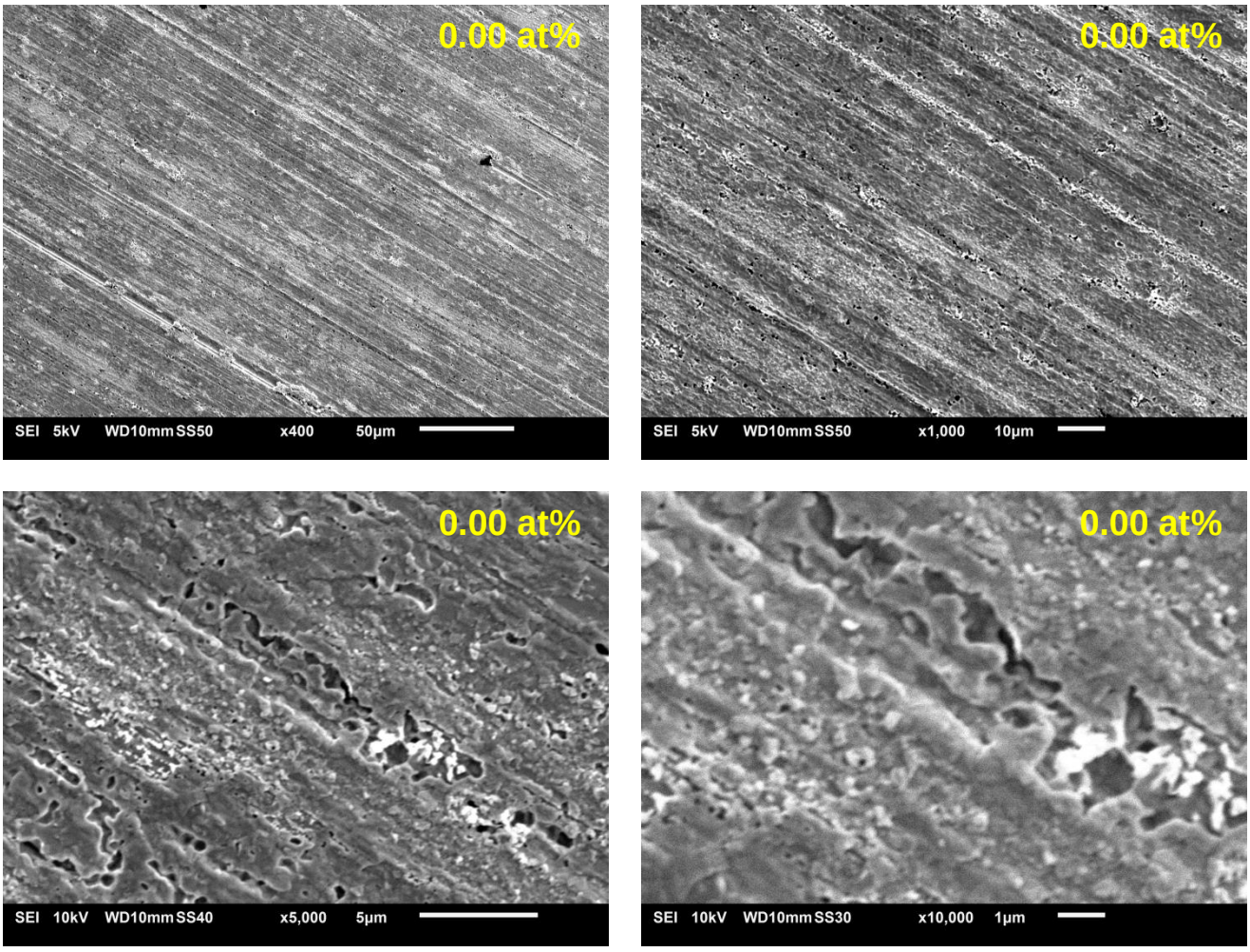

Figure 23: Annealed sample after testing in GC at -0.7 V vs RHE. Magnification starting upper left clockwise: 400x, 1000x, 5000x and 10000x. The yellow percentage in the picture represents the atomic S content.

4.2.3 Pre-reduction

The production of the pre-reduced samples consisted of two parts: first the chemical bath deposition step where the samples were immersed for a longer period so the S content would reach a high value. The second step was a pre-reduction step in which a large part of the S was leached out of the sample till the S content was only a few at% and was ready for use in GC experiments. In Figure 24 the samples just after CBD are shown. From these pictures in Figure 24 clearly Ag_2S crystals are visible.

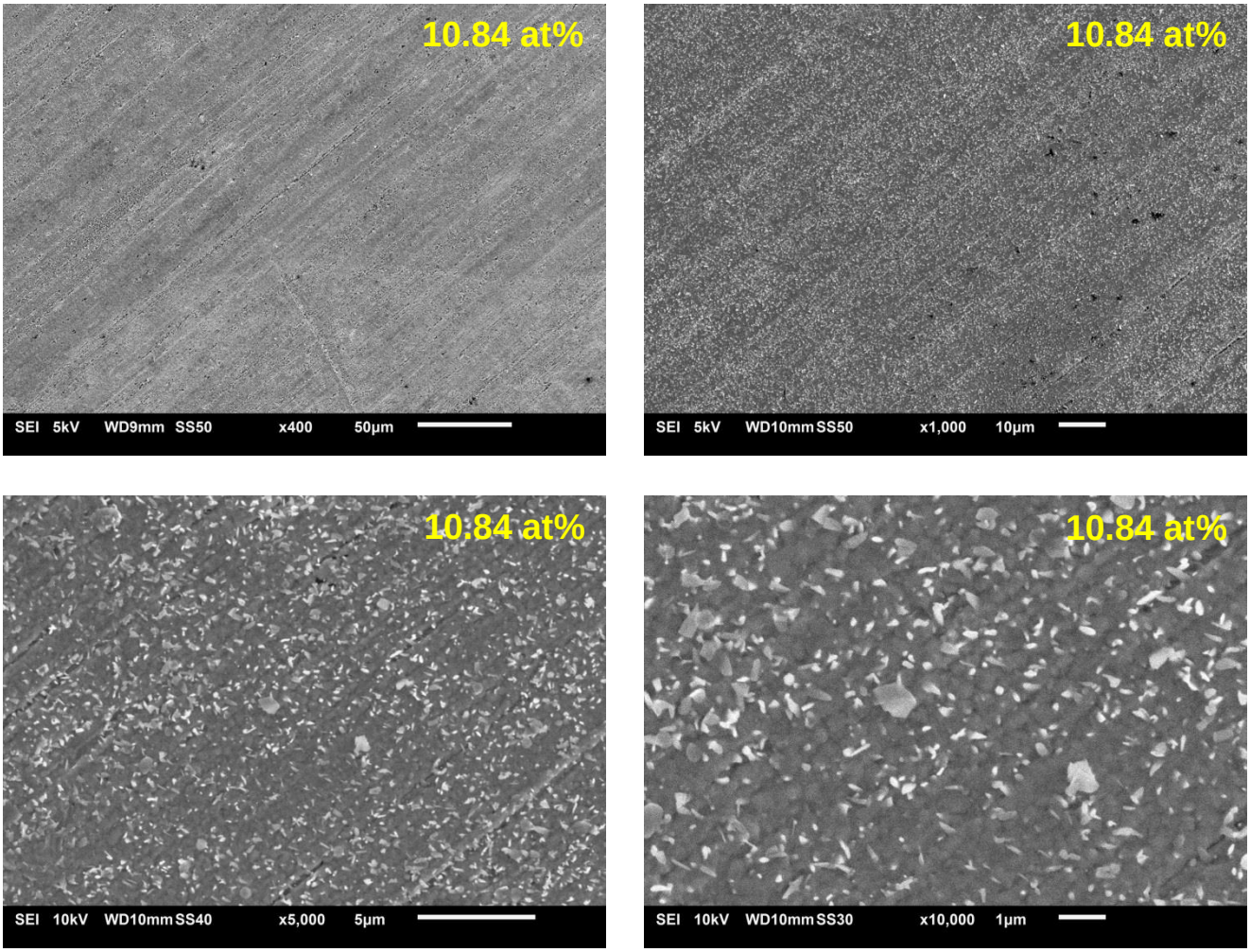

Figure 24: Pre-reduced after CBD, Magnification starting upper left clockwise: 400x, 1000x, 5000x and 10000x. The yellow percentage in the picture represents the atomic S content.

Figure 25 is the sample of Figure 24 but then after pre-reduction for 8 seconds at a potential of -1.0 V vs RHE. The sample after pre-reduction looks very similar to the annealed sample after GC operation. This result was expected because the sample is reduced therefore a similar reaction take place at the surface of the catalyst.

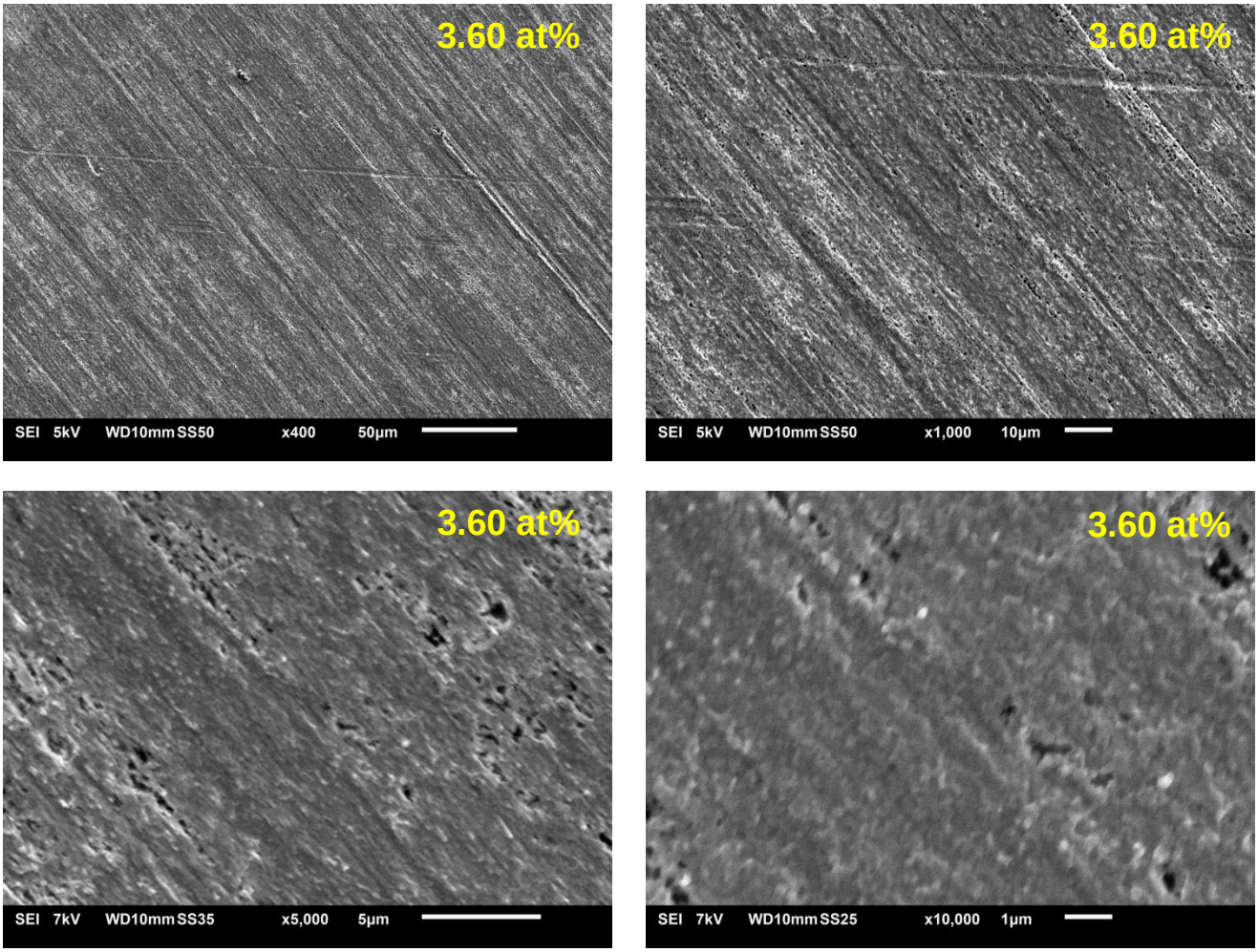

Figure 25: Pre-reduced sample after pre-reduction: Magnification starting upper left clockwise: 400x, 1000x, 5000x and 10000x. The yellow percentage in the picture represents the atomic S content.

Figure 26 is the same sample as in Figure 24 and Figure 25 after being used in GC operation for 1 hour at -0.7 V vs RHE. From the three different kinds of samples (Blanco Ag, annealed and pre-reduced) is the pre-reduced sample the one with the roughest surface. It is much more 'etched' than the annealed sample after use in the GC. A possible explanation would be that the S content initially was 10.84 at% and after two times reducing it declined until finally no S was left in the sample. This means that a large amount of the phases that were present at the surface of this sample were actually Ag_2S. So when all the S was leached out, i.e. 10.84 % of the atoms that make up the structure are lost, which leads to formation of cavities. Also when it is realised that the EDX electron beam penetrates the material approximately 1.2 µm, therefore the S content closer to the surface is probably higher, it is reasonable to say that this the reason for the rough and with cavities covered surface.

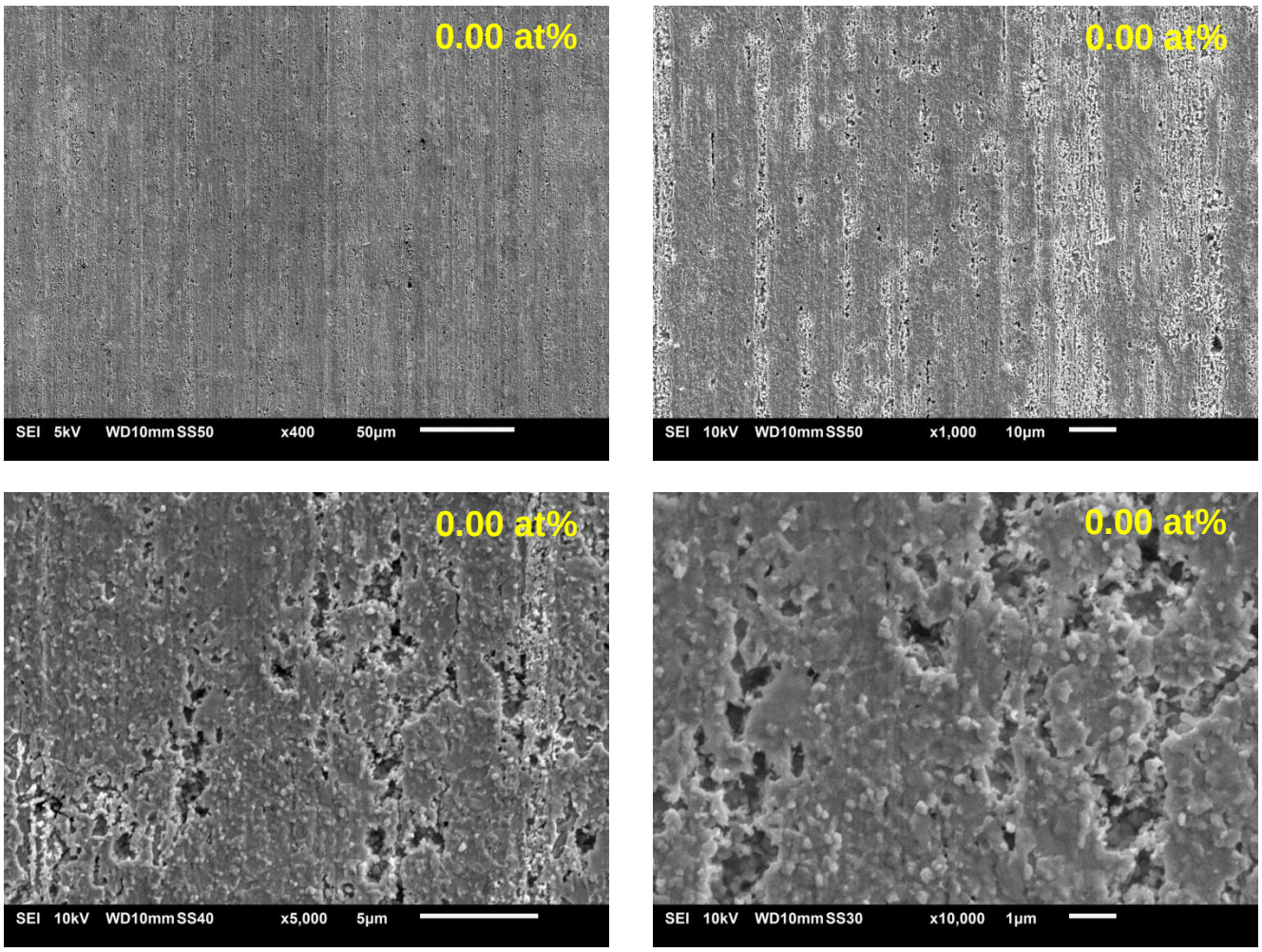

Figure 26: Pre-reduced sample after operation in GC. Magnification starting upper left clockwise: 400x, 1000x, 5000x and 10000x. The yellow percentage in the picture represents the atomic S content.

If the 10,000 times magnified image of a pre-reduced sample in Figure 26 is compared with the at the same magnification of an annealed sample in Figure 23 and that of a Blanco Ag sample in Figure 21 it is expected that the electrochemical surface of the pre-reduced sample is the largest followed by the annealed sample and then the Blanco Ag sample.

4.2.4 Conclusions SEM and EDX

From the SEM and EDX results the most important conclusions are that the addition of S to polycrystalline Ag affects the surface morphology. There is also a big difference between the surface before use in a electrochemical cell and afterwards. The produced S-doped Ag catalysts are not very stable, because at al potentials all of the S is lost after GC operation in an electrochemical cell. The amount of S that is measured by EDX is not necessarily the amount of S that is present at the surface of the catalyst. Since EDX measures deeper (Figure 52, Appendices) than the surface and the S content is expected to be higher at the surface than deeper in the sample, probably the S content at the surface is higher. In Table 4 in the Appendices there is an overview of all the samples that were used in this thesis. In this table for each sample the code, type, testing and all of the EDX results are summarized.

4.3 XRD

To get more insight in the structural properties of the material of the catalyst XRD measurements were conducted. The XRD measurements were all performed on a Bruker D8 advance X-ray Powder Diffractometer with a Co X-ray diffraction source. For the identification of the peaks JCPDS No. 14-0072 was used that resembles monoclinic α-Ag_2S (acanthite) phase of Ag_2S.

First the pre-reduced samples will be treated, because of a high S content in these samples the Ag_2S peaks will be best visible and this will help to identify the smaller Ag_2S peaks of the other samples with a lower S content. Next the -0.7 V vs RHE sample series after use in the electrochemical cell will be presented. On this same series also GIXD measurements are performed. Finally the stability of an annealed sample will be discussed.

Because of the nature of the samples, 0.125 mm pure Ag films, the samples were very easily bended. Especially after use in the electrochemical cell the samples were deformed because to ensure the cell was airtight the screws had to be tightened. As a consequence of the deformation of the samples it was not possible to compare the samples on a potential peak shift since this peak shift could also be the result of the bending the sample.

4.3.1 Pre-reduced samples

The effect of longer immersion time on the structure of the Ag sample can be seen in Figure 27 these long S-doped samples resemble the pre-reduced samples. From Figure 27 it is clearly visible that next to the metallic Ag peaks (marked with ●) a lot of α-Ag_2S peaks can be distinguished, however not very dominantly compared to the metallic Ag peaks. As the S content increases in the samples the Ag_2S peaks increase in intensity, this is seen in Figure 27 in the 2θ region from 25˚ to 40˚. Since the amount of S changes after every production and operation step apart from the colouring the pre-reduced samples also have a code which can be found in the legend of the graphs.

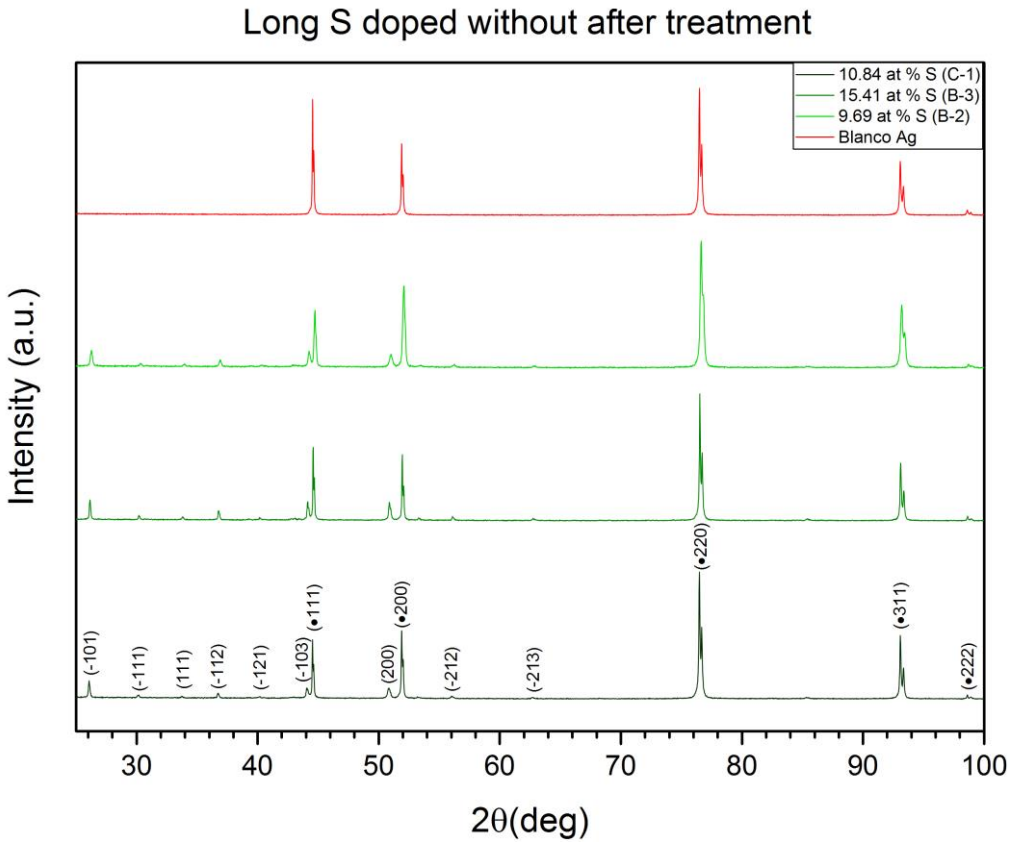

Figure 27: XRD patterns for the samples that were doped for an increased amount of time before being pre-reduced. Peaks marked with ● represent reflections of Ag metal. To prevent confusion the different graphs have been coded.

After the samples were pre-reduced a large amount of the S in each sample was lost. This is also confirmed by the X-ray diffraction pattern where almost all reflections of Ag_2S are lost for all three samples. One sample was pre-reduced for too long which, resulted in a final S content of 0.00 at%, the XRD pattern of this sample is then again similar to a Blanco Ag sample. The metallic peaks of the pre-reduced samples with a S content of 4.00 at% and the one with 0.00% have not changed during the pre-reducing step. Of these two samples only the Ag_2S peaks have disappeared from the pattern, and the reflection pattern more resembles the one of the Blanco Ag. The XRD pattern of the sample that contained a S content of 3.60 at% did change the (●111) peak has become more intense while the (●200) has decreased in intensity. And it is the only sample that still has some characteristic Ag_2S peaks is the sample that contained a S content of 3.60 at% these peaks are: (-101), (200).

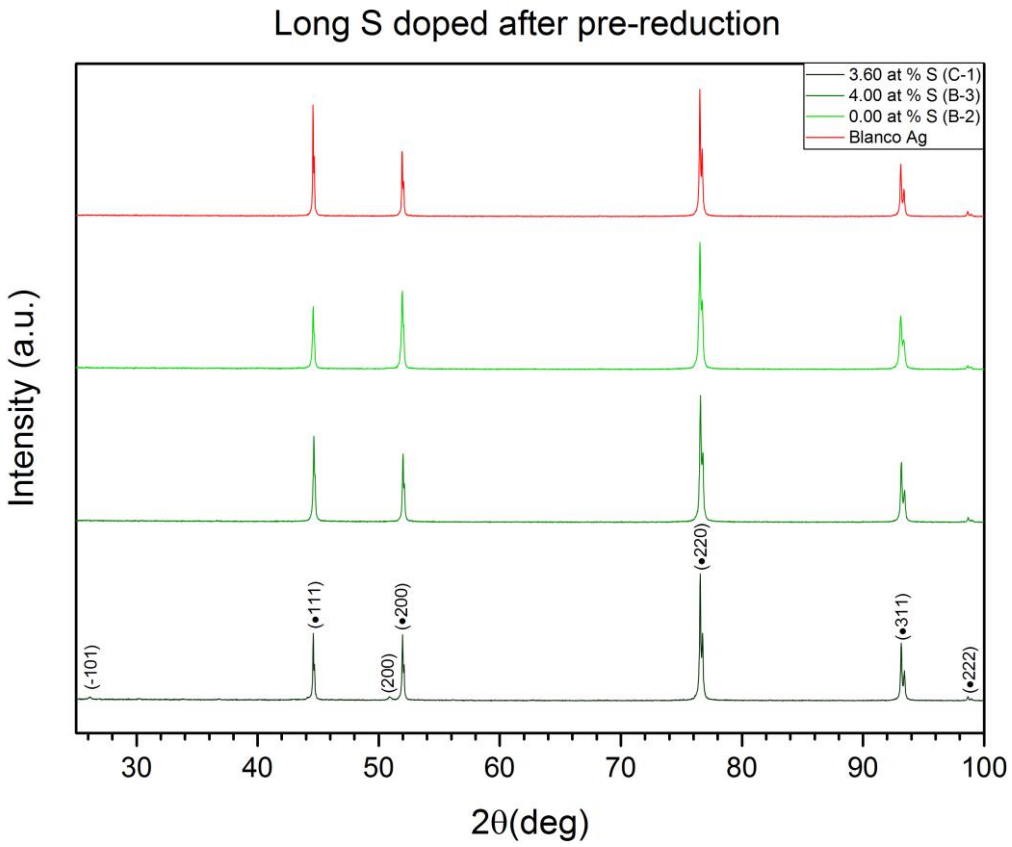

Figure 28: XRD patterns long S-doped samples after pre-reduction. Peaks marked with ● represent reflections of Ag metal. To prevent confusion the different graphs have been coded.

The XRD patterns of the samples after being used in the GC (Figure 29) are similar to the ones after the pre-reduction step. The (-101) and (200) peak that were present in the pre-reduced sample with a S content of 3.60 at% in Figure 28 were lost after GC operation as can be seen in Figure 29.

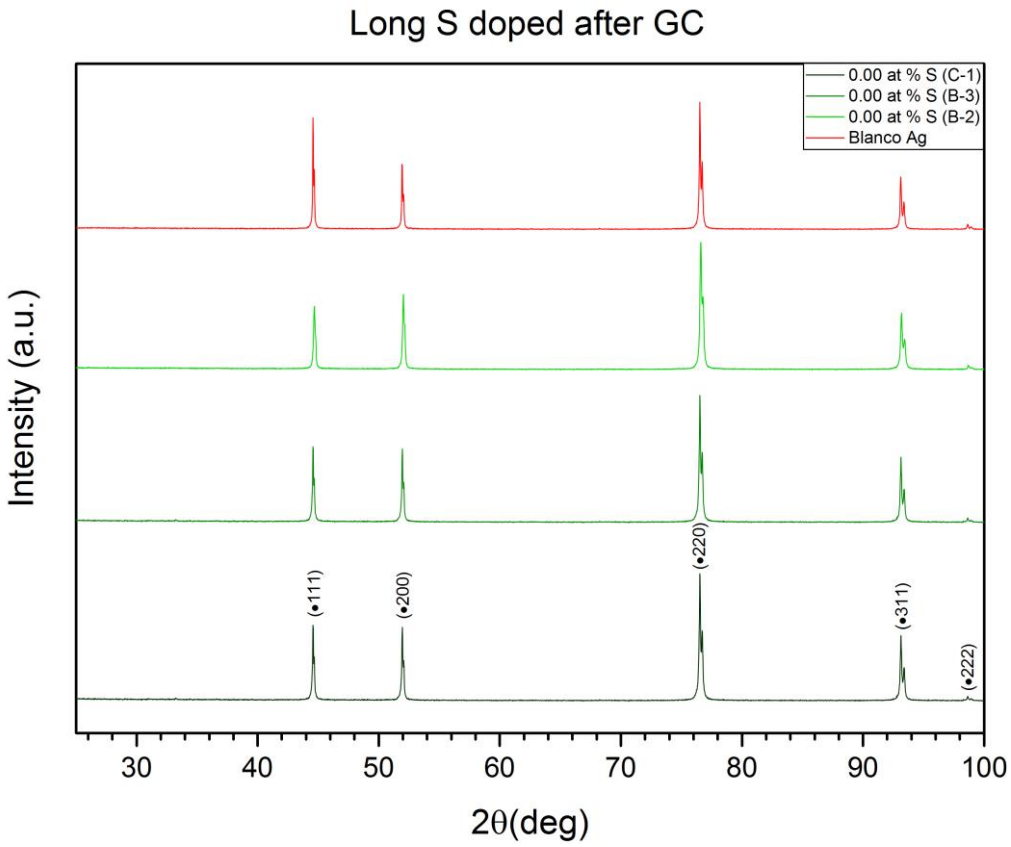

Figure 29: XRD patterns long S-doped samples after operation in GC. Peaks marked with ● represent reflections of Ag metal. To prevent confusion the different graphs have been coded.

From these pre-reduced samples it can be seen what the effect is on the structure of the sample when S is added in large quantities. After a sample is used in the CO_2RR the S content is however lost and therefore most of the peaks shown in Figure 27 will not be visible.

4.3.2 Comparison different samples

In Figure 30 different samples (e.g. Blanco Ag, annealed sample and a pre-reduced sample) are compared that were all tested at an overpotential of -0.7 V vs RHE. These patterns show that the changes between the different samples are very small. The proportion of the intensity of the peaks among the different samples is more or less the same. From Figure 30 it is noted that in all samples the (●220) peak is most intense and then followed by the (●111) peak.

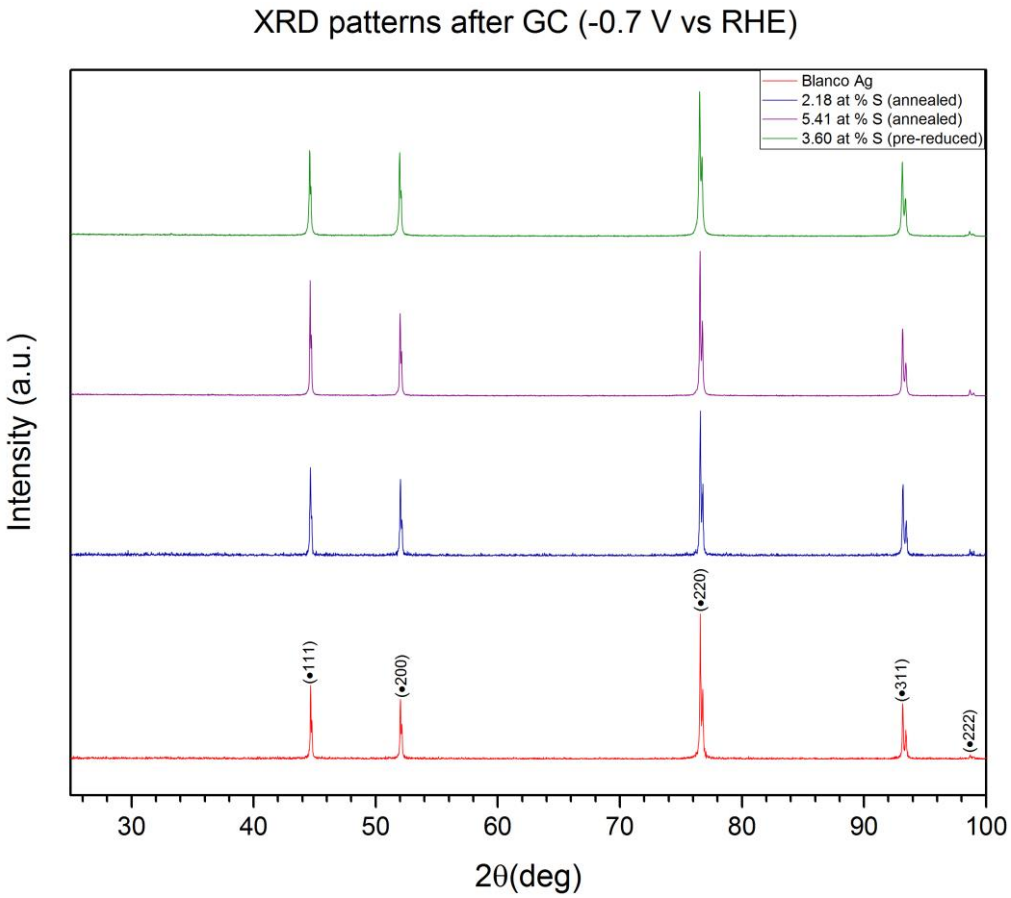

Figure 30: XRD patterns after GC operation at -0.7 V vs RHE. Peaks marked with ● represent reflections of Ag metal.

The XRD patterns of the samples tested at potentials (-0.4; -0.55 and -0.8 V vs RHE) are similar to those of the samples that are tested in Figure 30 and can be found in the appendix in respectively Figure 53, Figure 54 and Figure 55.

Since XRD is a bulk technique the X-rays focus on the deeper parts of a sample. The CO_2RR however happens on the surface of the sample, therefore the XRD results miss some information about the structure of the sample just beneath the surface. Because XRD focusses on the bulk the patterns of the XRD measurements are almost the same since the bulk is less affected by doping and GC operation. So to overcome this problem Grazing Incidence X-Ray Diffraction (GIXD) measurements were performed.

4.3.3 GIXD

GIXD focuses more on the structure just beneath the surface, as explained in the experimental section. Maybe by looking at the structure just beneath the surface we can get more insight in the differences between the samples.

The GIXD measurements were only conducted for the samples that were tested at -0.7 V vs RHE because in this set there was a clear difference seen in the S content, doping method and the performance of the samples. For the identification of the peaks the JCPDS No. 65-2871 file was used, this resembles an Ag structure. The X-ray source used in the GIXD measurements is Cu therefore the same reflections are at a different 2θ angle than the XRD a pattern which has a Co X-ray source. In Figure 31 the GIXD patterns are shown for the four different samples in the -0.7 V vs RHE set. The samples that were annealed show different characteristics if compared with the Blanco Ag or the pre-reduced sample. In the doped and annealed sample the (●111) peak is more prominent than the (●200) peak. In the 2θ range from 60° until 116.7° the (●311) peak is dominant while the other peaks are small and similar in size. The Blanco Ag and pre-reduced sample on the other hand have patterns that are very alike. The (●200) peak is more intense than the (●111) peak contrariwise in comparison with the annealed samples. At higher 2θ values the (●220), (●311) and (●222) peak are more or less the same size. The (●400) is in all the samples of this set very small and the (●331) and (●420) peak are more intense in the Blanco Ag and pre-reduced samples with respect to the two annealed samples.

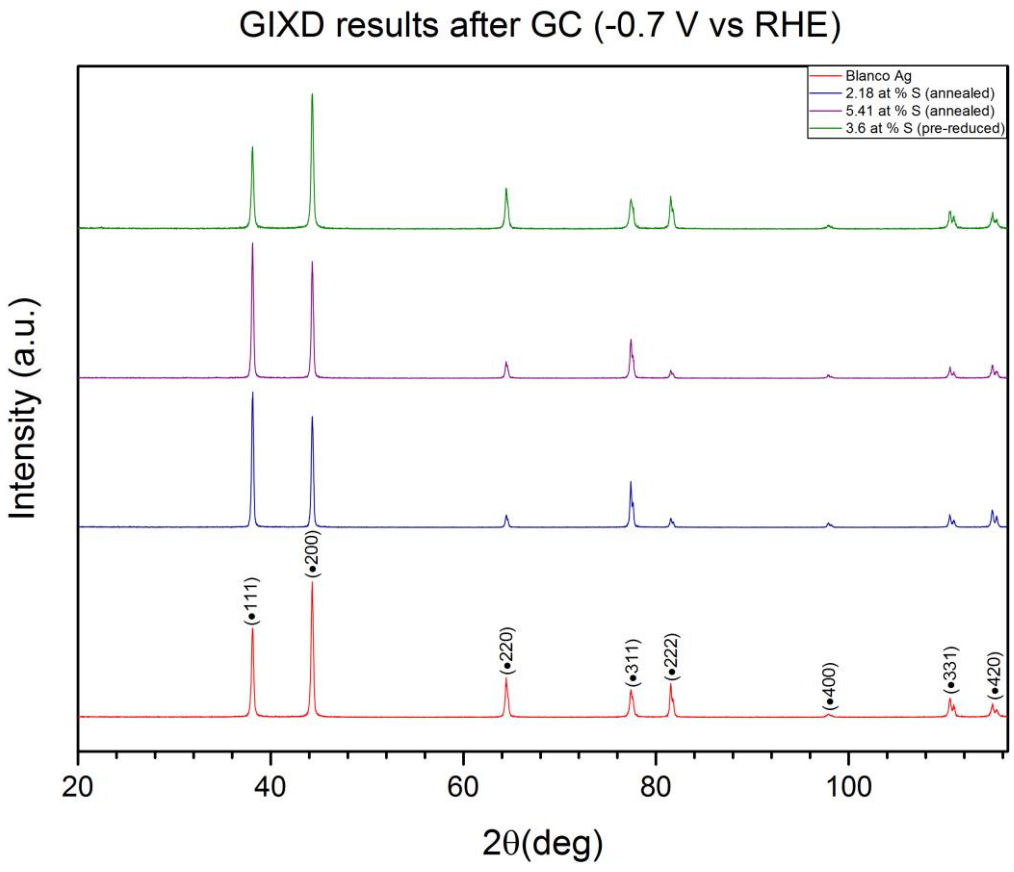

Figure 31: GIXD patterns of different samples after GC operation at -0.7 V vs RHE. Peaks marked with ● represent reflections of Ag metal.

The GIXD results are in agreement with literature about the relation between the facets of an Ag surface and the free energy change for the electrochemical reduction of CO_2 to CO. In an article by Rosen *et al.*[20] CO_2 reduction to CO was simulated with the help of DFT calculations to see if stepped surfaces on different facets would affect the free-energy change. From this modelling they found out that especially edge Ag (221) and (110) surfaces lowered the first PCET step in CO_2 reduction towards CO. The worst performing facet, they looked into, was the (100) facet and slightly better performing was the (111) peak. The (100) peak is parallel to the (200) peak and therefore have a reflection at the same place this causes that only one reflection is visible, but they are both present in the same quantities. This (200) peak is more dominant in the Blanco Ag and the pre-reduced sample, and could be a reason for the lower performance in GC testing. Hoshi *et al*.[57] also noted that the Ag (110) stepped facet has the highest CO current density followed by the flat (111) and (100) facet. Although the difference between (111) and (100) is very small and counterintuitive since the (111) peak is the most stable peak, the (111) peak has a higher activity for CO formation. Another explanation could be the difference in intensity of the higher coordinated facets on the different samples.

4.3.4 Stability

When the XRD patterns of the annealed sample are examined it is seen that the structure of the samples is hardly affected by the applied potential during GC measurements. The diffraction peaks due to the Ag are virtually unchanged. In Figure 32 this is represented by the before and after GC XRD pattern, only some very small Ag_2S peaks that are still present in the before GC pattern are lost during operation. The addition of S in the samples is in the XRD pattern the most clearly seen in the angles from 25° to roughly 52°. At all the samples the presence of S can be seen in this 2θ range. This same phenomena, where in the pre-GC XRD pattern Ag_2S peaks are visible in the lower 2θ range and the Ag peaks stay unchanged after GC operation, is also seen in an annealed sample with a lower S content which is depicted in Figure 57 in the Appendices. In the Appendices the stability of the annealed sample tested at -0.55 V vs RHE is depicted in Figure 57.

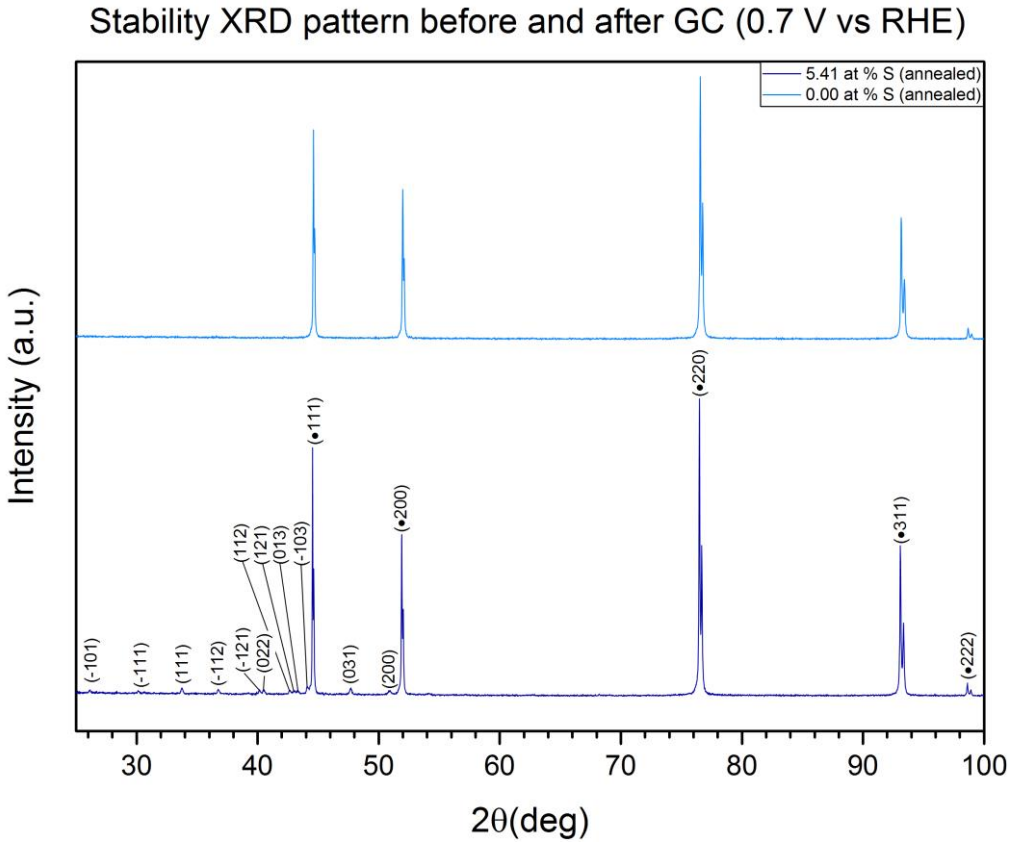

Figure 32: XRD pattern after operation in GC at 0.7 V vs RHE. The light blue pattern is the 'before GC' diffraction pattern and the dark blue is the 'after GC' pattern. Peaks marked with ● represent reflections of Ag metal.

4.3.5 Conclusions XRD and GIXD

From the XRD results the following conclusions can be drawn. The addition of S to Ag is visible in the XRD patterns, at least if the S content is high. At lower S contents the specific Ag_2S peaks are less intensive and less visible. Especially in the region of about 25˚ to 52˚ the α-Ag_2S peaks are best visible. When the S is completely removed from the samples only the metallic-Ag peaks are left and all α-Ag_2S peaks are gone. The XRD patterns of the different samples tested are very alike this is mainly because XRD is a bulk technique and thus focus on the deeper situated facets. Because the samples were very alike it was hard to draw conclusions from the XRD patterns. To bypass this problem and focus on the facets closer to the surface GIXD was used and this gave different results for the different type of samples. It must be noted that GIXD is not a one-to-one representation of the facets at the surface of the samples but more of an indication what are probably the facets at the surface but definitely not a certainty. For the two annealed samples that gave the best results of this series, the (●111) peak was the most intense and for higher 2θ angles the (●311) was most intensive. For the pre-reduced and Blanco Ag sample the (●200) peak was the most intensive and for higher 2θ angles the (●220), (●311) and (●222) were equal in intensity. From literature it was shown that the (111) peak is a slightly better than the (100) peak which is perpendicular to the (200) peak and therefore related, this could be an explanation why the annealed samples perform better than the pre-reduced and Blanco Ag sample. This effect of the (111) peak is also in accordance with the XRD results of the samples tested at -0.55 V vs RHE in Figure 54 and the samples tested at -0.8 V vs RHE in Figure 55.

4.4 CV

Cyclic Voltammetry (CV) measurements were performed to determine the 'active' potential range of the samples for GC operation. CV measurements were performed for the Blanco Ag, annealed and pre-reduced samples. The current-voltage curves were obtained with a scan rate of 20 mV/s at a potential range of 0 to -1.4 V vs RHE. All experiments were conducted with either a PARSTAT 4000A Potentiostat Galvanostat or a PARSTAT MC Multichannel potentiostat.

4.4.1 Blanco Ag

In Figure 33 the CV of a Blanco Ag sample is shown. The stability of Ag can be seen from the fact that there is a very small difference between the consecutive cycles of CV. The activity of the Blanco Ag sample at -1.4 V vs RHE, peak 1, is slightly lower (~2 mA) but in accordance with Hatsukade *et al.*[18]

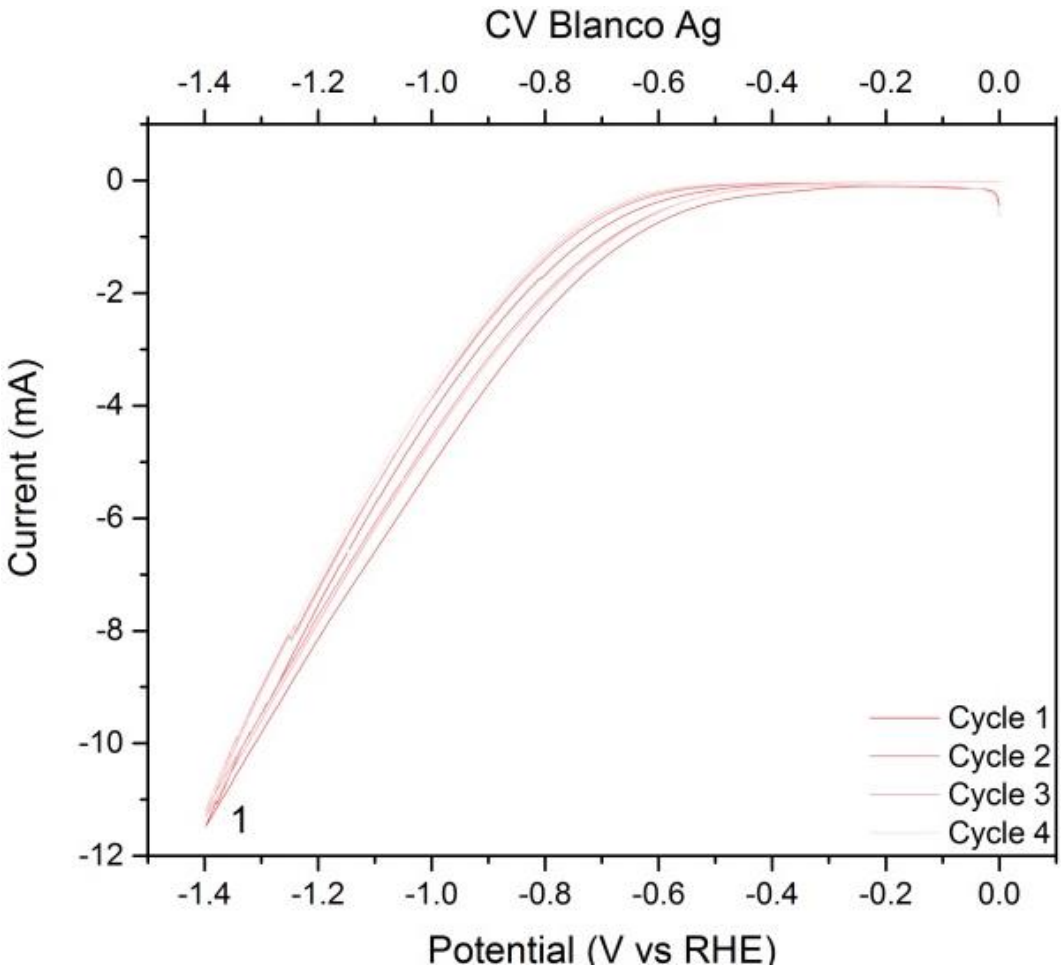

Figure 33: Cyclic voltammogram of a Blanco Ag sample.

4.4.2 Annealed samples

The CV of an annealed sample with a S content of 4.20 at% S is very different than the Blanco Ag sample as can be seen in Figure 34. The main difference is the large reduction peak 1 at -0.38 V vs RHE. This peak is the reduction of S, which leaches out of the sample. To be sure that this is definitely the reduction of S another CV was performed with a sample with an equal amount of S at a potential range from 0.8 V to -0.8 V vs RHE as shown in Figure 35. In Figure 35 the reduction peak of S of the cathodic scan (peak 1c) is at a potential of -0.41 V vs RHE. The peak at 0.11 V vs RHE (peak 1a) in the anodic scan is due to S adsorption. This is an irreversible process because the reduction peaks and oxidation peaks are not mirrored. From literature[58] there are two standard reduction reactions known for Ag_2S first there is: $Ag_2S + 2H^+ + 2e^- \leftrightarrow 2Ag + H_2S$ at a reduction potential of -0.0366 V vs SHE. And the other standard reduction is: $Ag_2S + 2e^- \leftrightarrow 2Ag + S^{2-}$ at -0.691 V vs SHE. It is assumed that the first reduction peak 1a is because of the first reduction reaction of Ag_2S as described above. Because this reduction is seen at a lower overpotential then the second reduction.

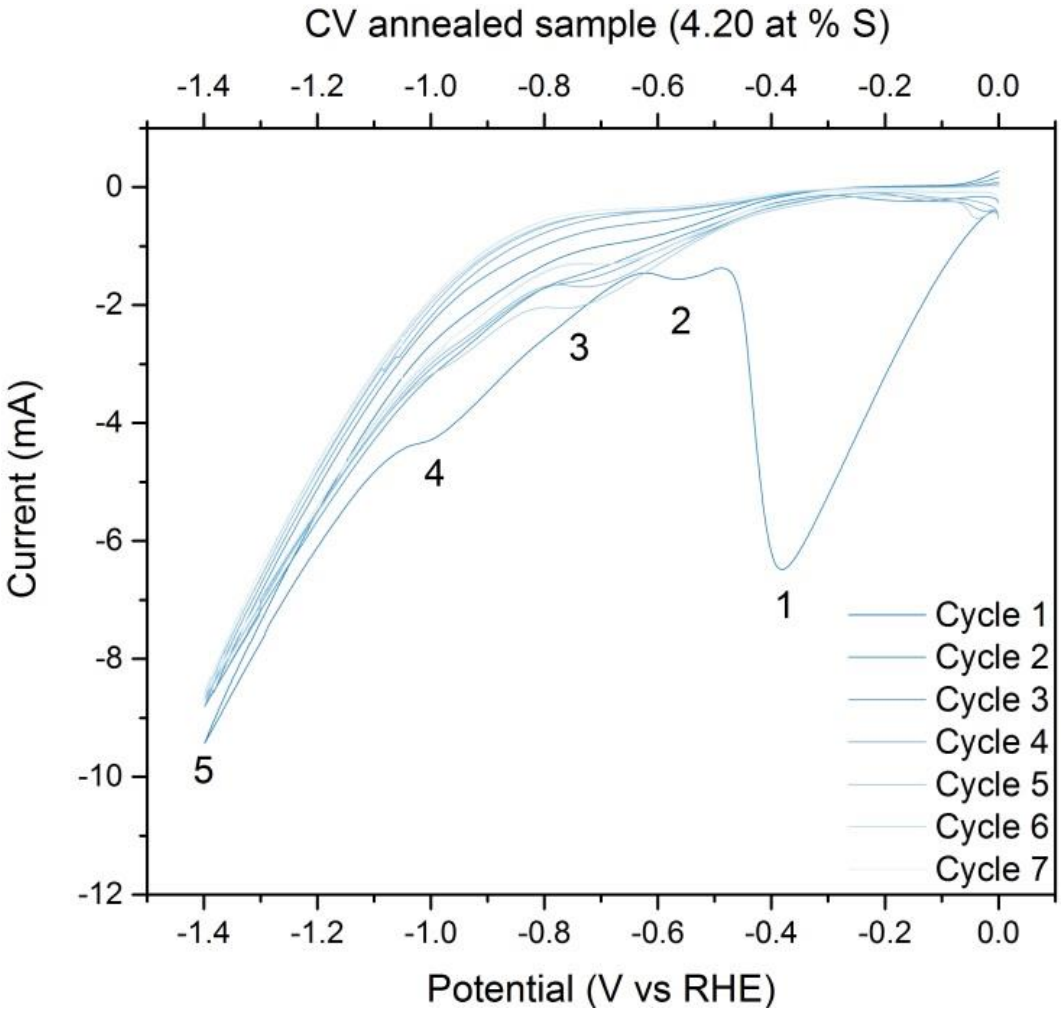

Figure 34: Cyclic voltammogram of an annealed sample with a 4.20 at% S content.

When we further observe Figure 34 the next cathodic peak is at -0.56 V vs RHE (peak 2) this peak is probably related to peak 1 and could be the reduction of the more stable S atoms in the Ag_2S structure since the entire peak is absent in the subsequent cycles. It is thought to be the reduction of Ag_2S due to the first reduction of Ag_2S, $Ag_2S + 2H^+ + 2e^- \leftrightarrow 2Ag + H_2S$.

Peak 3 in Figure 34 is visible from the second cycle until the last cycle this peak is probably because the formation of reaction intermediates in the CO_2RR. Because the peak is still visible after multiple cycles.

Peak 4 at -1.00 V is presumably like peak 1 the reduction of Ag_2S but in this case to another product $Ag_2S + 2e^- \leftrightarrow 2Ag + S^{2-}$. From the standard reduction potentials it is learned that this reduction takes place at an approximately 0.65 V[58] higher overpotential than the first reduction of Ag_2S therefore it is though that peak 4 is another reduction of Ag_2S.

Finally the annealed sample decreases in activity at the reduction peak at -1.4 V from -9.41 mA in the first cycle to -8.60 mA in the last cycle. Also shows this sample less activity than the Blanco Ag sample does at the same potential. After 7 cycles the shape of the voltammogram is similar to that of Blanco Ag as all S is lost, only peak 3 is still visible.

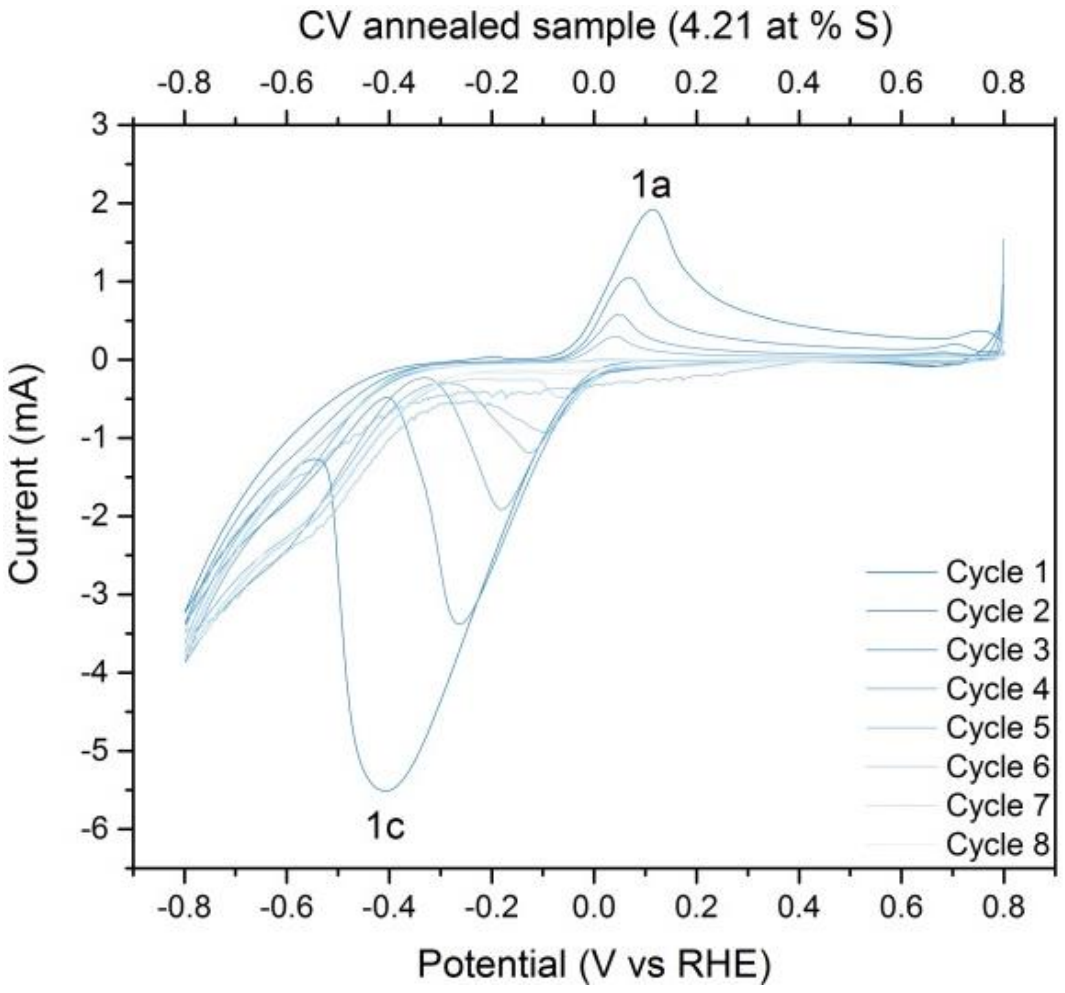

Figure 35: Cyclic voltammogram of an annealed sample with a 4.21 at% S content.

4.4.3 Pre-reduced sample

Figure 36 is the CV of a pre-reduced sample at a range from 0 to -1.4 V vs RHE. The first reduction peak in the cathodic scan at -0.47 V vs RHE is probably the reduction of S in Ag just as in Figure 34 the reduction of Ag_2S to H_2S. All of the S was leached out of the Ag sample. The next cathodic peak, peak 2, is at ~ -0.65 V vs RHE is probably because of the reduction of more stable sites of Ag_2S in the sample like in Figure 34. The third cathodic peak is found at -1.1 V vs RHE (peak 3a) this could probably the reduction of Ag_2S towards S^{2-}, a peak which is also present in Figure 34, which is again approximately at a -0.65 V higher overpotential than the assumed first reduction peak. But this peak is still present after ten cycles while all S was leached out of the sample at the end. Peak 3c which is located at -1.0 V could be the adsorption of the S that was leached out at peak 3a. This could not be checked by EDX because the amounts of adsorbed S are probably very small and limitations of EDX as explained in the SEM and EDX part of this report. Therefore it is not sure if peak 3a is definitly a S reducing peak and peak 3c is a peak caused by the adsorption of S. Certain is that there is enhanced activity at peak 3a but what is happening is not exactly clear, another possible explanation could be the CO_2RR intermediates, since it is still visible after multiple cycles.

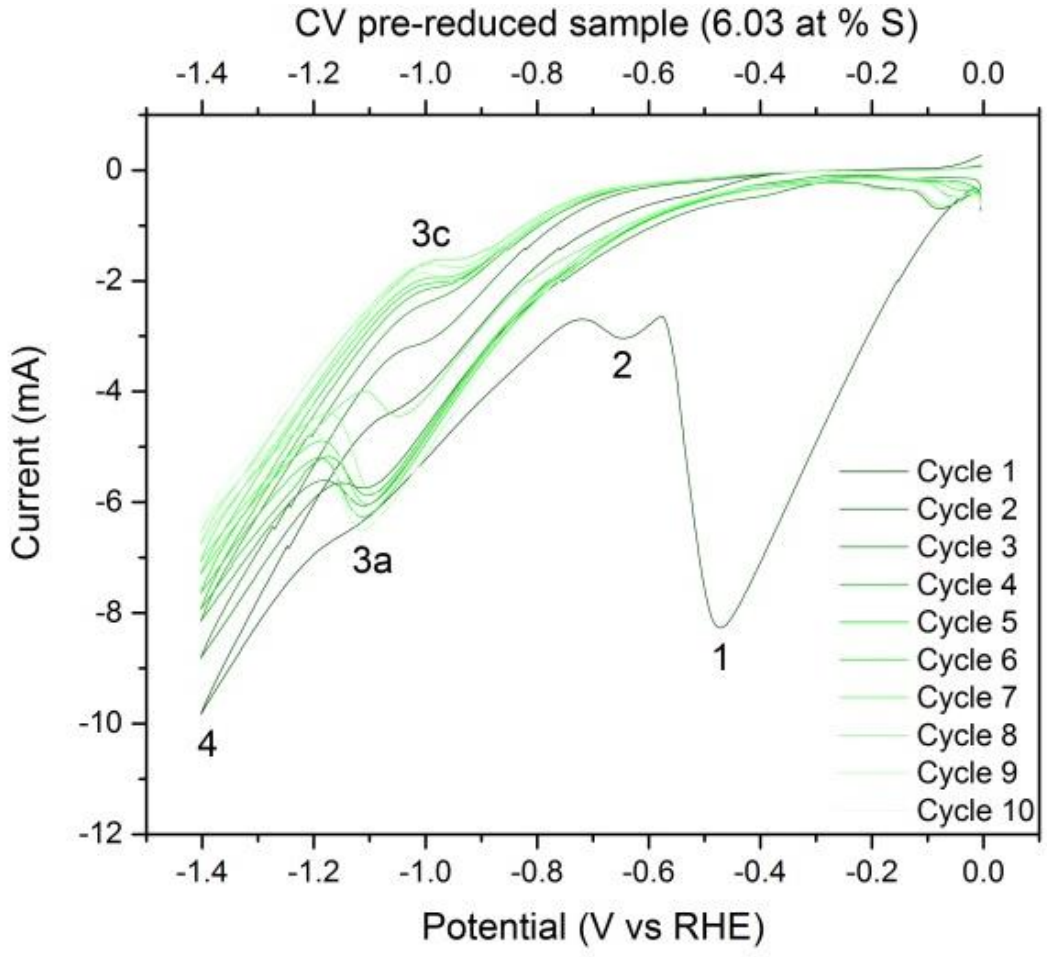

Figure 36: Cyclic voltammogram of a pre-reduced sample with a 6.03 at% S content.

Finally the activity of the samples decreases after multiple cycles at higher cathodic potentials, higher than -1.1 V vs RHE. The current at -1.40 V vs RHE decreases from -10 mA at the first cycle to -6.3 mA at the tenth cycle. A possible explanation for the decaying current density could be CO poisoning of Ag due to the S that is present in the sample. Another explanation could be Pt atoms from the counter electrode that diffused through the Nafion membrane that adhered to the surface of the sample which got poisoned by CO. Since the electrolyte $KHCO_3$ was saturated with CO_2, CO_2 was reduced and could have formed CO that poisonned the Pt that adhered to the surface of the catalyst which could have led to the decreasing current density over the course of ten cycles.

4.4.4 Comparison different samples

To compare the different CVs, the fourth cycle of a Blanco Ag, pre-reduced and annealed sample are shown together in Figure 37. This gives an insight how the different CV's relate to each other. The fourth cycle was chosen because for the annealed and pre-reduced sample this was approximately at half of the total amount of cycles performed in the CV and therefore gives a representation of the sample used in actual operation in an electrochemical cell. At -0.7 V the annealed sample shows a peak (peak 1) and shows more activity than the Blanco Ag and the pre-reduced sample. This is in agreement with the fact that the annealed sample at -0.7 V in the electrochemical cell,during GC measurements (see the Gas Chromatography section), had a higher total current density than the Blanco Ag and the pre-reduced sample. The CV in Figure 37 also suggests that the pre-reduced sample is more active than Blanco Ag sample, which is also in accordance with results in the GC measurements. Peak 1 therefore suggests that at lower overpotentials the addition of S is beneficial to the total activity of the sample. Peak 2 shows the difference in activty for the different samples at a high overpotential of -1.4 V vs RHE, suggesting that at higher overpotentials the catalytic effect of Ag prevails over the effect of S which is clearly visible in peak 1.

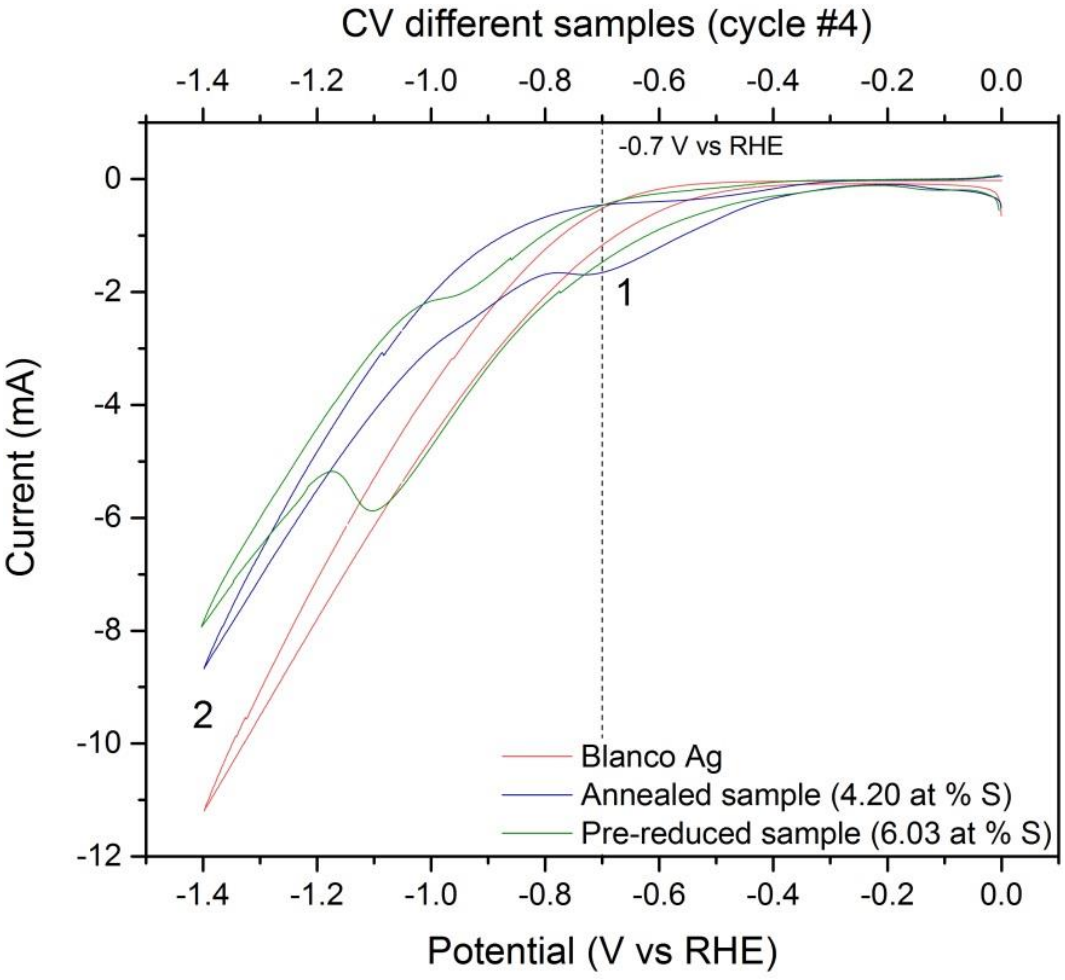

Figure 37: Cyclic voltammograms of three different samples at the 4th cycle.

4.4.5 Conclusions cyclic voltammetry

From CV experiments the following conclusions can be drawn. All of the S-doped samples (annealed and pre-reduced) have a very large reduction peak at the first cycle at roughly -0.4 to -0.5 V vs RHE. This is probably reduction of Ag_2S: $Ag_2S + 2H^+ + 2e^- \leftrightarrow 2Ag + H_2S$. This is an irreversible process because if an anodic scan is performed the oxidation peak is not at the same potential as the reduction peak and is smaller than the peak at the cathodic scan. Both the annealed sample as well as the pre-reduced sample showed a small peak just after the first big reduction peak, this could because of Ag_2S sites that were harder to reduce and therefore needed an higher overpotential. At the annealed sample there is another Ag_2S reducing peak at approximately -1.0 V vs RHE of the following reaction: $Ag_2S + 2e^- \leftrightarrow 2Ag + S^{2-}$. From literature it is known that the difference in potential between these standard reduction potentials is -0.65.[58] This difference in potential is approximately the same as difference in potential of these two peaks. The annealed samples lose these peaks after a single cycle which indicates that all the S is lost during the first cycle. The pre-reduced sample did not show this peak at -1.0 V vs RHE but at -1.1 V vs RHE, and were the peak at -1.0 V vs RHE for the annealed sample disappeared after a single cycle, the peak at the pre-reduced sample was still there after ten cycles. This peak could indicate the reduction of Ag_2S, but it could also be a peak present because of CO_2RR intermediates. The current density of the pre-reduced sample decreased at higher potentials over the length of the experiment. The annealed sample also showed decreasing activity but less than pre-reduced sample. The annealed sample showed another small peak at -0.7 V vs RHE, which decreased over time but was fairly stable. The different samples were finally compared at a single overpotential of -0.7 V vs RHE. At this potential the annealed sample with a S content of 4.20 at% showed the highest current density, followed by the pre-reduced sample and finally the Blanco Ag sample. At high overpotentials (-1.4 V vs RHE) the Blanco Ag sample has the highest current density followed by the annealed sample and lastly the pre-reduced sample.

4.5 Gas Chromatography

Gas chromatography (GC) measurements were performed to monitor the ability of the different samples to convert CO_2 to CO. Measurements were performed for all different samples at three potentials: -0.55, -0.7 and -0.8 V vs RHE. An additional measurement at -0.4 V vs RHE was performed on an annealed sample to see if this type of sample was able to reduce CO_2 to CO at such a low overpotential. It was decided not to perform a GC measurement at -0.4 V vs RHE on a Blanco Ag sample because from literature there were no examples found of CO formation at this low overpotential for a Blanco Ag sample. Besides this, also the experiment with a Blanco Ag sample conducted at -0.55 V vs RHE produced very small amounts of CO, this was an extra reason not to test the Blanco Ag sample at an overpotential of -0.4 V vs RHE. This experiment at the potential of -0.4 V vs RHE was neither performed for the pre-reduced sample because this type of sample showed at -0.55 V vs RHE hardly any activity to form CO and was therefore expected not to convert any CO_2 to CO at -0.4 V vs RHE. Before all GC measurements the internal resistance, *iR*, was determined in all experiments this had a value of 30±3 Ω. Because of the low resistance, which falls into the margin of error range therefore it was decided not to adjust the overpotentials used in this thesis. In this thesis we are primarily interested in the production of CO, but it was possible other products could have been formed. Of course there is the direct competition with the HER but Ag is also capable of forming formate, which is another two electron CO_2RR product. Although this was not in the scope of this research, for completion a sample of the catholyte of the annealed sample tested at -0.8 V vs RHE was inspected for organic compounds with the help of Nuclear Magnetic Resonance (NMR). NMR measurements were only performed on one sample because of time limitations, therefore only the sample most prone to produce formate, the annealed sample at -0.8 V vs RHE, was investigated. This gave only a single peak, this peak corresponds to acetone that was used to clean the NMR tube. Because the NMR tube was not properly dried there was probably still some acetone residue in the NMR tube which is coherent with the result from the NMR measurement. There were no peaks found for formate therefore it is concluded that there was no formate present in the catholyte or the amounts were below the detection limits of the equipment.

As explained in the theory section we are interested in both the FE which is a measure for the selectivity of the catalyst and the current density which is a measure for the activity of the catalyst. The FE was calculated as explained in Equation 2 in the Theory part of this thesis. Since the FE did not add up to 100% for every sample these values were normalized so the total FE added up to 100%. By normalizing these values comparing the FE of the samples was possible.

The values of the current densities are based upon the current measured by the potentiostat. The individual current densities are the product of the normalized FE and the individual current densities. The formula used to calculate the current density is shown in Equation 13 in the Experimental methods section. The formula used to calculate the FE is shown in Equation 14 in the Experimental methods section.

4.5.1 Current density

Since only H_2 and CO were formed during GC operation the total current density is made up by the sum of the H_2 and CO current densities. By showing the total current density for the Blanco Ag and annealed samples in Figure 38 next to the H_2 current density in Figure 39 it is immediately seen that the amount of electrons that are used in the hydrogen formation of the total amount of electrons used is very high. By increasing the overpotential the current density increases as well. Only the annealed sample tested at -0.4 V vs RHE has a total and H_2 current density of 0.115 mA/cm^2 that is very close to that of the Blanco Ag sample tested at -0.55 V vs RHE. The total current density of the annealed sample tested at -0.55 V vs RHE increased with 98% to 0.32 mA/cm^2 in comparison with the Blanco Ag sample. There is also a correlation between the S content of the annealed samples and the total and H_2 current density. At all potentials the total and H_2 current densities of the doped annealed samples are higher than the Blanco Ag samples. A higher S concentration results in higher total and H_2 current densities, as can clearly be seen from the annealed samples tested at -

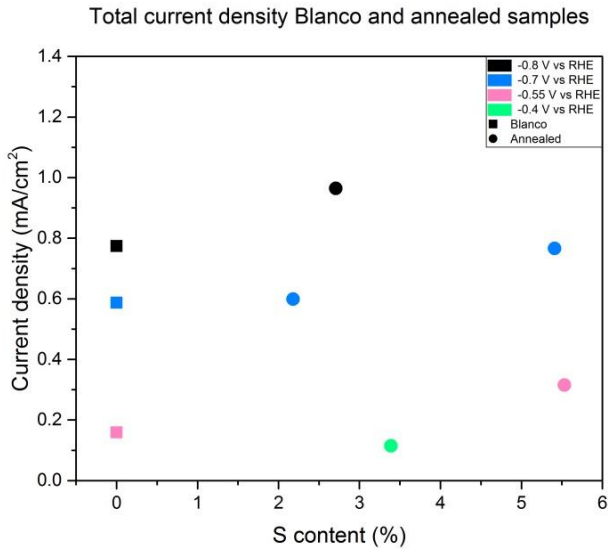

Figure 38: Total current density Blanco Ag and annealed samples.

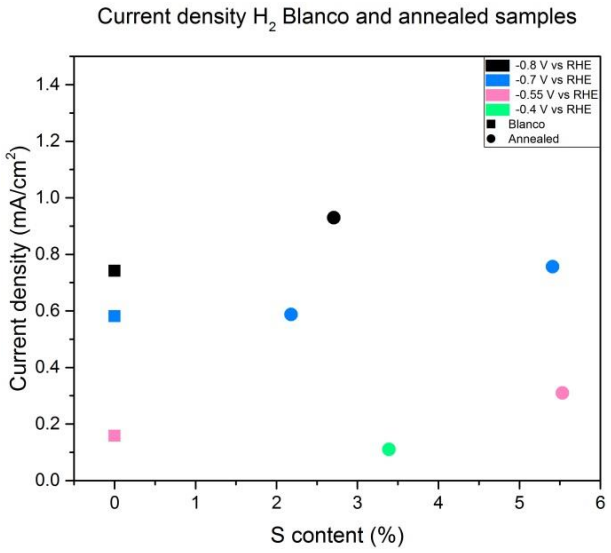

Figure 39: H_2 current density Blanco Ag and annealed samples.

0.7 V vs RHE in Figure 38 and Figure 39. At -0.7 V vs RHE with a S content of 2.18 at% (0.60 mA/cm^2) and 5.41 at% (0.71 mA/cm^2) increased with 2% and 31% in comparison with the Blanco Ag sample. Where the annealed sample tested at -0.8 V vs RHE performed the best with a total current density of 0.96 mA/cm^2 an increase of approximately 25%. The total current densities of the Blanco Ag samples are comparable with values found in literature[i]: Ma *et al.*[36], Hatsukade *et al.*[18], Hsieh *et al.*[37] measured a total current density of ~0.1 mA/cm^2, ~0.25 mA/cm^2 and 0.45 mA/cm^2 respectively at a potential of -0.6 V vs RHE for Ag foil. In these articles by Ma *et al.*[36] and Hatsukade *et al.*[18] also the total current density is almost totally made up by the partial H_2 current density. The values for the total current density of the Blanco Ag sample at -0.7 V vs RHE is with 0.59 mA/cm^2 higher than the total current density measured by Ma *et al.*[36] and Hatsukade *et al.*[18] They measured a total current density for Ag foil of 0.3 mA/cm^2 and 0.4 mA/cm^2 at -0.7 V vs RHE. But Hsieh *et al.*[37]

[i] The articles mentioned here all used CO_2 saturated 0.1 M $KHCO_3$ as an electrolyte with a pH of 6.8.

measured a higher total current density for Ag foil of 0.7 mA/cm^2 at -0.7 V vs RHE. At -0.8 V vs RHE the total current density of Ag foil measured by Ma *et al*.[36] and Hatsukade *et al.*[18] and Hsieh *et al*.[37] were 0.8 mA/cm^2, 0.5 mA/cm^2 and 1 mA/cm^2 respectively this result is in line with the measured current density, 0.77 mA/cm^2 in this research.

Figure 40 shows the current density for CO of the Blanco Ag and annealed samples. Again just as the total and H_2 current density, the current density for CO rises with increasing potentials. The CO current density is also for every overpotential higher than the Blanco Ag samples. There is no correlation between increasing S content of the sample and the CO current density as can be seen from the samples tested at -0.7 V vs RHE. The sample with a S content of 5.41 at% has a slightly lower CO current density, 0.010 mA/cm^2, versus 0.012 mA/cm^2 for the sample with a S content of 2.18 at%. The increase in CO current density for the 2.18 at% and 5.41 at% annealed samples are 83% and 61% respectively if compared with the Blanco Ag sample which had a CO current density of 0.0064 mA/cm^2. The S content of 2.18 at% is also closer to the amount Lim *et al.*[1] used in their calculations and was therefore expected to perform better. The doped annealed sample tested at -0.4 V vs RHE has only a slightly lower CO current density with 0.0051 mA/cm^2 than the doped annealed sample tested at -0.55 V vs RHE with a partial CO current density of 0.0055 mA/cm^2. The annealed samples both perform better on partial CO current density than the Blanco Ag sample tested at -0.55 V vs RHE which only has a very low CO partial current density of $6.39 \cdot 10^{-4}$ mA/cm^2 so the addition of S caused an increase of 88% in CO current density in comparison with the Blanco Ag sample. The doped annealed sample tested at -0.8 V vs RHE only has a minor higher CO current density (0.034 mA/cm^2) than the Blanco Ag (0.032 mA/cm^2) tested at that same potential. These observations from Figure 40 suggest that the addition of S primarily affects the performance of the catalysts at low overpotentials (-0.4, -0.55, -0.7 V vs RHE). To compare these values presented with literature the partial CO current densities of Ag foil of two articles are shown: At -0.6 V vs RHE Ma *et al.*[36] and Hatsukade *et al.*[18] measured a negligible and 0.007 mA/cm^2 respectively at -0.6 V vs RHE, at -0.7 V vs RHE they measured 0.025 mA/cm^2 and 0.05 mA/cm^2 respectively. And finally Ma *et al.*[36] and Hatsukade *et al.*[18] reported a CO partial current at -0.8 V vs RHE for Ag foil of 0.15 mA/cm^2 and 0.25 mA/cm^2. Although these values measured for the CO current density in this research are lower than that recorded in literature, there is an improvement seen for the S-doped annealed samples in regard with the Blanco Ag samples.

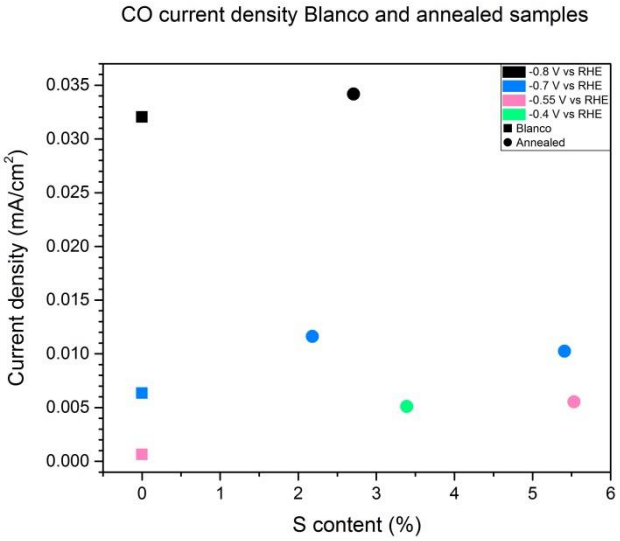

Figure 40: CO current density Blanco Ag and annealed samples

In Figure 41 the total current density of the Blanco Ag samples and the pre-reduced samples are depicted. Figure 42 shows the outcome for the H_2 partial current density of the Blanco Ag and pre-reduced samples. The total and H_2 current densities for the pre-reduced sample are at each overpotential higher in respect with the Blanco Ag samples. At -0.8 V vs RHE the difference between the Blanco Ag sample with ~0.74 mA/cm^2, and the pre-reduced sample with ~1.29 mA/cm^2 is an increase of about 74%. At that same potential of -0.8 V vs RHE the annealed sample only reached a current density of ~0.93 mA/cm^2 which is an increase of 25% in comparison with the Blanco Ag sample. At -0.7 V vs RHE the total current density of the pre-reduced sample is 0.71 mA/cm^2 this is an increase of 21% in regard with the Blanco Ag sample that had a current density of 0.59 mA/cm^2. The total current density of the pre-reduced sample is in between the total current densities of the annealed samples tested at the same potential: annealed sample (2.18 at%) 0.599 mA/cm^2; pre-reduced (3.6 at%) 0.709 mA/cm^2; annealed (5.41 at%) 0.767 mA/cm^2. These total current densities for the annealed and pre-reduced samples tested at -0.7 V vs RHE suggest a relationship between the total current density and the S content.

The pre-reduced sample tested at -0.55 V vs RHE has a slightly higher total current density than the Blanco Ag sample due to pre-reducing for too long this sample contained 0.00 at% S. If we then look at Figure 42 the current densities for H_2 are almost the same as the total current densities. This is confirmed by Figure 41 indicating that pre-reduced samples have a very low CO current density and are predominately active for H_2 production.

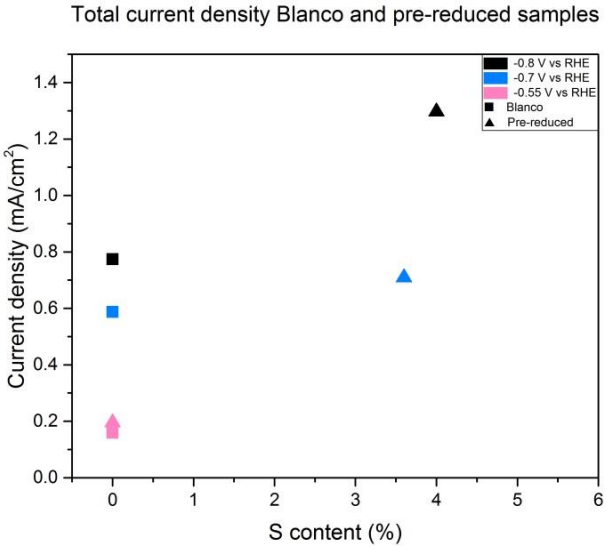

Figure 41: Total current density of the Blanco Ag and pre-reduced samples.

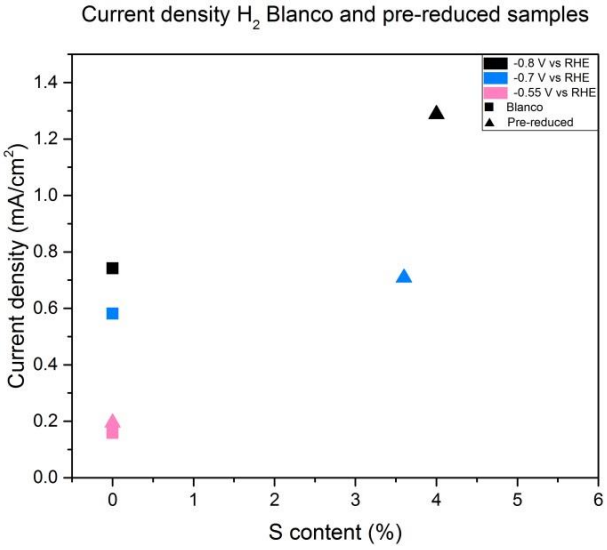

Figure 42: H_2 current density of the Blanco Ag and pre-reduced samples.

This statement is also in agreement with Figure 43 that shows the CO current density of the samples at the different potentials. The pre-reduced sample that had a S content of 0.00% and was tested at -0.55 V vs RHE had the same current density for CO as the Blanco Ag tested at the same potential. The pre-reduced sample tested at -0.7 V vs RHE had the same CO current density as the Blanco Ag and pre-reduced sample tested at -0.55 V vs RHE, which is a tenfold lower than the CO current density for the Blanco Ag sample at the same potential. At -0.8 V vs RHE the activity for CO formation is around three times as low as the Blanco Ag sample at the same potential. Where the annealed samples at all overpotentials had a higher CO current density than the Blanco Ag samples the pre-reduced samples showed at all overpotentials lower current densities.

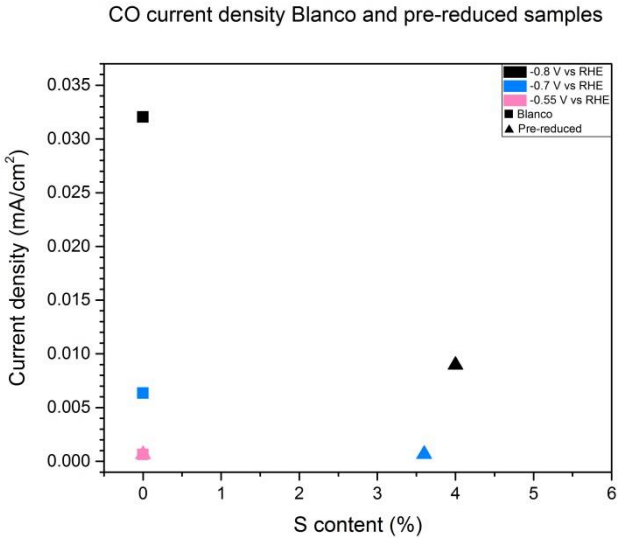

Figure 43: CO current density Blanco Ag and pre-reduced samples

4.5.2 Faradaic efficiency

In Figure 44 the FE of all the different samples tested are shown the solid colours represent CO FE and the colour with a mesh pattern represents the FE of H_2. The total FE of most of the samples fall into a 5% error margin of 100% and were therefore found to be trustworthy. However the annealed sample tested at -0.4 V vs RHE and the Blanco Ag and the annealed sample tested at -0.55 V vs RHE have a total FE of about 80%. A possible explanation for this result is that instead of CO_2, Ag_2S is reduced this could explain the loss of electrons in the total FE, which is only based upon CO and H_2.

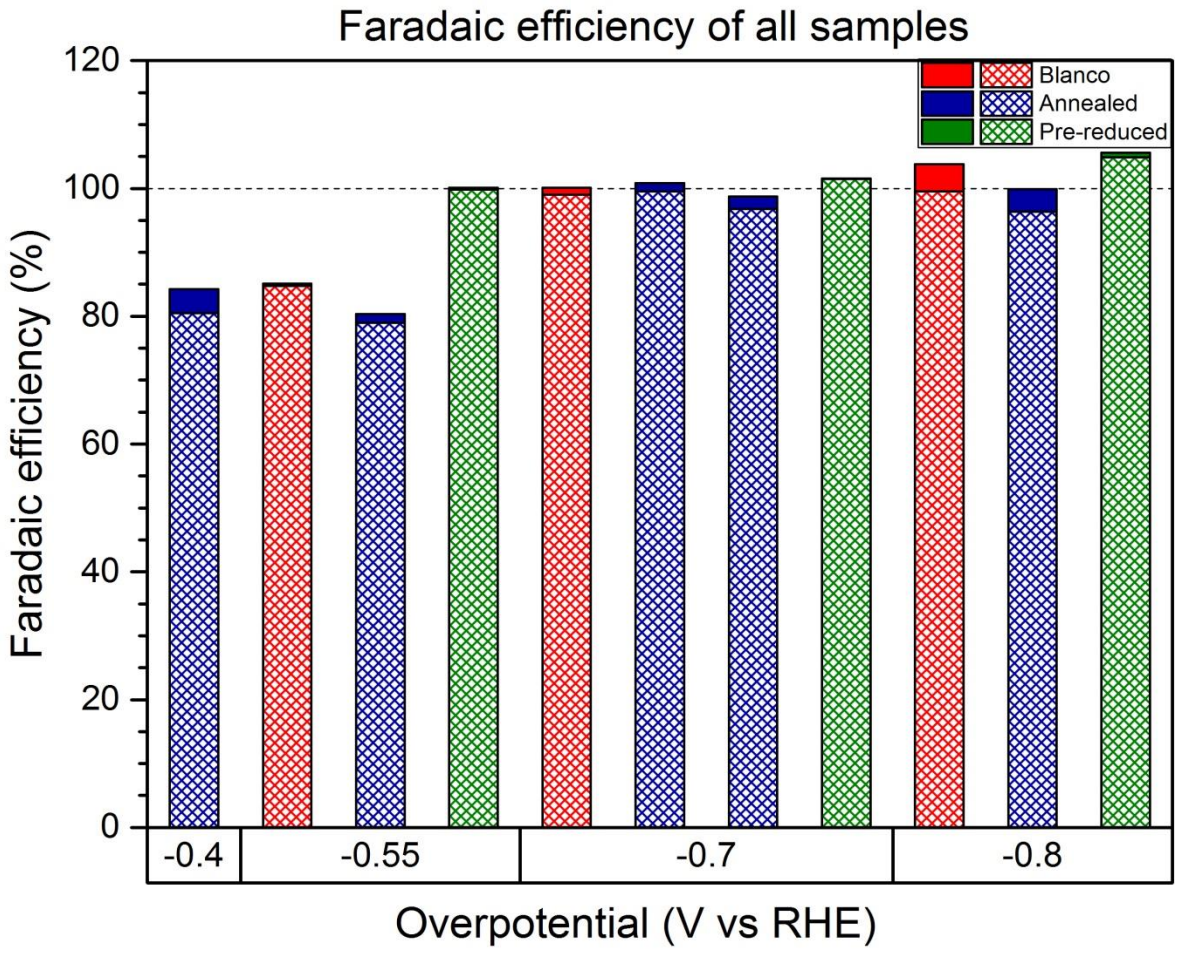

Figure 44: FE of all samples. Solid colours represent the CO FE the meshed colours represent the FE of H_2.

To compare the FE of the different samples, the FE were therefore normalized to 100% as can be seen in Figure 45. All of the samples produce predominantly H_2 and the CO FE is small.

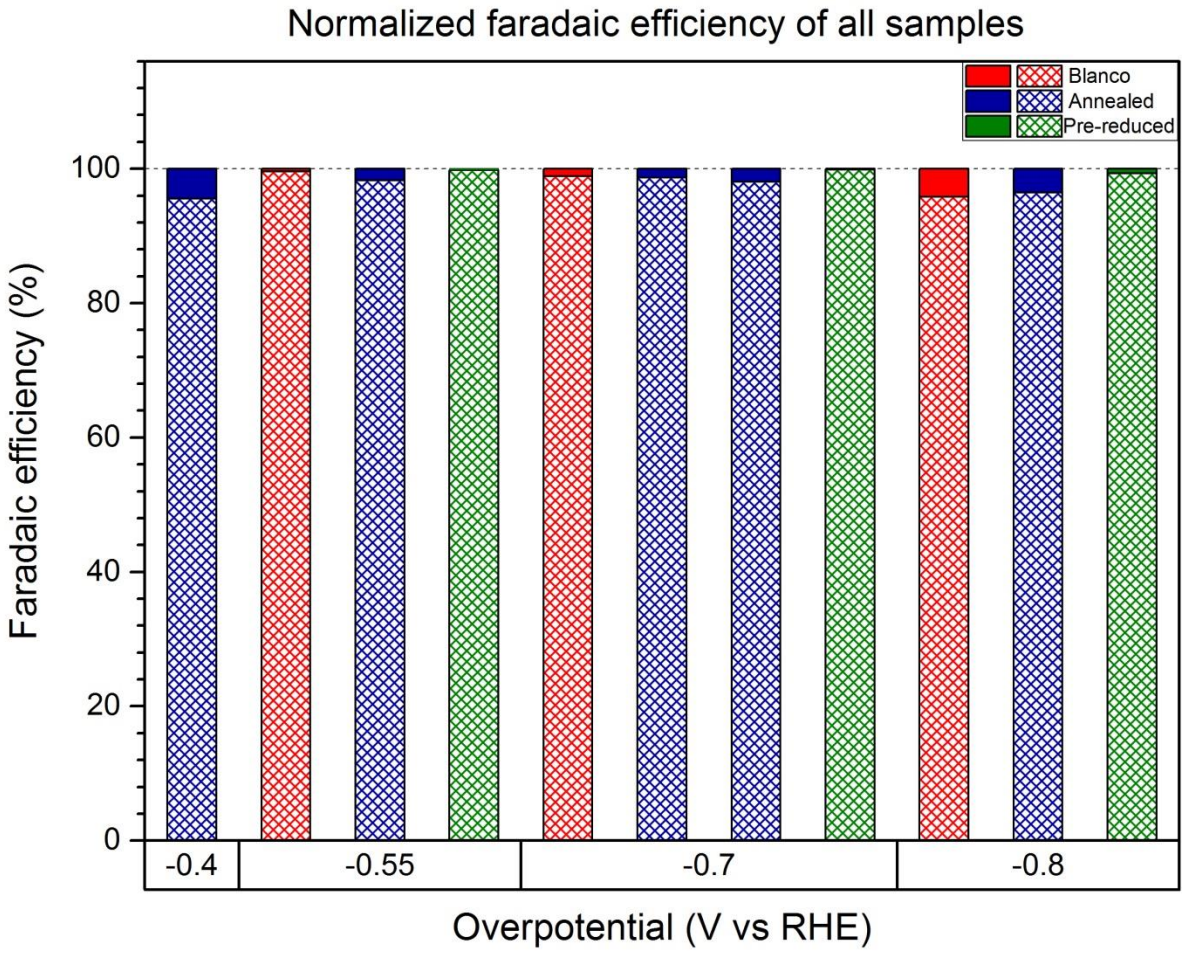

Figure 45: Normalized FE of all samples. Solid colours represent the CO FE the meshed colours represent the FE of H_2.

In Figure 46 the CO FE is shown for all tested samples. It can be seen that the annealed samples have a higher CO FE at lower overpotentials. At -0.4 V vs RHE the highest FE of all of the samples is reached with a value of ~4.44 %. At -0.55 V vs RHE again the FE of the annealed sample is the highest, 1.75%, of the three different samples tested at this potential. This is an increase of 336% if compared with the Blanco Ag at this potential. The Blanco Ag sample has only a FE of ~0.40 % and is therefore performing similar to the pre-reduced sample which has a FE of ~0.33%, it must be noted that the S content of the pre-reduced sample is 0.00% like the Blanco Ag sample. This low FE for a Blanco Ag sample is however in agreement for a flat Ag surface of Hsieh *et al*.[37] The reason why the pre-reduced sample is performing this poorly is not yet clear. At -0.7 V vs RHE the annealed samples have the best FE of all the samples at that potential. There is also a correlation between the S content in the sample and the FE which, is in agreement with article of Lim *et al.*[1] where they used a S content of ~2.1 at%. The annealed sample at -0.7 V vs RHE with a S content of 2.18 at% with a FE of ~1.94% performs better than the annealed sample with a S content of 5.41 at% and a FE of ~1.34%. The CO FE of the annealed samples with 5.41 at% and 2.18 at% increased with respectively 24% and 80% in comparison with the Blanco Ag sample with a CO FE of 1.08%. In literature at -0.7 V vs RHE, FE of ~10% are reported for polycrystalline Ag[18,36,37] which is almost a tenfold higher than the result in this research. The pre-reduced sample is performing the worst of all tested samples with only a FE of ~0.0934%. At the highest overpotential tested, -0.8 V vs RHE, the Blanco Ag sample has the highest FE of 4.14 % with the annealed sample with a FE of ~3.55% just below it. However the current density for CO at this potential is higher for the annealed sample than the Blanco Ag, but because the total current density of the annealed sample was also higher the CO FE is lower. The result of a CO FE of 4.14 % at an overpotential of -0.8 V vs RHE for a Blanco Ag sample is rather low, in literature FE of 20 % are considered normal.[18,36,37] The pre-reduced sample has the lowest FE, ~0.691%, in comparison with the other samples tested at -0.8 V vs RHE.

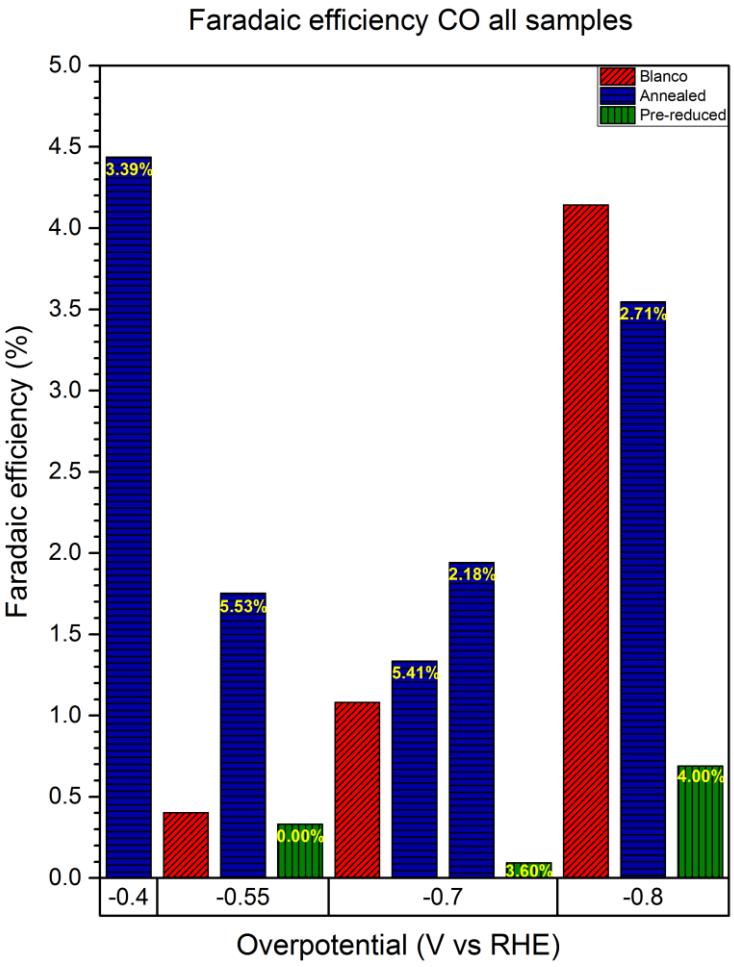

Figure 46: CO FE of all samples. The yellow percentage in the annealed and pre-reduced columns represent the at% S in the sample.

If we look at trends in the CO FE of the samples it is seen that if the overpotential increases the CO FE on the Blanco Ag samples increases as well. Although the FE of the Blanco Ag samples are rather low the general trend, higher CO FE at higher overpotentials, is correct. The annealed samples on the other hand perform significantly better at the lower overpotentials, suggesting that the S could have a positive effect on the FE to CO. At all overpotentials the pre-reduced samples performs poorly, the sample tested at -0.55 V vs RHE with a S content of 0.0 at% S has a similar result as the Blanco Ag sample. At -0.7 V vs RHE the pre-reduced sample performs worst of all samples. The pre-reduced sample has the highest CO FE at -0.8 V vs RHE.

4.5.3 Stability

Next to the performance based upon the current density and FE the stability of the samples is also discussed. EDX measurements performed after testing the samples in the electrochemical cell with an applied potential showed that all S was lost. To see how the samples performed over the course of 1 hour in operation in the electrochemical cell, the measured produced CO concentration (ppm) was plotted against the time (minutes). Figure 47 shows the CO production for the samples tested at -0.4 V vs RHE, the annealed sample did not produce CO over the whole of the experiment but only at sparse moments and at low concentrations. There is despite the sparse activity a decreasing trend seen in the production of CO over the length of the experiment. The produced CO concentration of the different type of samples tested at -0.55 V vs RHE can be seen in Figure 48. The production of CO is even sparser than at -0.4 V vs RHE, the Blanco Ag sample shows only one production peak just like the pre-reduced sample. From this result it can be concluded that pre-reduced and Blanco Ag are not active at all for the production of CO at these potentials, and this one spike could be a measurement mistake. The only sample that is producing CO on multiple moments is the annealed sample, but only at three on a total of twenty measuring points. However it seems like the amount of produced CO is decreasing for the annealed sample at -0.55 V vs RHE.

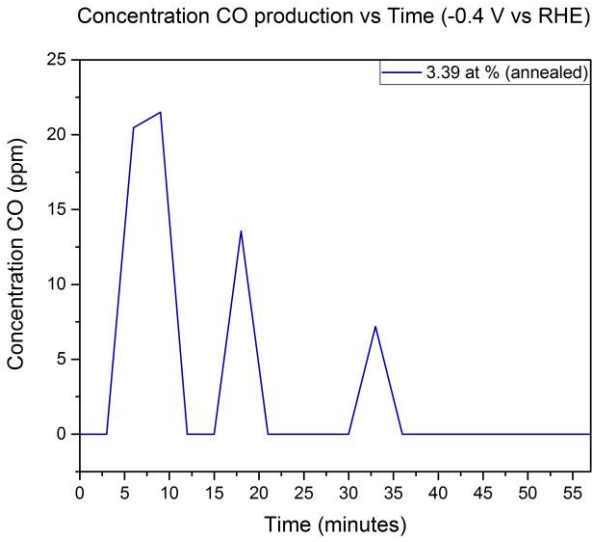

Figure 47: Concentration CO production versus time annealed sample (-0.4 V vs RHE).

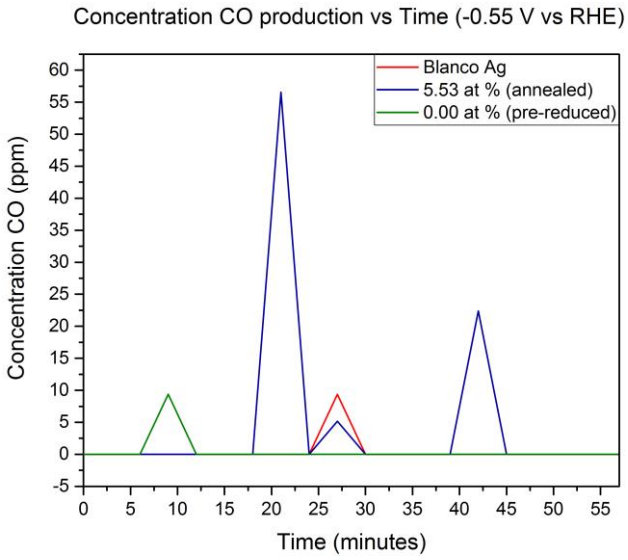

Figure 48: Concentration CO production versus time Blanco Ag, annealed and pre-reduced samples (-0.55 V vs RHE).

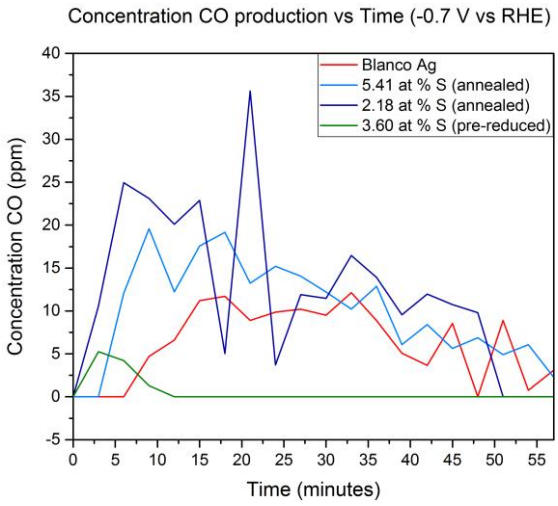

Figure 49: Concentration CO production versus time Blanco Ag, annealed and pre-reduced samples (-0.7 V vs RHE).

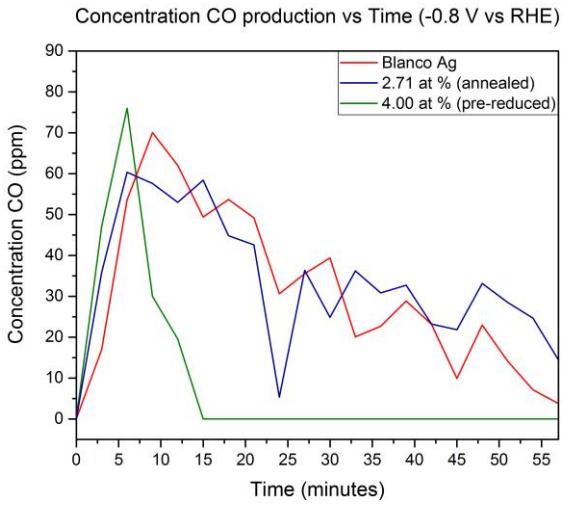

Figure 50: Concentration CO production versus time Blanco Ag, annealed and pre-reduced samples (-0.8 V vs RHE).

Figure 49 depicts the produced CO concentration for the samples at an overpotential of -0.7 V vs RHE. Here is the production of all of the samples more constant over time. At all of the samples the CO production seems to decline over time. The annealed sample with an S content of 2.18 at% produces the most CO but after a high concentration in the beginning the production decreases. There is one large peak at 21 minutes but this could also be an error in the measurement. The annealed sample with a S content of 5.41 at% follows the same trend as the other annealed sample and the production steadily decreases over time. The Blanco Ag sample starts slowly and has a lower production in the beginning as the annealed samples but again the production is falling over the course of the experiment. The pre-reduced sample started with a small production of CO and then after ~10 minutes the production of CO stops and no more CO is produced throughout the experiment.

At a higher potential of -0.8 V vs RHE the CO production (Figure 50) for all of the samples is a lot higher, but here as well is for all samples a steady decline seen in the production of CO. The Blanco Ag sample after initially reaching a peak in production at 9 minutes steadily declines towards zero at the end of the experiment. The production of the annealed sample is very similar to that of the Blanco Ag sample. At the start a high concentration of produced CO but after this peak a continuous decrease of production. The pre-reduced sample follows the trend as seen at the other potentials, a peak and then immediately a decline to no production at all. The CO concentration of the pre-reduced peak at 6 minutes is the highest of all the samples at this overpotential.

General conclusions are that all of the graphs see a decrease in CO production in the course of an hour-long experiment with an applied potential and CO_2 bubbling. At low overpotentials (-0.4 and -0.55 V vs RHE) the production of CO is sparse and the concentration is low therefore these experiments should be approached with caution and not to bold statements can be made upon these outcomes. The pre-reduced samples always follow a similar production path, at one moment CO is produced and then it suddenly stops producing CO. A possible reason for this could be CO poisoning of the surface of the catalyst. Another general remark is that at the first measurement at 0 minutes there is no CO measured this is logical because the potential is only supplied after the first sample is in injected into the GC. The next measurement is usually not the highest CO concentration this is probably because the

CO is first diffusing into the electrolyte and is only released to the overhead compartment in the cell when the electrolyte is saturated with CO.

4.5.4 Conclusions Gas Chromatography experiments

The following conclusions can be drawn from the GC measurements. The addition of S to Ag is beneficial to the CO current density as well as the total current density. Especially at low overpotentials the CO current density increases significantly. At -0.4 V vs RHE the CO current density for the annealed sample (0.0051 mA/cm^2) was higher than the Blanco Ag sample tested at -0.55 V vs RHE and similar to that of the annealed sample tested at -0.55 V vs RHE (0.0055 mA/cm^2). At -0.7 V vs RHE the annealed samples again performed better when compared with the Blanco Ag sample where the CO current density of the annealed sample with a S content of 2.18 at% increased with 83% to 0.012 mA/cm^2. And the annealed sample with a S content of 5.41 at% increased with 61% to 0.010 mA/cm^2. This result is also in harmony with the article of Lim *et al.*[1] since the sample with a S content of 2.18 at% is performing better. The CO current density was the highest for the annealed sample tested at -0.8 V vs RHE with 0.034 mA/cm^2 which was slightly higher than the Blanco Ag sample tested at that overpotential. The total current densities of the Blanco Ag samples were in accordance with literature, but the CO current densities were smaller than described in literature. The total current densities are at every potential higher than the Blanco Ag samples and comparable to the annealed samples. Of every sample the largest part of the total current density is made up by the H_2 current density. This is in the case of the pre-reduced samples the most extreme were CO current density is very low and the H_2 current density is high.

The CO FE is the highest at an overpotential of -0.4 V vs RHE with ~4.44%. At -0.55 V vs RHE the annealed sample performs the best with a CO FE of 1.75%, an increase of 336% if compared with the Blanco Ag sample. At -0.7 V vs RHE the annealed samples perform the best. The sample with a S content of 2.18 at% had a FE of 1.94%, an increase of 80% with the CO FE of the Blanco Ag of 1.08%. The annealed sample with a S content of 5.41 at% had a 24% higher CO FE than the Blanco Ag sample with 1.34%. This difference in S content is again in accordance with Lim *et al.*[1] At the highest overpotential however the Blanco Ag had the highest CO FE of 4.14% and the annealed sample slightly lower with 3.55%. The pre-reduced samples had al overpotentials very low CO FE. If these CO FE of the Blanco Ag samples for each potential are compared to results from literature they are significantly lower. But if we solely look at the results presented in this thesis the annealed samples outperform the Blanco Ag samples at lower overpotentials.

From examining the concentration of produced CO for all the samples, it was concluded that especially at low overpotentials the results are not always very reliable. The production is not consistent and only at sparse moments CO is formed. Were the result of -0.55 V vs RHE is most unreliable, the result of -0.4 V vs RHE does show a decreasing trend in CO production over time. A decreasing trend in the produced CO concentration is also seen at -0.7 V vs RHE and -0.8 V vs RHE. After an initial CO concentration peak the concentration steadily decreases, this implicates that the samples are not stable for a long time.

4.6 Electrochemical Surface Area measurements

Although the surfaces of the Blanco Ag samples were relatively flat, despite some ridges, no deliberate actions was undertaken to nanostructure or in any other way morphologically change the surface of the samples. However the SEM images have shown that there is a difference in the roughness of the surface of the samples. The doping of the samples caused the surface to crack and altered the relatively flat surface of the Blanco Ag samples. So to exclude the altering of the surface morphology on the performance of the samples Electrochemical Surface Area Measurements (ECSA) were performed. The precise proceedings in measuring the ECSA can be found in the experimental section.

In Figure 51 the outcome of the ECSA measurement are shown for the samples tested at -0.7 V vs RHE in GC operation. In the legend the surface 'A' is given in C/cm^2 in this way a relative area measurement is given to each sample. As predicted the flat surface of the Blanco Ag sample has the lowest surface area. Whereas the pre-reduced sample with a S content of 10.84 at%, before pre-reduction, had the largest surface area. For the annealed samples there is again a positive relation between the atomic S content and the ECSA.

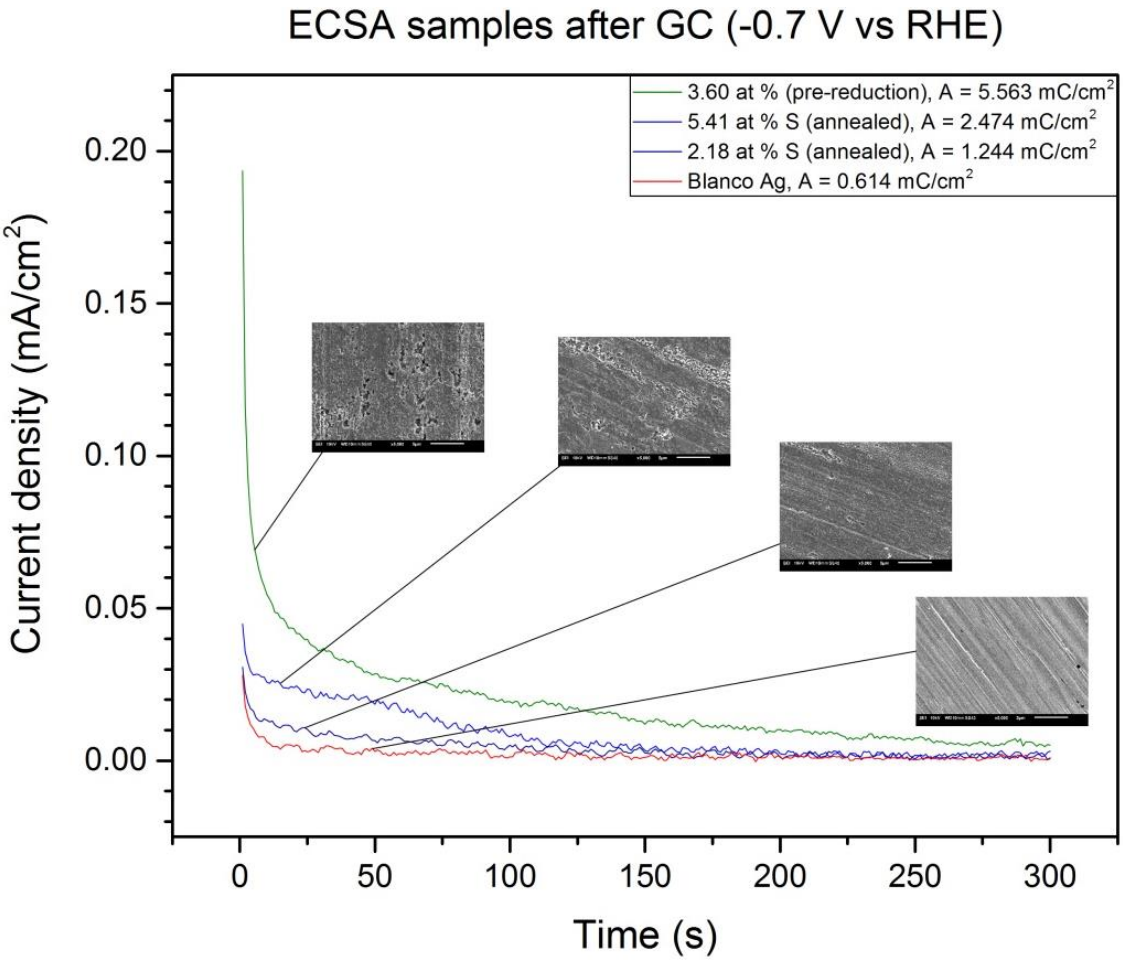

Figure 51: ECSA of the different samples after GC operation at -0.7 V vs RHE including SEM pictures of the concerned sample.

By ECSA measurements the expectation that was raised from the SEM results is confirmed, the ECSA decline in the following way: Pre-reduced samples > Annealed samples > Blanco

Ag samples. The results of the experiments seem to be reliable because the forming of a monolayer Ag_2O or AgOH resembles a charge of roughly 400 µC/cm^2 for an Ag surface.[54] The Blanco Ag samples tested at -0.55, -0.7 and -0.8 V vs RHE had respectively a charge of 441, 614 and, 442 µC/cm^2. The ECSA measurements of the potentials of -0.4, -0.55, -0.8 V vs RHE can be found in the Appendices in Figure 58, Figure 59 and Figure 60 respectively. The Blanco Ag sample surface of each overpotential series was used as a reference for that particular overpotential series because there was a difference between the surface areas of the Blanco Ag samples, and in the -0.7 V vs RHE case it was more than 1.5 times as high as the theoretical value. The values of the ECSA measurement and the normalized value of this surface area is depicted in, Table 1, Table 2 and Table 3 for an overpotential of respectively -0.55 V, -0.7 V and -0.8 V vs RHE. The normalized surface area of -0.4 V vs RHE is depicted in Table 5 in the Appendices.

Table 1: ECSA of the samples that were tested at -0.55 V vs RHE in the electrochemical cell.

Type	S content (at%)	ECSA (mC/cm^2)	Normalized ESCA
Blanco Ag	-	0.441	1
Annealed	5.53	1.974	4.476
Pre-reduced	0.0	2.43	5.510

Table 2: ECSA of the samples that were tested at -0.7 V vs RHE in the electrochemical cell.

Type	S content (at%)	ECSA (mC/cm^2)	Normalized ESCA
Blanco Ag	-	0.614	1
Annealed	2.18	1.244	2.026
Annealed	5.41	2.474	4.029
Pre-reduced	3.60	5.563	9.060

Table 3: ECSA of the samples that were tested at -0.8 V vs RHE in the electrochemical cell.

Type	S content (at%)	ECSA (mC/cm^2)	Normalized ESCA
Blanco Ag	-	0.442	1
Annealed	2.71	2.064	4.670
Pre-reduced	4.00	3.013	6.817

If these results from the ECSA measurements are combined with the current densities measured during GC operation there is no one-to-one relationship between these two quantities that holds for every result.

At -0.55 V vs RHE (Table 1) the total current density of the Blanco Ag sample is 0.159 mA/cm^2 and the total current density for the annealed sample is 0.315 mA/cm^2, the ECSA is however almost 4.5 times as large which is not in agreement with the factor two between the total current densities. For the pre-reduced sample has a 5.5 times larger ECSA than the Blanco Ag but the total current density is only 0.195 mA/cm^2, which is only 1.2 times as high.

The lack of a one-to-one correlation between ECSA and the total current density also becomes clear when the results of the -0.7 V vs RHE samples are reviewed (Table 2). The Blanco Ag sample had the lowest value of all of the samples in this series and all of the ECSA are larger than that of the Blanco Ag, but the difference in current densities are much smaller than the gain in ECSA. The total current density for the Blanco Ag sample is 0.587 mA/cm^2, the annealed sample with a 2.18 at% has an ECSA of ~2 times the size as the Blanco Ag sample but the current density is only 0.599 mA/cm^2. The annealed sample with a S content of 5.41 at% with a total current density of 0.767 mA/cm^2 and a ECSA of ~4 times as high as the Blanco Ag. From the SEM images it was qualitatively clear that it had the largest surface area of all the samples and this is also quantitatively affirmed by the ECSA measurements. The ECSA of the pre-reduced sample was ~9 times as large as the Blanco Ag but the current density is with 0.709 mA/cm^2 only 1.21 times as high.

Table 3 shows the ECSA results for the -0.8 V vs RHE series. The current densities for both the annealed (0.964 mA/cm^2) and pre-reduced (1.297 mA/cm^2) sample are higher than the Blanco Ag sample (0.774 mA/cm^2). But where the annealed sample has a roughly 4.7 times larger ECSA the current density is just ~1.25 times as high. And the pre-reduced sample has a 6.8 times higher ECSA but the current density is only 1.4 times higher.

4.6.1 Conclusion ECSA measurements

The ECSA measurements have given us more insight in the surface area that is actually used during the electrochemical conversion of CO_2. Although the ECSA for the annealed and pre-reduced samples is in the order of 2 till 9 times as high as the Blanco Ag samples, this is not true for the total current densities which is at most only 1.4 times as large as the Blanco Ag samples of the same potential set. It is possible that the surface of the samples is also energetically changed due to addition of S that would enable the formation of an oxide multilayer. This would explain the large differences in ECSA between the different samples, because from the SEM images it is questionable if some of the surfaces are really 9 times larger.

5 Discussion

In this chapter the results and outcomes of this thesis will be discussed.

5.1 Theory

Regarding the article of Lim *et al.*[1] there are a lot comments to be made. First of all by using DFT calculations it is possible to create an ideal world where atoms can be placed in every order, orientation, or place imaginable. Unfortunately the real, experimental world does not work like that. In the article by Lim *et al.*[1] they replaced in a set array of 4x4x3 Ag atoms one Ag atom with a S atom, in this way according to DFT calculations the overpotential would be lowered with more than 0.50 V, which is in the field of CO_2RR an impressive decrease of needed overpotential. But as stated before atoms in the real world do not abide rules set by a computer (i.e. human), they form energetically favourable structures. In the case of Ag and S that is acanthite, α-Ag_2S, as was shown with XRD. This also correlates with phase diagrams found in literature.[40] Furthermore it must be noted that the potentials cannot be regarded as absolute values because there is no mentioning of the type of electrolyte where the reactions would take place in. Another problem is leaching of S from the catalyst: the difference between the theoretical reduction overpotential and the theoretical leaching potential is -0.58 - -0.38 = 0.20 V. This is a very small potential window and little room to increase the current density by increasing the overpotential.

5.2 Samples

In total three methods were tried to dope an Ag surface, next to the annealed and pre-reduced samples doping through immersing the surface in a 1-Octanethiol solution was also tested. However the thiols formed on the surface of the Ag were too unstable and degraded within 24 hours, therefore this method was not further investigated.

Before polycrystalline Ag samples were used as the substrate a 300 nm Ag layer was sputtered on a polished and thoroughly cleaned Ti sample. The doping method was the same as used for the polycrystalline sample the only difference was the lower concentration of 0.1 mM S_8 instead of 1 mM S_8, because of a thinner Ag layer of 300 nm instead of 125 µm. When the samples were used for CO_2RR the layer of Ag at different potentials the layer Ag dissociated from the Ti substrate. This was the reason to stop using sputtered Ag but instead use an all Ag electrode as substrate for S doping.

It was hard to control the final amount of S in the Ag sample. Especially to control the temperature which had a direct correlation with the final S content. The subsequent step in the production had a very large effect on the final performance of the sample. The anneal treatment showed a better partial CO current density and a higher CO FE than the pre-reduced samples. Probably because the anneal treatment caused a better distribution across the Ag sample than the pre-reduced case, and therefore better resembling the proposed

system by Lim *et al*.[1] The pre-reduced samples on the other hand were doped for much longer times reaching higher S contents. This method was described by Huang *et al*[21]*.* In this research Cu_2O-derived Cu catalyst doped with S by immersing Cu in to an ammonium polysulfide solution. The S-doped Cu with a S content of 2.7 at% showed a very high selectivity towards formate with the highest current density. Huang *et al.*[21] used S because on a Pt surface it poisons the HER, something they also wanted to accomplish on the Cu catalyst. To see if the enhanced formate production was also seen at other similar catalysts (group 11) the S-doping was also tried on a cleaned but further no oxide derived Ag film. They tested an S-doped Ag catalyst with a S content of 1.9 at% and one with a S content of 15.7 at%. An increase in current density was found from -3.4 mA/cm^2 (Blanco Ag) to -9.8 mA/cm^2, and the FE increased from 73.5 to 88.4% for the S-doped Ag sample at an overpotential of -1.0 V vs RHE. Other than these results no other information is given about the results of the S-doped Ag catalyst (e.g. stability, electrochemical surface area, etc.). So the experiment was slightly adjusted with another S solution and a different pre-reducing overpotential. The formed Ag_2S layer on the top was very brittle and easily damaged when picked up with a tweezer. Because no anneal step was applied and the sample was immediately pre-reduced no re-distribution/diffusion step of the S atoms took place. By removing these S atoms the surface morphology was changed causing a more nano-structured surface.

Although there are more techniques to dope Ag with S it was decided to stick to the chemical bath deposition using an acetonitrile + S_8 solution. This was due to the simplicity, safety and if the energy transition is taken into account the electrochemical reduction should be implemented on a global scale and therefore it should be able to be implemented on a large scale.

With the help of ECSA measurements it was able to quantify the surface change of the samples which was clearly visible with SEM images. The pre-reduced samples had the largest ECSA followed by the annealed samples and the Blanco Ag had the smallest ECSA as expected. The change however between the Blanco Ag and the pre-reduced was almost 9 times in the most extreme case, this seems a bit much. This could be because of an energetically changed surface energy because of the doping with S. Causing multiple oxide layers to form on the surface of the sample, this would then again give a false representation of the surface area. A solution for this problem could be to use AFM together with ECSA measurements in this way it is possible to check the results of the ECSA.

5.3 Stability

The amount of CO produced for each sample decreased over the time the experiment was conducted. This is a normal phenomenon of Ag catalyst in the CO_2RR and could be because of the following reasons: Yano *et al.*[59] proposed that the decreased activity for CO formation was because of the forming of graphite on the surface of the electrode. In the first period of operation they measured a high CO FE but after approximately 10 minutes this decreased suddenly. When examined with EDX carbon and oxygen were present, they rule out the formation of adsorbed intermediates because they would be removed in the ultra-high vacuum of electron probe micro-analyser. In this research not at all samples carbon was detected in after GC EDX measurements but for some samples it was, this could be because

of graphite formation. Delacourt *et al.*[60] name another reason for the decrease of CO FE.[60] The increase of the HER current causes the pH of the electrolyte near the surface of the catalyst to rise, because of this rise the amount of dissolved CO_2 there will fall. Subsequently the amount of CO produced will decrease. Another reason for the decline in CO production could be impurities present in the electrolyte. Wuttig & Surendranath[61] investigated the poisoning effect of impurities on the CO_2RR capabilities of different electrodes. Even when very pure electrolyte salts and water were used for the electrolyte in a rotating disc experiment with an applied potential of -1.0 V vs RHE still traces of Zn and Pb were found on the surface of the electrode. These impurities caused the decrease of CO current density and increased the current density for H_2. These trace metals together with Pt which may came loose from the Pt counter electrode, diffused through the Nafion membrane and were adsorbed on the surface of the electrode. Subsequently formed CO on the surface of the catalyst poisoned the Pt which caused the decrease of CO production.

Besides the instability of CO production also the sample itself is not stable when a potential is applied to the sample. This followed from XRD and EDX measurements taken after GC operation. In all cases all of the S was lost. The XRD patterns did not show the characteristic α-Ag_2S patterns and in the EDX measurement no S was detected. Also SEM pictures have shown that the overall morphology changed by GC operation. This could be the cause of the S leaching out of, where S first was present in the structure of α-Ag_2S after GC it was gone, causing a more pored morphology. The leaching of S from the samples was also detected with CV measurements. Immediately after the beginning of the cathodic scan the reduction of S starts and reaches a peak at approximately -0.4 V vs RHE for all samples. Later in the voltammogram there appears another peak, -1.0 V vs RHE that is thought to be because of the reduction of S. Next to these S reduction peaks also the activity of the electrodes decreased over time which could cause a lower CO production and thus performance.

The ultimate goal of CO_2RR is to be a full-fledged alternative of fossil fuels for our carbon-based products. Therefore the catalysts need to be apart from efficient and highly active also durable. They need to be useable for long periods of times and should not be replaced very often, for this S-doped Ag catalyst it has been proven that it is not stable enough for large scale implementation.

5.4 Performance catalysts

The use of the GC together with potentiostat was the most important method to determine the performance of the catalysts. However during this thesis there were some problems with the GC. Multiple times it was down, mainly due to inadequate use that led to liquid injection into the GC. When liquid is injected into the GC this has to be removed with the help of a bake-out i.e. heating the system to evaporate all liquids inside. To maintain quality of the data a calibration should be performed after each bake out this was however after most of the bake-outs not the case. Ideally every month a calibration should be performed to safeguard the quality of the measurements.[35] But this influence was probably of a minor effect since the calibrations after different bake-outs were similar. The FE of the different samples especially at low overpotentials reached values as high as 180% but also sometimes very low with only 30%. The reason for these outliers was in all cases a very high amount of H_2 detected while at other moments virtually no H_2 was detected. When H_2 was

produced on the surface of the catalyst it was released in gaseous form and was (partly) dissolved in the catholyte. When the catholyte was saturated with H_2 the H_2 would be released to the overhead compartment of cathodic part of the electrochemical cell. Causing immediately a large spike in the H_2 production if at that moment of release the GC was injected with a sample. When a sample was injected just before a bubble of H_2 was released this could cause a very low amount of H_2 and therefore a very low overall FE. These extremities in measured H_2 were excluded from the data to ensure a total FE of approximately 100%. Next to the sudden release of large amounts of H_2, it is known that because of its small size it is hard to accurately measure H_2.[35] To check the quality of the measurements a base measurement was performed i.e. a normal GC measurement of an hour but without applied potential. This gave an average measured fraction of 28.3±1.5 ppm of H_2 and although this is a very small amount it gives insight in the difficulty to accurately determine the amount of H_2 formed. This value was subtracted from the measured H_2 to only take into account the amount H_2 produced.

These sudden increases in production were not measured for CO, the CO production did however decline after long operation but this was believed to be caused by inactivation of the catalyst as described before and will be discussed in more detail later.

Another problem regarding GC measurements was the flow rate of CO_2 into the electrochemical cell. The flow of CO_2 was controlled by a mass flow controller (MFC) (EL-FLOW, Bronkhorst) but it was suspected that this MFC did not gave a good result i.e. the set values on the MFC did not agree the real values of supplied gas. To check these values the flow of the MFC was measured with a flowmeter (ProFLOW 6000, Restek) and when needed adjusted on the MFC. This could however been a mistake since where the MFC was calibrated for CO_2 the flowmeter could be used to measure all gases and was not calibrated to only measure CO_2.

When the results of the different samples are examined it is seen that the annealed samples show a higher CO FE at lower overpotentials especially at -0.4 and -0.55 V vs RHE. At -0.55 V vs RHE an increase of more than 3 times the CO FE of an Ag Blanco sample at that overpotential. But it has to be noted that because of imperfect cell design some (abnormal) measured points were excluded from the data.

At -0.7 V vs RHE two annealed samples were tested, the one with a S content of 5.41 % had an increased CO FE of 23% in comparison with the Blanco Ag sample. The annealed sample with a S content of 2.18% had an increased CO FE of 80% in comparison with the Blanco Ag sample. At the highest overpotential tested (-0.8 V vs RHE) the Blanco Ag sample has the highest CO FE of all samples with 4.1% followed by the annealed sample with 3.5% and the lowest CO FE is from the pre-reduced sample with 0.7%. So it seems the addition of S is beneficial for the CO FE in the overpotentials of -0.7 V vs RHE and lower. Also the activity for CO production increases over sevenfold at the potential of -0.55 V vs RHE. At -0.7 V vs RHE the current density increases in comparison with the Blanco Ag over 60% for the annealed sample with 5.41 at% S and ~83% for the sample with 2.18 at% S. This is a significant increase and also the amount of S calculated by Lim *et al*.[1] is in line with this result. At an overpotential of -0.8 V vs RHE the CO FE of the Blanco Ag sample is higher with 4.1% in comparison with the annealed sample with a CO FE of 3.5% but the total current density of the annealed sample is with 0.97 mA/cm^2 higher than that of the Blanco Ag sample with

0.797 mA/cm^2. Therefore the partial CO current density is also higher for the annealed sample with 0.034 mA/cm^2 vs 0.032 mA/cm^2 which is an increase of 6.7%. Also for the activity of the samples the addition of S seems beneficial.

Although the annealed samples performed in comparison with the Blanco Ag very good the other S-doped samples performed the worst of all samples, the pre-reduced samples. With negligible CO FE's and CO current densities but with very high H_2 current densities.

A possible explanation for the poor CO current density and CO FE of the pre-reduced samples could be the increased amount of S-vacancies that are there because of the longer immersion time and the pre-reducing of the sample. The influence of S-vacancies is also seen in MoS_2 where the increase in S-vacancies causes enhanced HER.[62] This enhanced HER reaction could cause a suppressing effect on the CO formation in the pre-reduced samples. Although Ag is a different material this good be an explanation for the enhanced HER that is seen with the pre-reduced samples. This could also be an explanation why annealed samples with a higher S content had higher H_2 current densities.

If we however compare the results of this thesis with results recorded in literature it does not look very good. Polycrystalline flat surface Ag catalyst reaches in literature[18,36,37] at -0.7 V vs RHE an CO FE of 10% and at -0.8 V vs RHE 20%. In this thesis for a polycrystalline flat surface Ag sample only a CO FE of 1.08% was measured and at -0.8 V vs RHE only 4.14%. Also the CO current density is compared with literature was low, were Hatsukade *et al.*[18] at -0.7 V vs RHE measured a CO current density of 0.03 mA/cm^2 and Ma *et al.*[36] at the same potential measured 0.05 mA/cm^2. At -0.8 V vs RHE Hatsukade *et al.*[18] measured 0.3 mA/cm^2 and Ma *et al.*[36] measured a CO current density of 0.2 mA/cm^2. While in this research for the Blanco Ag sample at -0.7 V vs RHE a CO current density of 0.0064 mA/cm^2 was measured and at -0.8 V vs RHE a CO current density of 0.032 mA/cm^2 was measured also for a Blanco Ag sample. The annealed samples in this thesis had higher CO current densities than the Blanco Ag samples but these were not orders of magnitude larger therefore the comparison with the Blanco Ag samples from this thesis with polycrystalline Ag from literature is justified. At -0.7 V vs RHE the CO current density in literature is 5-8 times larger and at -0.8 V vs RHE it is 6-9 times larger.

So the samples tested in this thesis all performed less than results published in literature. If these poor results (i.e. CO current density and CO FE) together with the instability of the samples both in CO production as in the loss of all S are put together a possible explanation for this behaviour could be the reason why in the first place the doped samples perform better, the addition of S. In the first moments when looking at the CO production over time the S seems to be beneficial to the CO production. But since all S was lost during experiments in the electrochemical cell for all samples at all potentials, which was proven by CV, XRD, GIXD and EDX. This S that was leached out of could have formed a layer or in another way block the sites that were used for the reducing of CO_2 to CO. The pre-reduced samples which probably had a higher S content, because of longer immersion time, were faster poisoned by S than the annealed samples that had probably a lower S content. The S that was leached out the samples even affected the cell and the tip of the reference electrode. PMMA, which is colourless and transparent, became more opaque by a thin black tarnish layer just as the tips of the reference electrodes that turned black. This layer of S therefore also affected the Blanco Ag samples that also performed not as good as they

should in S-free environment. Thus it is believed that the use of S at first sight is beneficial but eventually suppresses the CO_2 reducing capabilities.

The intention of this research was to look into the effect of S on the electrochemical reduction of CO_2 to CO on an Ag flat surface. From the start it was suspected that the CO current densities and CO FE measured would not be as high as the best results in literature since effective and proven changes on the surface morphology were deliberately not performed to look solely at the effect of S. Therefore comparing the samples of this research with the best results in literature is not very useful. But it was not expected that the performance was this poor even in comparison with flat polycrystalline Ag.

6 Conclusion

By examining available literature on the subject and conducting various experiments it is now possible to answer the sub-questions and finally the main research question.

Two methods were investigated to dope an Ag electrode with the desired ~2.1 at% S. The method where Ag samples were immersed in a solution of acetonitrile and S_8 and were post-treated with an anneal treatment was the best method to produce the S-doped samples. The other method that included a pre-reducing after treatment gave lesser results.

To see the effect of the S on the Ag the different samples were characterized and tested with SEM, EDX, XRD, GIXD, CV, GC and ECSA. The doping step caused S to get included into the structure of the Ag samples and thereby also changing the morphology of the electrode. Samples that were produced with the annealing step saw an increased CO FE and CO current density at the lower overpotentials. At the highest overpotential the Blanco Ag sample had a higher CO FE. Samples produced with the help of the pre-reduction method showed poor results at both the CO FE as well the CO current density. A possible explanation for this result could be the large amount of S-vacancies in the sample.

During operation the CO production of all the sampled decreased over time, this issue was most clearly seen with the pre-reduced samples. This phenomenon could be caused by S that was leached out of samples and thereby suppressing the CO_2 reduction towards CO. The leaching of the S happened at all potentials with every doped sample, therefore the S-doped samples were assessed as unstable.

When the results of the experiments conducted in this thesis were compared to the literature it was found that all samples show a very poor result both in CO FE as in CO current density. So although it was expected that S would enhance the CO_2 reducing capabilities towards CO, the in comparison poor results and instability of the samples make S-doped flat surface Ag electrodes not qualified for the task of CO_2 reduction.

7 Future outlook

Probably the S content of the Ag samples were a lot higher because of measurement restrictions of EDX. A solution to overcome this fundamental problem is to use XPS instead which can solely focus on the top layer of the sample. Although the CBD technique is very simple, safe and easy to scale up it is still hard to control, so it is recommended to look into other techniques. To get more insight in the reactions happening at the surface, CV should be performed in a CO_2-free electrolyte to see if certain peaks are really caused by CO_2 intermediates. The CO_2RR should thereby also be tried in a different electrolyte, a slight alkaline environment could have a positive effect on the leaching potential of S. Although the addition of S is beneficial to the efficiency of the catalyst all of the S is lost and therefore probably also its positive effect. The leaching of S out of Ag makes S-doped Ag catalyst therefore unfit for large-scale implementation which is eventually our main goal: producing fuels and plastics from CO_2 from the air so the amount of atmospheric CO_2 will not increase. Unless this leaching problem is not resolved the experimental work done on the doping of Ag with S it is better to cease investigation in this subject and focus on other techniques that have proven to work or are promising. This can also be concluded if we compare the outcome of the GC experiments, the results are consistently less than results showed in literature.

However from a more fundamental science point of view it is very interesting to further look into S-doping since it can also learn us more about the general aspects of doping which can help us further. Also literature shows us promising results where S-doped Ag can be really beneficial to the performance of the electrode. However the doping of a flat Ag surface as performed in this thesis has probably no future.

8 Appendices

8.1 SEM

Figure 52 shows an EDX energy table which is used to estimate the penetration depth of the electrons used in EDX. To find the penetration depth 2 parameters are needed the density (kg/m^3) of the material that is analysed and the voltage used in operation (kV). The density of Ag is 10.49 kg/m^3 but since the Ag is S-doped (ρ_{Ag2S} = 7.23 kg/m^3) the density is set to 9.50 kg/m^3. The voltage used in EDX operation is 20 kV. When a line is drawn from the density scale bar through the voltage scale bar with the help of the previous stated values and this line is extended to the last scale bar, the penetration depth is found to be approximately 1.2 µm.

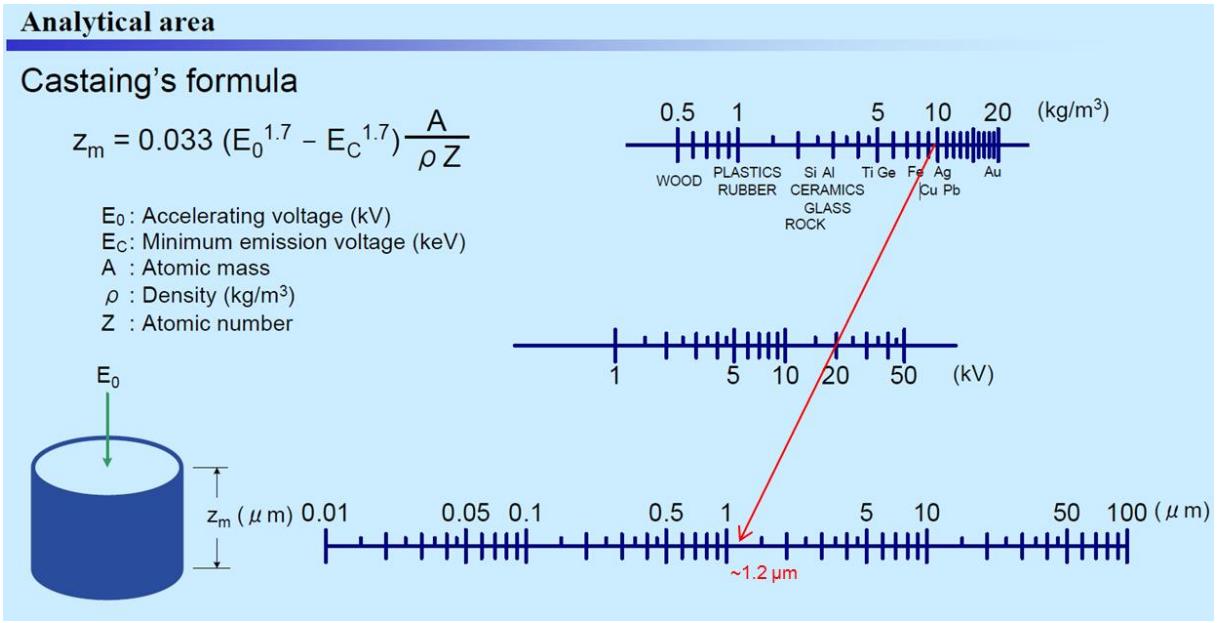

Figure 52: Energy table for EDX penetration depth analysis. Including line for the estimation of penetration depth of S-doped Ag.[63]

Table 4: Overview samples used in this thesis

Code	Type	Test	Overpotential V vs RHE	EDX 1			EDX 2			EDX 3			EDX Average			ECSA (mC/cm^2)
				Ag at%	*S at%*	*C at%*	*Ag at%*	*S at%*	*C at%*	*Ag at%*	*S at%*	*C at%*	*Ag at%*	*S at%*	*C at%*	
1-1*	Annealed	GC	-0.4 V vs RHE	83.61	3.09	13.3	83.72	3.76	12.52	82.77	2.98	14.25	86.6	3.39	10.02	1.142
3-B	Blanco Ag	GC	-0.55 V vs RHE	-	-	-	-	-	-	-	-	-	-	-	-	0.441
01	Annealed	GC	-0.55 V vs RHE	80.34	5.88	13.78	81.99	5.43	12.58	80.66	5.27	14.06	81.00	5.53	13.47	1.974
B-2	Pre-reduced	PR**	-0.55 V vs RHE	71.43	9.29	19.28	74.27	8.87	16.85	89.09	10.91	0	78.26	9.69	12.05	-
B-2	Pre-reduced	GC	-0.55 V vs RHE	100	0	0	100	0	0	100	0	0	100.00	0.00	12.04	2.43
2-B	Blanco Ag	GC	-0.7 V vs RHE	-	-	-	-	-	-	-	-	-	-	-	-	0.614
2-1	Annealed	GC	-0.7 V vs RHE	80.44	4.87	14.70	79.65	5.64	14.71	79.95	5.71	14.34	80.01	5.41	14.58	2.474
2-4	Annealed	GC	-0.7 V vs RHE	83.86	2.05	14.09	84.53	2.2	13.28	85.44	2.3	12.25	84.61	2.18	13.21	1.244
C-1	Pre-reduced	PR	-0.7 V vs RHE	88.79	11.21	0	89.61	10.39	0	89.08	10.92	0	89.16	10.84	0.00	-
C-1	Pre-reduced	GC	-0.7 V vs RHE	96.42	3.58	0	95.83	4.17	0	96.96	3.04	0	96.40	3.60	0.00	5.563

Code	Type	Test	Overpotential V vs RHE	EDX 1			EDX 2			EDX 3			EDX Average			ECSA (mA/cm^2)
				Ag at%	*S at%*	*C at%*	*Ag at%*	*S at%*	*C at%*	*Ag at%*	*S at%*	*C at%*	*Ag at%*	*S at%*	*C at%*	
A-B	Blanco Ag	GC	-0.8 V vs RHE	-	-	-	-	-	-	-	-		-	-	-	0.442
2-2	Annealed	GC	-0.8 V vs RHE	13.04	2.15	84.81	14.18	2.95	82.87	13.15	3.03	83.82	13.46	2.71	83.83	2.064
B-3* **	Pre-reduced	PR	-0.8 V vs RHE	84.76	15.24	0	84.42	15.58	0	-	-	-	84.59	15.41	0.00	-
B-3	Pre-reduced	GC	-0.8 V vs RHE	81.13	4.33	14.54	96.49	3.51	0	83.16	4.16	12.4	86.93	4.00	8.98	3.013
1-CV	Annealed	CV	-0.8 - 0.8 V vs RHE	82.52	4.15	13.33	80.74	4.05	15.21	81.63	4.44	13.93	81.63	4.21	14.16	
2-5*	Annealed	CV	-1.4 - 0.0 V vs RHE	95.86	4.14	0	81.7	4.28	14.02	96.34	3.66	-	92.3	4.2	3.51	
3-B-CV	Blanco Ag	CV	-1.4 - 0.0 V vs RHE	-	-	-	-	-	-	-	-	-	-	-	-	
B-1	Pre-reduced	PR	-1.4 - 0.0 V vs RHE	88.39	11.61	0	87.79	12.21	0	-	-	-	88.09	11.91	0.00	
B-1	Pre-reduced	CV	-1.4 - 0.0 V vs RHE	93.38	6.62	0	93.29	6.71	0	81.39	4.76	13.85	89.35	6.03	4.62	

***4 EDX measurements**

****Pre-reduction, S content is S content before pre-reduction.**

*****2 EDX measurements**

8.2 XRD

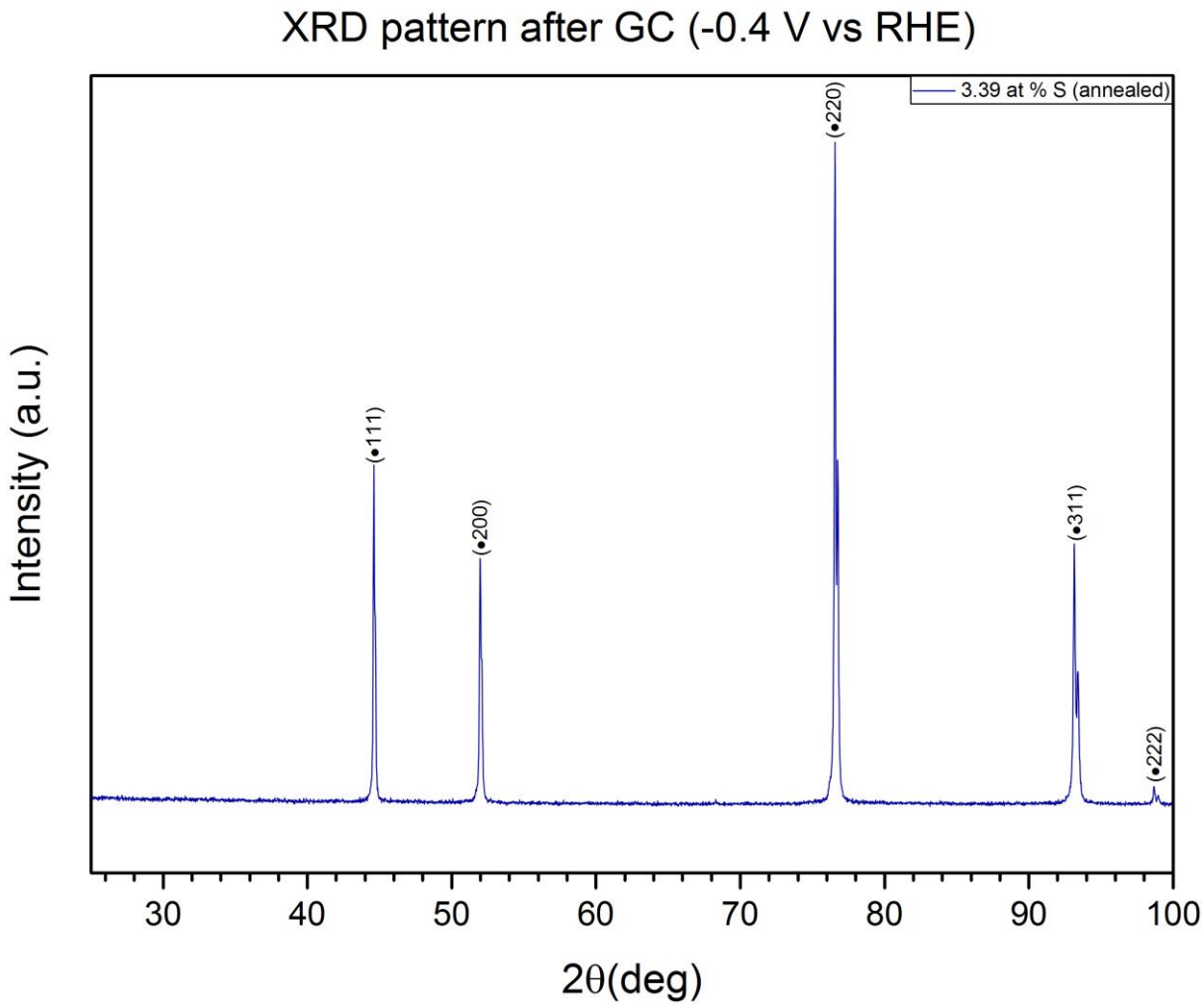

Figure 53: XRD pattern annealed sample after GC operation at -0.4 V vs RHE. Peaks marked with • represent reflections of Ag metal.

In Figure 53 the XRD pattern of annealed sample after GC operation at -0.4 V vs RHE is shown. This pattern is very similar to all of the patterns of the different samples in Figure 30.

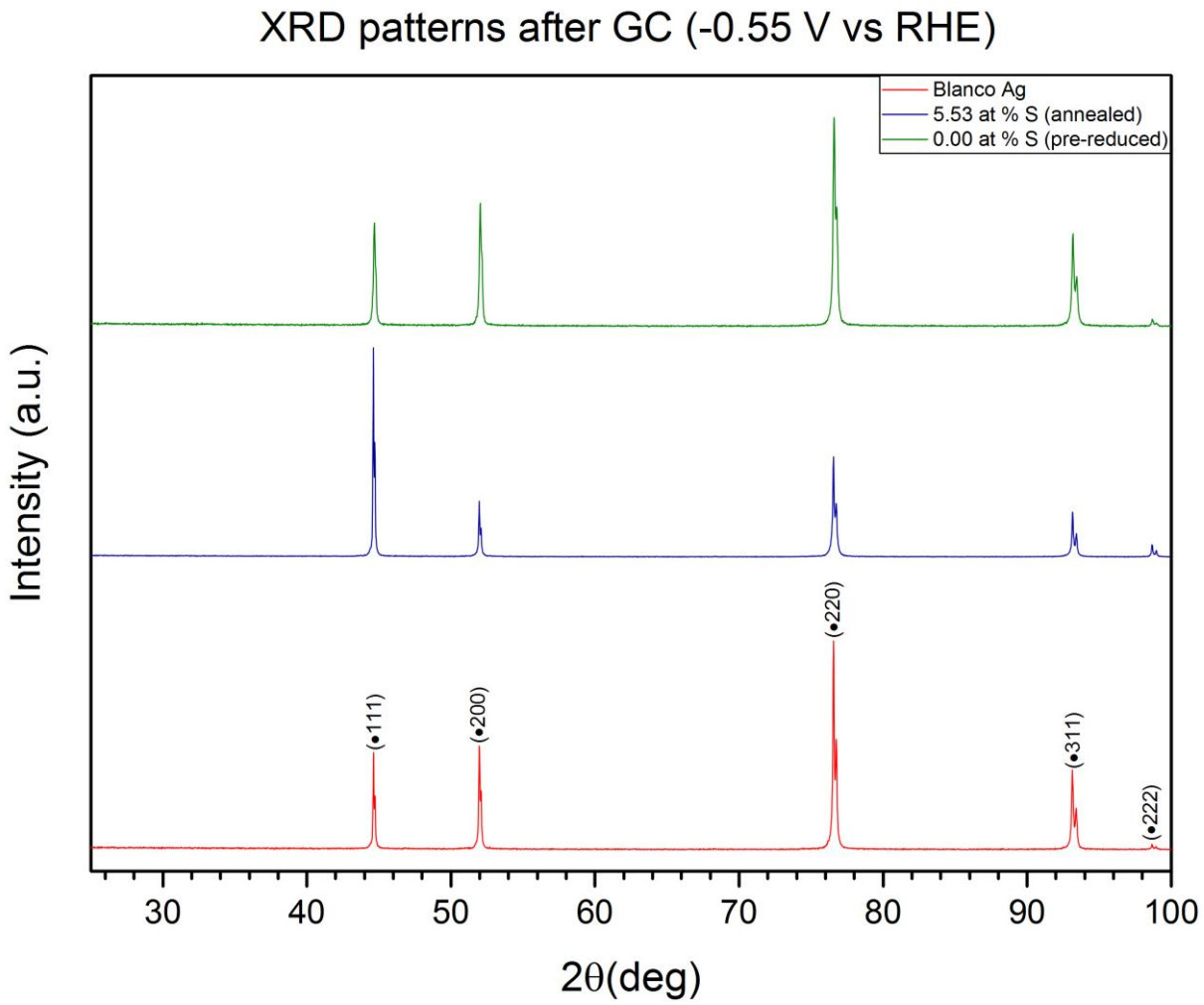

Figure 54: XRD patterns different samples after GC operation at -0.55 V vs RHE. Peaks marked with ● represent reflections of Ag metal.

In Figure 54 the XRD patterns of the samples tested at -0.55 V vs RHE are shown. At this overpotential the annealed sample performed by far the best as can be seen in the Gas Chromatography section of this report. The pre-reduced sample had a S content of 0.00 at% due to too long pre-reducing therefore the XRD pattern is almost similar to that of the Blanco Ag sample. The pattern of the annealed sample is similar to that of the GIXD pattern of the annealed samples with a very intense (111) peak, however the (200) and (220) peak are not that intense.

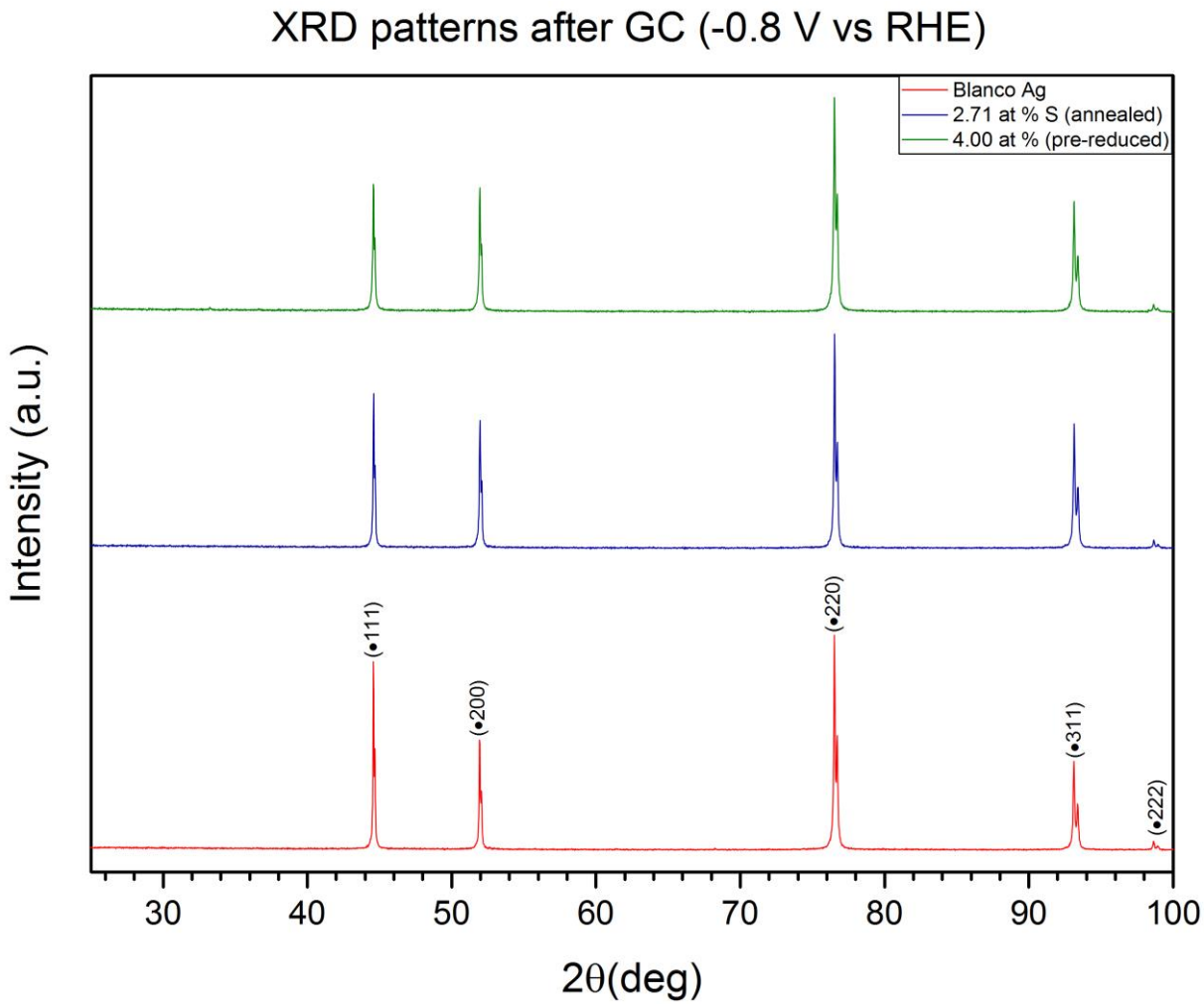

Figure 55: XRD patterns different samples after GC operation at -0.8 V vs RHE. Peaks marked with • represent reflections of Ag metal.

In Figure 55 the XRD patterns of the samples tested at -0.8 V vs RHE are shown. At this overpotential the annealed sample had the highest CO current density and the Blanco Ag sample had the highest CO FE as stated in the Gas Chromatography section of this thesis. The XRD patterns are however very similar. The only difference is the relation between the intensity of the (111) and (200) peak. A possible explanation for the difference in CO current density could be the intensity of the (111) peak. This is also explained in the XRD section of this report.

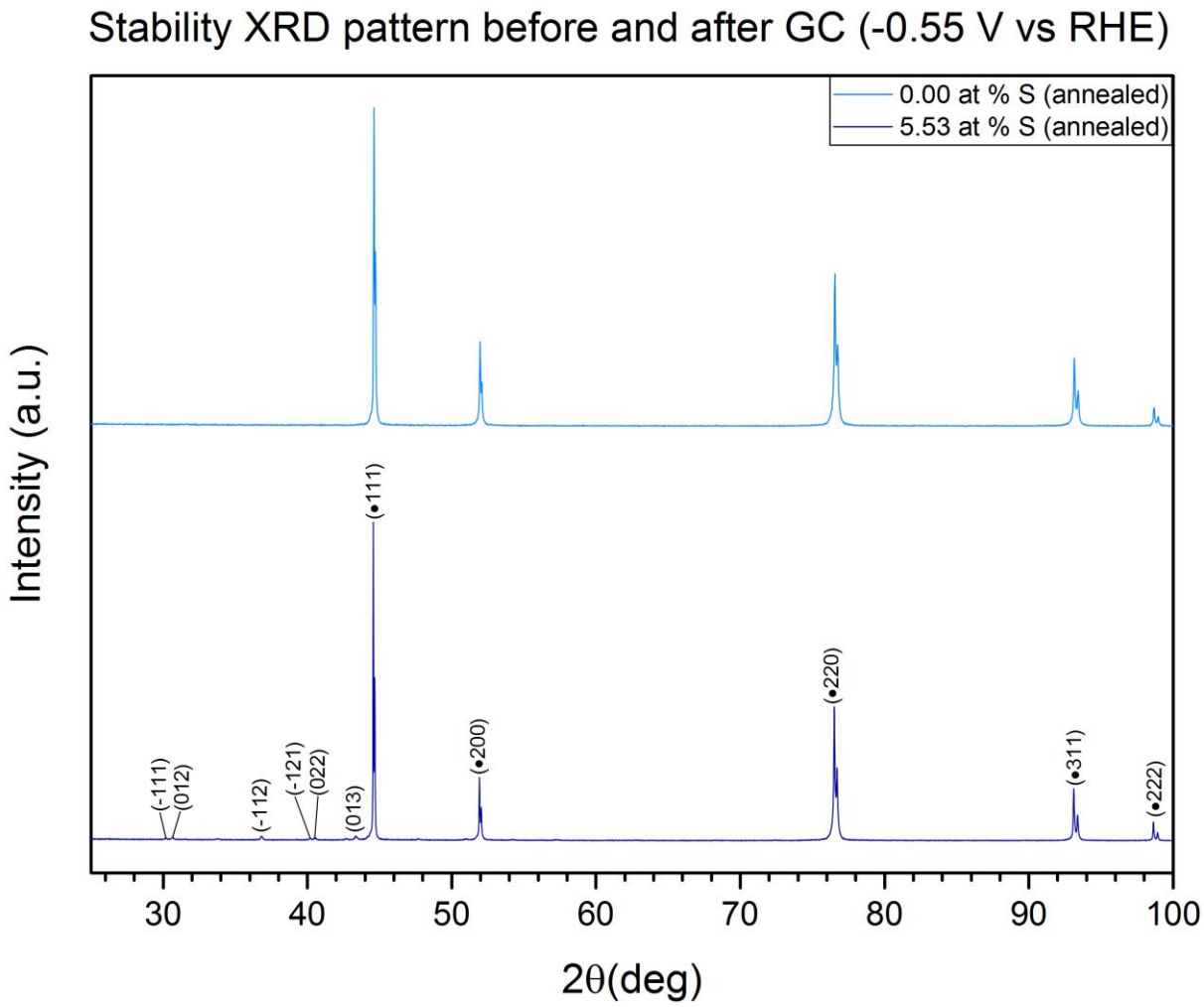

Figure 56: XRD patterns annealed sample before and after GC operation at -0.55 V vs RHE. The light blue pattern is the 'before GC' diffraction pattern and the dark blue is the 'after GC' pattern. Peaks marked with ● represent reflections of Ag metal.

In Figure 57 the XRD pattern of an annealed sample before and after GC operation at -0.55 V vs RHE is shown. It is clearly seen that the metallic-Ag peaks are not really affected by GC operation but that the α-Ag_2S peaks are all gone after GC operation.

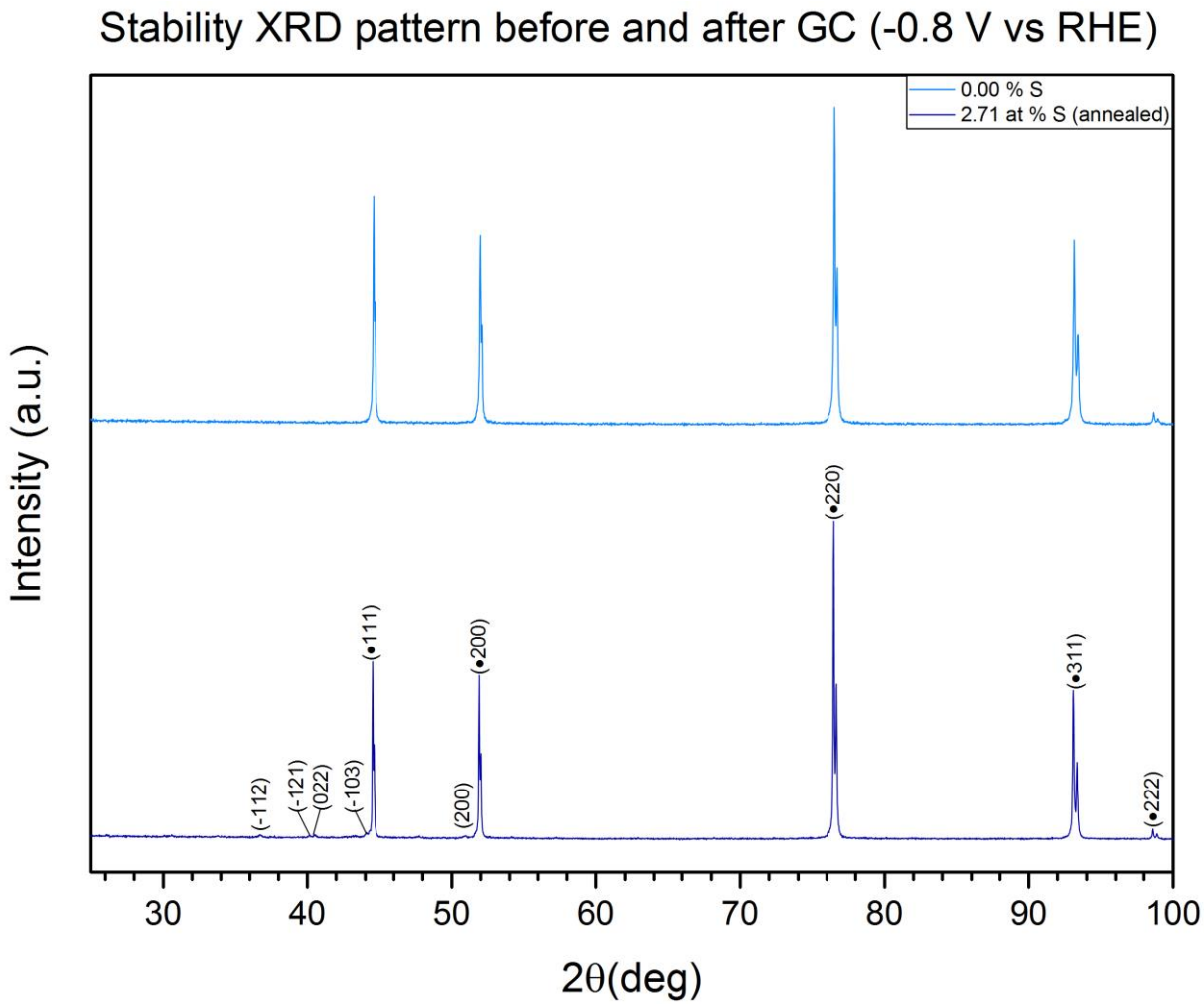

Figure 57: XRD patterns annealed sample before and after GC operation at -0.8 V vs RHE. The light blue pattern is the 'before GC' diffraction pattern and the dark blue is the 'after GC' pattern. Peaks marked with ● represent reflections of Ag metal.

In Figure 57 the XRD pattern of an annealed sample before and after GC operation at -0.8 V vs RHE is shown. It is clearly seen that the metallic-Ag peaks are not really affected by GC operation but that the α-Ag_2S peaks are all gone after GC operation.

8.3 ECSA

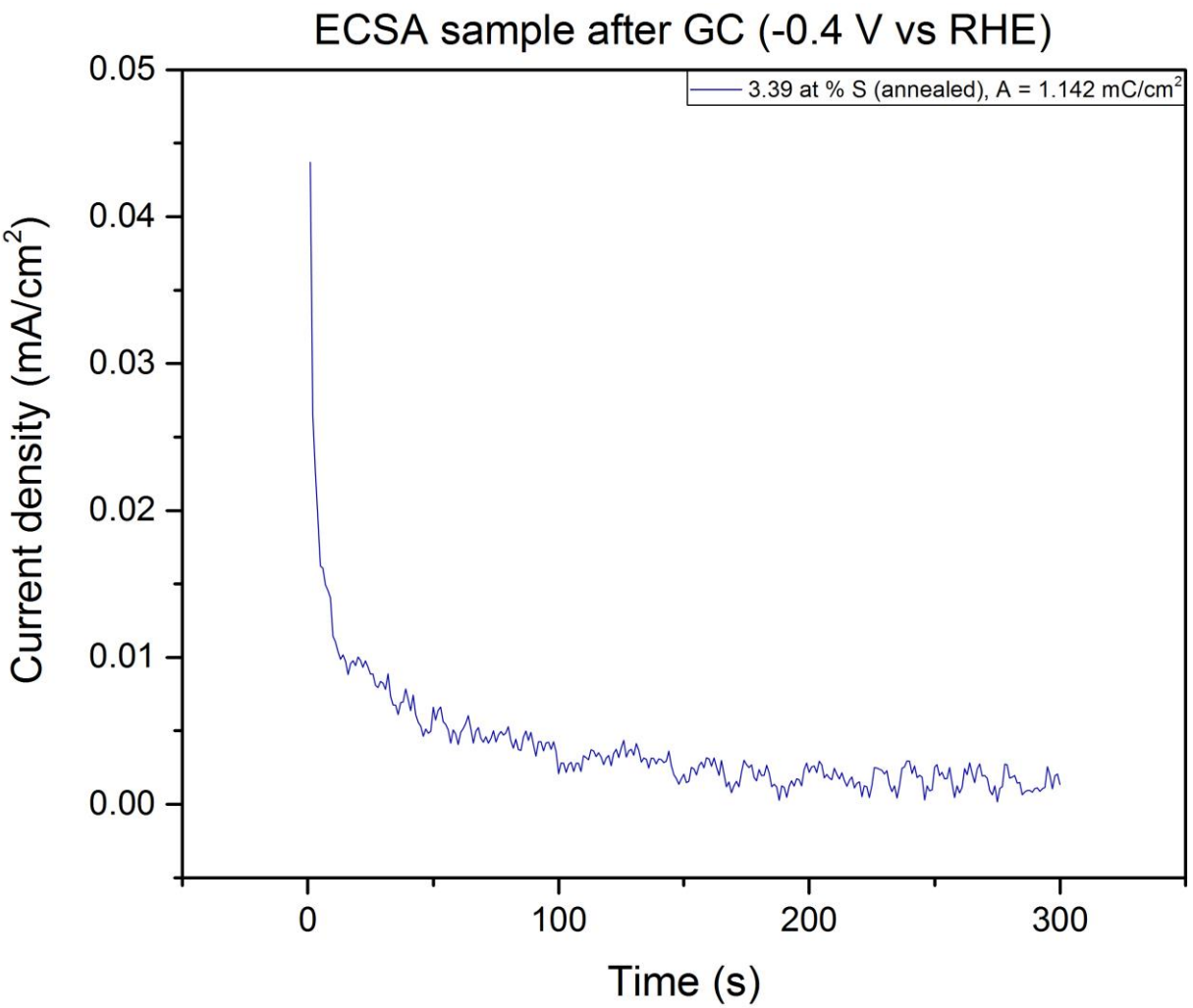

Figure 58: ECSA of an annealed sample after GC operation at -0.4 V vs RHE.

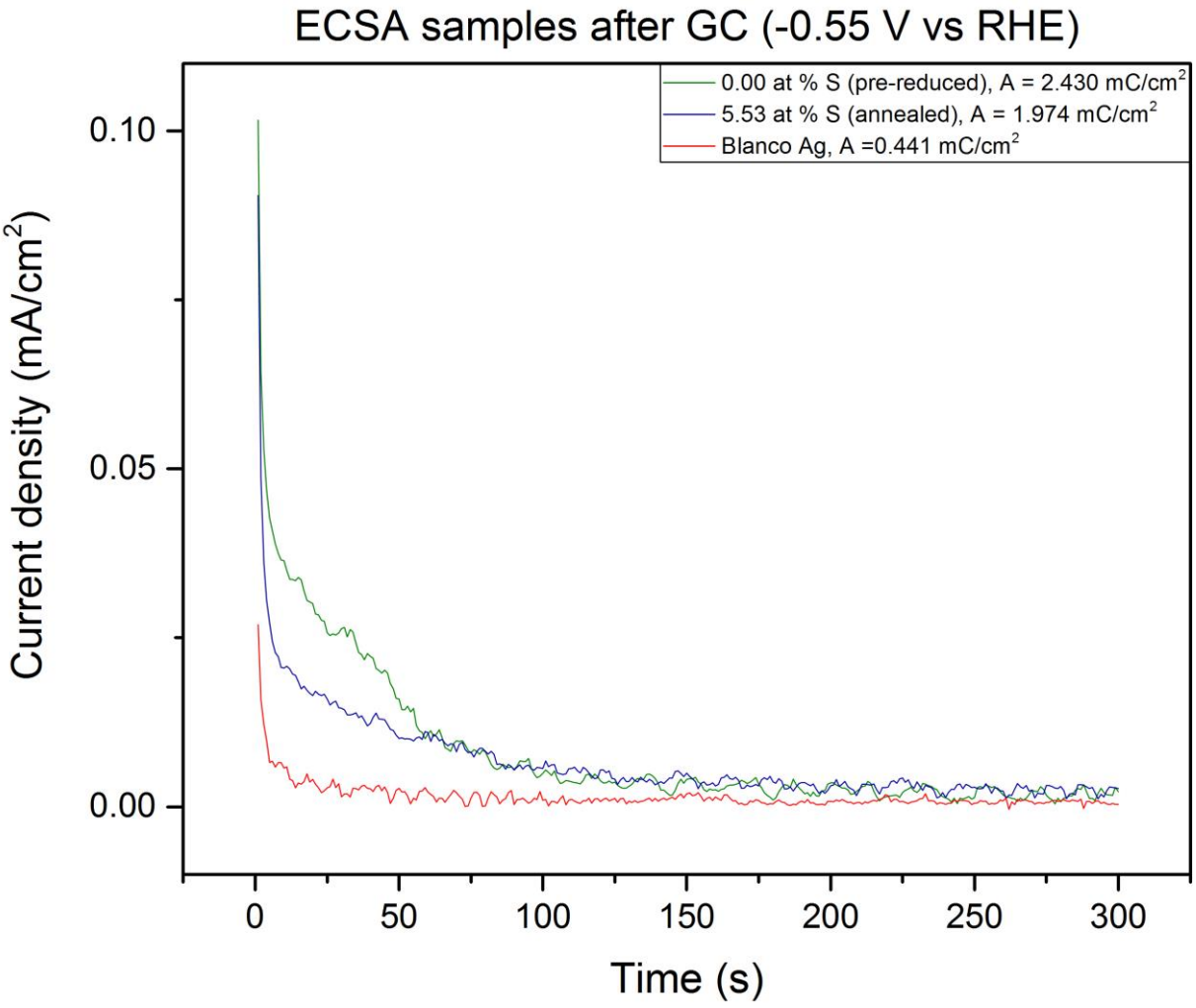

Figure 59: ECSA of annealed, pre-reduced and Blanco Ag sample after GC operation at -0.55 V vs RHE.

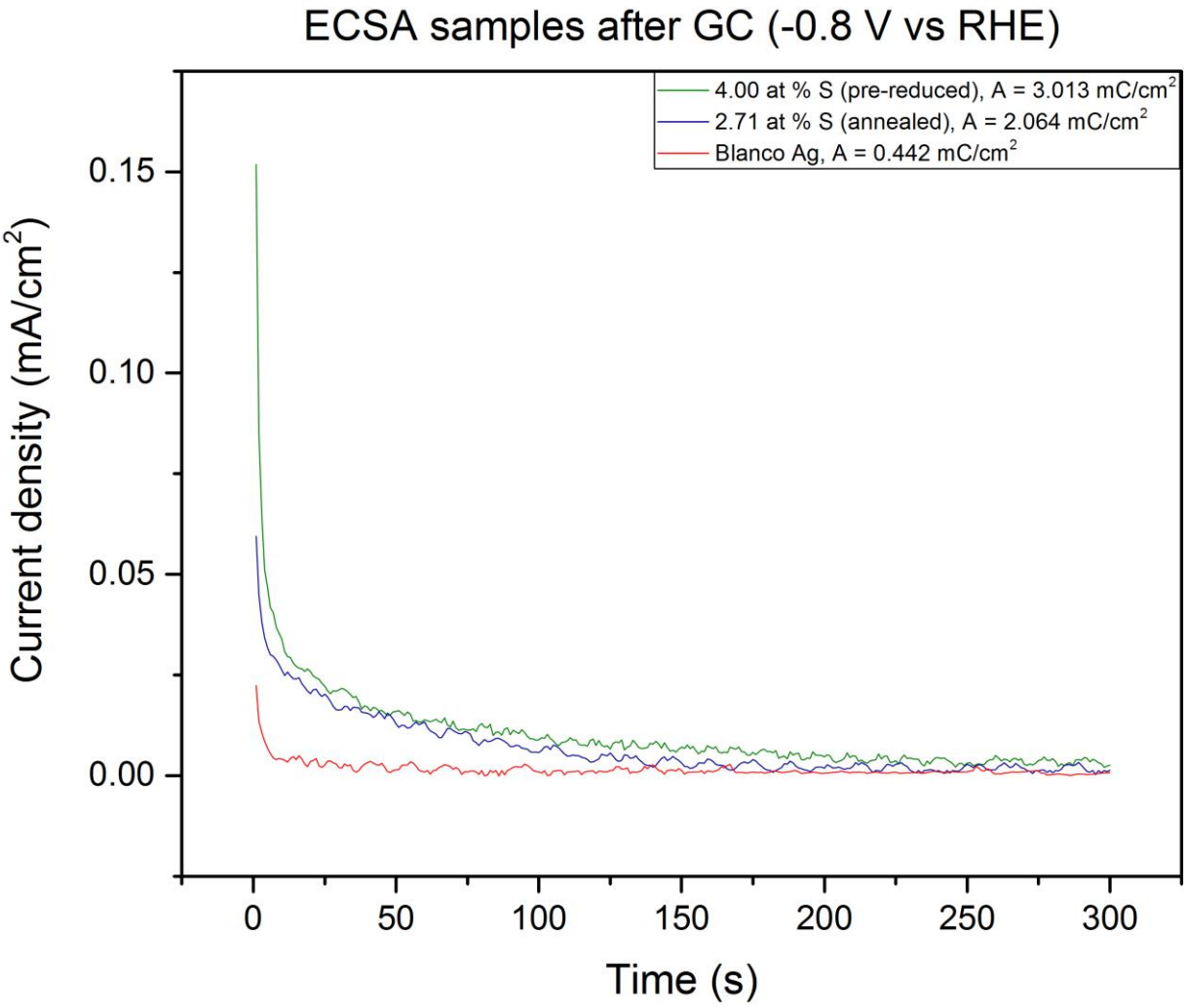

Figure 60: ECSA of annealed, pre-reduced and Blanco Ag samples after GC operation at -0.8 V vs RHE.

Table 5: ECSA of the annealed sample that was tested at -0.4 V vs RHE in the electrochemical cell.

Type	S content (at%)	ECSA (mC/cm^2)	Normalized ESCA
*Monolayer Ag_2O or AgOH on Ag**	-	0.400	1
Annealed	3.39	1.142	2.855

* There was no Blanco Ag sample tested at -0.4 V vs RHE therefore the theoretical value of a single monolayer of Ag_2O or AgOH on an Ag surface was used as a reference surface area.

9 Bibliography

1. Lim, H.-K. *et al.* Embedding Covalency into Metal Catalysts for Efficient Electrochemical Conversion of CO 2. *J. Am. Chem. Soc.* **136,** 11355–11361 (2014).

2. Le Quéré, C. *et al.* Global Carbon Budget 2016. *Earth Syst. Sci. Data* **8,** 605–649 (2016).

3. Ruddiman, W. F. The Anthropocene. *Annu. Rev. Earth Planet. Sci* **41,** 45–68 (2013).

4. Archer, D. *et al.* Atmospheric Lifetime of Fossil Fuel Carbon Dioxide. *Annu. Rev. Earth Planet. Sci.* **37,** 117–134 (2009).

5. Lewis, S. L. & Maslin, M. A. Defining the Anthropocene. *Nature* **519,** 171–180 (2015).

6. Scripps Institution of Oceanography. Keeling Curve. *Scripps Institution of Oceanography* (2018). Available at: https://scripps.ucsd.edu/programs/keelingcurve/. (Accessed: 27th March 2018)

7. Ramanathan, V. & Feng, Y. Air pollution, greenhouse gases and climate change: Global and regional perspectives. *Atmos. Environ.* **43,** 37–50

8. IPCC. *Fifth Assesment Report. Summary for Policy Makers*. *Climate Change 2014: Impacts, Adaptation and Vulnerability - Contributions of the Working Group II to the Fifth Assessment Report* (2014).

9. UNFCC. United Nations Framework Convention on Climate Change. *Rev. Eur. Community Int. Environ. Law* **1,** 270–277 (1992).

10. UNFCCC. Paris Agreement. *Conf. Parties its twenty-first Sess.* **58,** 32 (2015).

11. Agency, I. E. *Key world energy statistics*. (2017).

12. Mulder, F. M. Implications of diurnal and seasonal variations in renewable energy generation for large scale energy storage. *J. Renew. Sustain. Energy* **6,** 033105 (2014).

13. Kyriakopoulos, G. L. & Arabatzis, G. Electrical energy storage systems in electricity generation: Energy policies, innovative technologies, and regulatory regimes. *Renew. Sustain. Energy Rev.* **56,** 1044–1067 (2016).

14. Soloveichik, G. L. Battery Technologies for Large-Scale Stationary Energy Storage. *Annu. Rev. Chem. Biomol. Eng.* **2,** 503–527 (2011).

15. Pires, J. C. M., Martins, F. G., Alvim-Ferraz, M. C. M. & Simões, M. Recent developments on carbon capture and storage: An overview. *Chem. Eng. Res. Des.* **89,** 1446–1460 (2011).

16. Kumar, B. *et al.* New trends in the development of heterogeneous catalysts for electrochemical CO2 reduction. *Catal. Today* **270,** 19–30 (2016).

17. Zhu, D. D., Liu, J. L. & Qiao, S. Z. Recent Advances in Inorganic Heterogeneous Electrocatalysts for Reduction of Carbon Dioxide. *Adv. Mater.* **28,** 3423–3452 (2016).

18. Hatsukade, T., Kuhl, K. P., Cave, E. R., Abram, D. N. & Jaramillo, T. F. Insights into the electrocatalytic reduction of CO 2 on metallic silver surfaces. *Phys. Chem. Chem. Phys.* **16,** 13814–13819 (2014).

19. Durst, J. *et al.* Electrochemical CO2 Reduction – A Critical View on Fundamentals, Materials and Applications. *Chim. Int. J. Chem.* **69,** 769–776 (2015).

20. Rosen, J. *et al.* Mechanistic Insights into the Electrochemical Reduction of CO2 to CO on Nanostructured Ag Surfaces. *ACS Catal.* **5,** 4293–4299 (2015).

21. Huang, Y., Deng, Y., Handoko, A. D., Goh, G. K. L. & Yeo, B. S. Rational Design of Sulfur-Doped Copper Catalysts for the Selective Electroreduction of Carbon Dioxide to Formate. *ChemSusChem* **11,** 320–326 (2018).

22. Shinagawa, T., Larrazábal, G. O., Martín, A. J., Krumeich, F. & Pérez-Ramírez, J. Sulfur-Modified Copper Catalysts for the Electrochemical Reduction of Carbon Dioxide to Formate. *ACS Catal.* **8,** 837–844 (2018).

23. Yoo, J. S., Christensen, R., Vegge, T., Nørskov, J. K. & Studt, F. Theoretical Insight into the Trends that Guide the Electrochemical Reduction of Carbon Dioxide to Formic Acid. *ChemSusChem* **9,** 358–363 (2016).

24. Peterson, A. A. & Nørskov, J. K. Activity descriptors for CO 2 electroreduction to methane on transition-metal catalysts. *J. Phys. Chem. Lett.* **3,** 251–258 (2012).

25. Kuhl, K. P. *et al.* Electrocatalytic conversion of carbon dioxide to methane and methanol on transition metal surfaces. *J. Am. Chem. Soc.* **136,** 14107–14113 (2014).

26. Huang, Y., Handoko, A. D., Hirunsit, P. & Yeo, B. S. Electrochemical Reduction of CO 2 Using Copper Single-Crystal Surfaces: Effects of CO* Coverage on the Selective Formation of Ethylene. *ACS Catal.* **7,** 1749–1756 (2017).

27. Albo, J. *et al.* Copper-Based Metal–Organic Porous Materials for CO2 Electrocatalytic Reduction to Alcohols. *ChemSusChem* **10,** 1100–1109 (2017).

28. Lu, Q. & Jiao, F. Electrochemical CO2 reduction: Electrocatalyst, reaction mechanism, and process engineering. *Nano Energy* **29,** 439–456 (2016).

29. Wu, J. *et al.* Incorporation of Nitrogen Defects for Efficient Reduction of CO2via Two-Electron Pathway on Three-Dimensional Graphene Foam. *Nano Lett.* **16,** 466–470 (2016).

30. Feng, D.-M., Zhu, Y.-P., Chen, P. & Ma, T.-Y. Recent Advances in Transition-Metal-Mediated Electrocatalytic CO2 Reduction: From Homogeneous to Heterogeneous Systems. *Catalysts* **7,** 373 (2017).

31. Lu, Q., Rosen, J. & Jiao, F. Nanostructured metallic electrocatalysts for carbon dioxide reduction. *ChemCatChem* **7,** 38–47 (2015).

32. Grote, J. P. *et al.* Screening of material libraries for electrochemical CO2 reduction catalysts – Improving selectivity of Cu by mixing with Co. *J. Catal.* **343,** 248–256 (2016).

33. Kortlever, R., Shen, J., Schouten, K. J. P., Calle-Vallejo, F. & Koper, M. T. M. Catalysts and Reaction Pathways for the Electrochemical Reduction of Carbon Dioxide. *J. Phys. Chem. Lett.* **6,** 4073–4082 (2015).

34. Verma, S., Kim, B., Jhong, H. R. M., Ma, S. & Kenis, P. J. A. A gross-margin model for defining technoeconomic benchmarks in the electroreduction of CO2. *ChemSusChem* **9,** 1972–1979 (2016).

35. Pander III, J. E., Ren, D. & Yeo, B. S. Practices for the collection and reporting of electrocatalytic performance and mechanistic information for the CO_2 reduction reaction. *Catal. Sci. Technol.* **7,** 5820–5832 (2017).

36. Ma, M., Trześniewski, B. J., Xie, J. & Smith, W. A. Selective and Efficient Reduction of Carbon Dioxide to Carbon Monoxide on Oxide-Derived Nanostructured Silver Electrocatalysts. *Angew. Chemie - Int. Ed.* **55,** 9748–9752 (2016).

37. Hsieh, Y.-C., Senanayake, S. D., Zhang, Y., Xu, W. & Polyansky, D. E. Effect of Chloride Anions on the Synthesis and Enhanced Catalytic Activity of Silver Nanocoral Electrodes for CO_2 Electroreduction. *ACS Catal.* **5,** 5349–5356 (2015).

38. Koper, M. T. M. Theory of multiple proton–electron transfer reactions and its implications for electrocatalysis. *Chem. Sci.* **4,** 2710 (2013).

39. Firet, N. J. & Smith, W. A. Probing the Reaction Mechanism of CO 2 Electroreduction over Ag Films via Operando Infrared Spectroscopy. *ACS Catal.* **7,** 606–612 (2017).

40. Sharma, R. C. & Chang, Y. A. The Ag-S (Silver-Sulfur) system. *Bull. Alloy Phase Diagrams* **7,** 263–269 (1986).

41. Masis, M. M. Resistive Switching in Mixed Conductors Ag2S as a Model System. (Universiteit Leiden, 2012).

42. Liu, S. *et al.* Rational Design of Silver Sulfide Nanowires for Efficient CO 2 Electroreduction in Ionic Liquid. *ACS Catal.* **8,** 1469–1475 (2018).

43. Kim, C. *et al.* Achieving Selective and Efficient Electrocatalytic Activity for CO 2 Reduction Using Immobilized Silver Nanoparticles. *J. Am. Chem. Soc.* **137,** 13844–13850 (2015).

44. Park, H., Kim, H., Hwang, E., Ahn, S. H. & Kim, S.-K. Electrochemical Reduction of Carbon Dioxide Using Ag Catalysts Prepared by Electrodeposition in the Presence of Additives. *J. Nanosci. Nanotechnol.* **17,** 7843–7851 (2017).

45. Choi, J. *et al.* Electrochemical CO2 reduction to CO on dendritic Ag-Cu electrocatalysts prepared by electrodeposition. *Chem. Eng. J.* **299,** 37–44 (2016).

46. Sun, K. *et al.* Enhanced electrochemical reduction of CO_2 to CO on Ag electrocatalysts with increased unoccupied density of states. *J. Mater. Chem. A* **4,** 12616–12623 (2016).

47. Liu, X., Liu, Z., Lu, J., Wu, X. & Chu, W. Silver sulfide nanoparticles sensitized titanium dioxide nanotube arrays synthesized by in situ sulfurization for photocatalytic hydrogen production. *J. Colloid Interface Sci.* **413,** 17–23 (2014).

48. Baše, T. *et al.* Carborane-thiol-silver interactions. A comparative study of the molecular protection of silver surfaces. *Surf. Coatings Technol.* **204,** 2639–2646 (2010).

49. Zhou, W., Apkarian, R., Wang, Z. L. & Joy, D. Fundamentals of Scanning Electron Microscopy (SEM). in *Scanning Microscopy for Nanotechnology* 1–40 (Springer New

York, 2006).

50. Epp, J. X-ray diffraction (XRD) techniques for materials characterization. in *Materials Characterization Using Nondestructive Evaluation (NDE) Methods* 81–124 (Elsevier, 2016).

51. Widjonarko, N. Introduction to Advanced X-ray Diffraction Techniques for Polymeric Thin Films. *Coatings* **6,** 54 (2016).

52. Elgrishi, N. *et al.* A Practical Beginner's Guide to Cyclic Voltammetry. *J. Chem. Educ.* **95,** 197–206 (2018).

53. Sparkman, O. D., Penton, Z. E. & Kitson, F. G. Gas Chromatography. in *Gas Chromatography and Mass Spectrometry: A Practical Guide* 15–83 (Elsevier, 2011).

54. Lu, Q. *et al.* A selective and efficient electrocatalyst for carbon dioxide reduction. *Nat. Commun.* **5,** 1–6 (2014).

55. Gomez Becerra, J., Salvarezza, R. C. & Arvia, A. J. The role of a slow phase formation process in the growth of anodic silver oxide layers in alkaline solutions-I. Electroformation of Ag(I) oxide layer. *Electrochim. Acta* **33,** 1431–1437 (1988).

56. Sheng, W., Myint, M., Chen, J. G. & Yan, Y. Correlating the hydrogen evolution reaction activity in alkaline electrolytes with the hydrogen binding energy on monometallic surfaces. *Energy Environ. Sci.* **6,** 1509 (2013).

57. Hoshi ', N., Kato, M. & Hori, Y. Electrochemical reduction of CO, on single crystal electrodes of silver Ag(111:) , Ag(100) and Agi 1101. *Iuumd Elcctroanalytical Chem.* **4,** 283–286 (1997).

58. Lide, D. R. *CRC handbook of chemistry and physics*. *a ready-reference book of chemical and physical data* (CRC Press, 2004).

59. Yano, H., Shirai, F., Nakayama, M. & Ogura, K. Electrochemical reduction of CO2 at three-phase (gas|liquid|solid) and two-phase (liquid|solid) interfaces on Ag electrodes. *J. Electroanal. Chem.* **533,** 113–118 (2002).

60. Delacourt, C., Ridgway, P. L. & Newman, J. Mathematical Modeling of CO2 Reduction to CO in Aqueous Electrolytes. *J. Electrochem. Soc.* **157,** B1902–B1910 (2010).

61. Wuttig, A. & Surendranath, Y. Impurity Ion Complexation Enhances Carbon Dioxide Reduction Catalysis. *ACS Catal.* **5,** 4479–4484 (2015).

62. Yin, Y. *et al.* Contributions of Phase, Sulfur Vacancies, and Edges to the Hydrogen Evolution Reaction Catalytic Activity of Porous Molybdenum Disulfide Nanosheets. doi:10.1021/jacs.6b03714

63. Jeol. Energy table for EDS analysis. Available at: http://studylib.net/doc/8126264/energy-table-for-eds-analysis. (Accessed: 11th July 2018)